Electronic Supporting Information

2-Azabutadiene Complexes of Rhenium(I): *S,N*-Chelated Species With Photophysical Properties Heavily Governed by the Ligand Hidden Traits

Adrien Schlachter,[a] Frank Juvenal,[a] Rodolphe Kinghat,[b] Abderrahim Khatyr,[b] Fabrice Guyon,[b] Paul-Ludovic Karsenti,[a] Carsten Strohmann,[c] Marek M. Kubicki,[d] Yoann Rousselin,[d] Pierre D. Harvey,[a] and Michael Knorr[b]*

a Département de Chimie, Université de Sherbrooke, Sherbrooke, Québec, Canada J1K 2R1.

b Institut UTINAM, UMR CNRS 6213, Université Bourgogne Franche-Comté, 25030 Besançon, France.

c Anorganische Chemie, Technische Universität Dortmund, 44227 Dortmund, Germany.

d Institut de Chimie Moléculaire UMR 5260, Université Bourgogne Franche-Comté, 21078 Dijon, France.

* E-mail: michael.knorr@univ-fcomte.fr

Table of Content

Table S1. Spectroscopic Characteristics of the Complexes

	IR ($\nu_{C\equiv O}$/cm^{-1})	$^{13}C\{^1H\}$ NMR ($CDCl_3$) ($\delta_{(C\equiv O)}$/ppm)	UV-visible (CH_2Cl_2) λ/nm (ε x 10^{-3} M^{-1}cm^{-1})
1a	2031, 1937, 1898	187.3, 189.4, 192.6	236 (25.5), 274 (16.9), 383 (10.3)
1b	2033, 1938, 1905	188.2, 189.8,191.8	231 (20.4), 267 (15.8), 352 (7.2), 384 (6.8)
1c	2034, 1940, 1903	188.1, 190.2,192.8	234 (21.7), 272 (18.4), 387 (8.9)
1d	2031, 1937, 1904	187.4, 189.9, 192.6	231 (31.9), 267 (23), 351 (10.2), 385 (9.6)
1e	2032, 1939, 1899	186.7, 189.9, 193.2	235 (17.3), 273 (19.1), 386 (11.9)
1f	2033, 1942, 1904	187.1, 189.3, 192.2	235 (20.5), 274 (17.1), 389 (8.2)
1g	2032, 1937, 1906	187.9, 188.9, 192.0	230 (26), 274 (11.9), 376 (5.9)
1h	2034, 1942, 1904	188.3, 190.3, 192.3	235(28.7), 286 (8.7), 395(2.3)
1i	2031, 1936, 1899	189.7, 191.1, 193.2	232 (28.9), 253 (29.5), 370 (8.3)
1j	2044, 1952, 1920	188.0, 191.0, 193.2	233 (22), 273 (16.1), 384 (7.1)

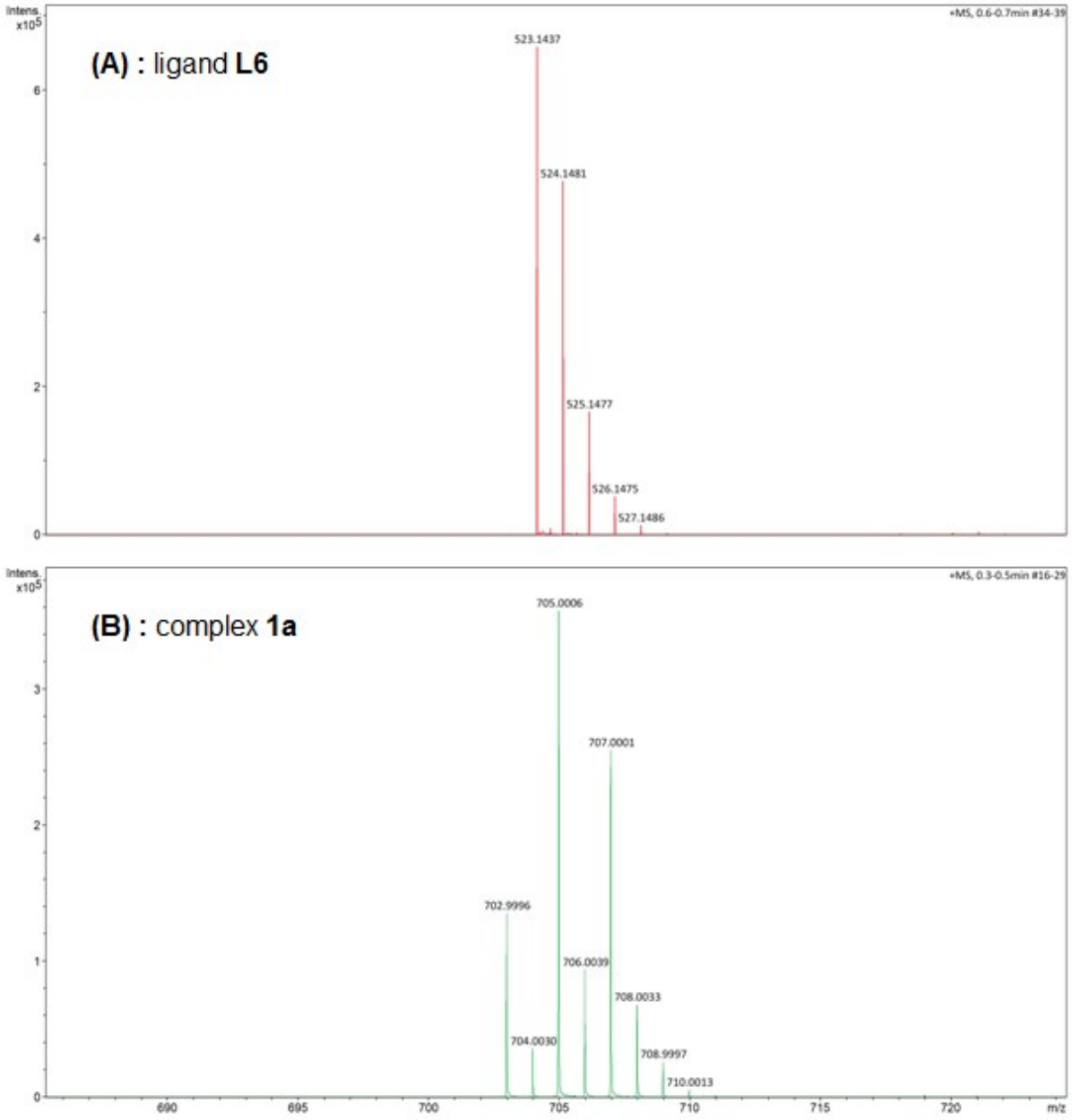

Figure S1. APCI mass spectra (positive mode) of: ligand **L6** (A) and complex **1a** (B).

a) **b)**

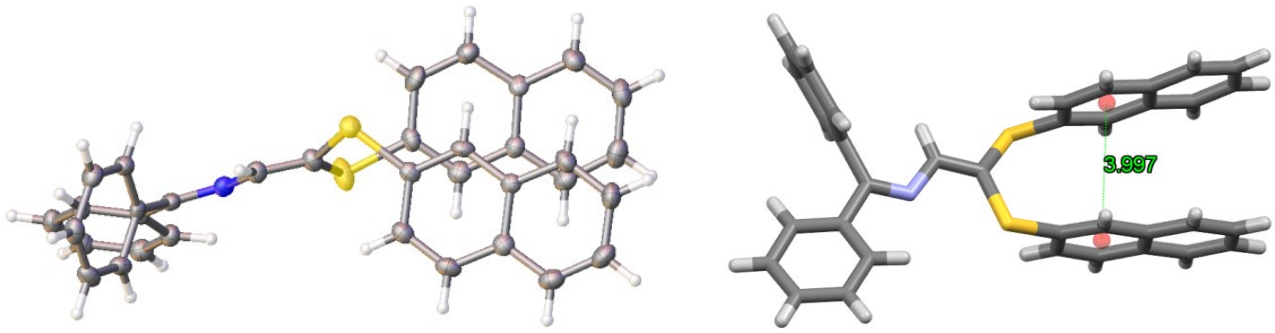

c)

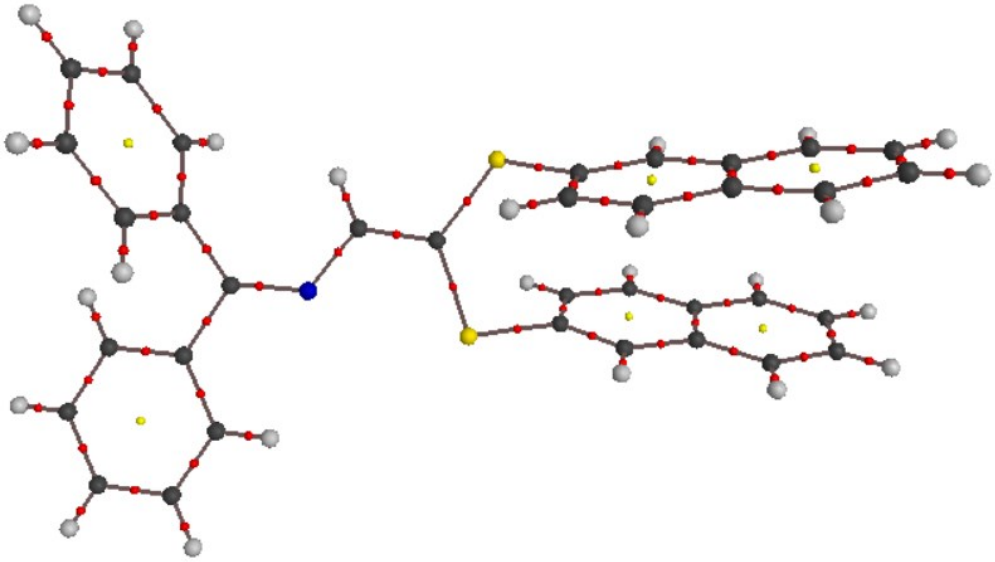

Figure S2. a) and b) Supposed π–π slipped interaction between the planes of phenyl fragments of the naphtyl substituents in the crystal of **L6**, 3.997 Å is the distance between the centroids of these planes, c) Molecular graph of **L6**, showing the bond critical points (red) and ring critical points (yellow).

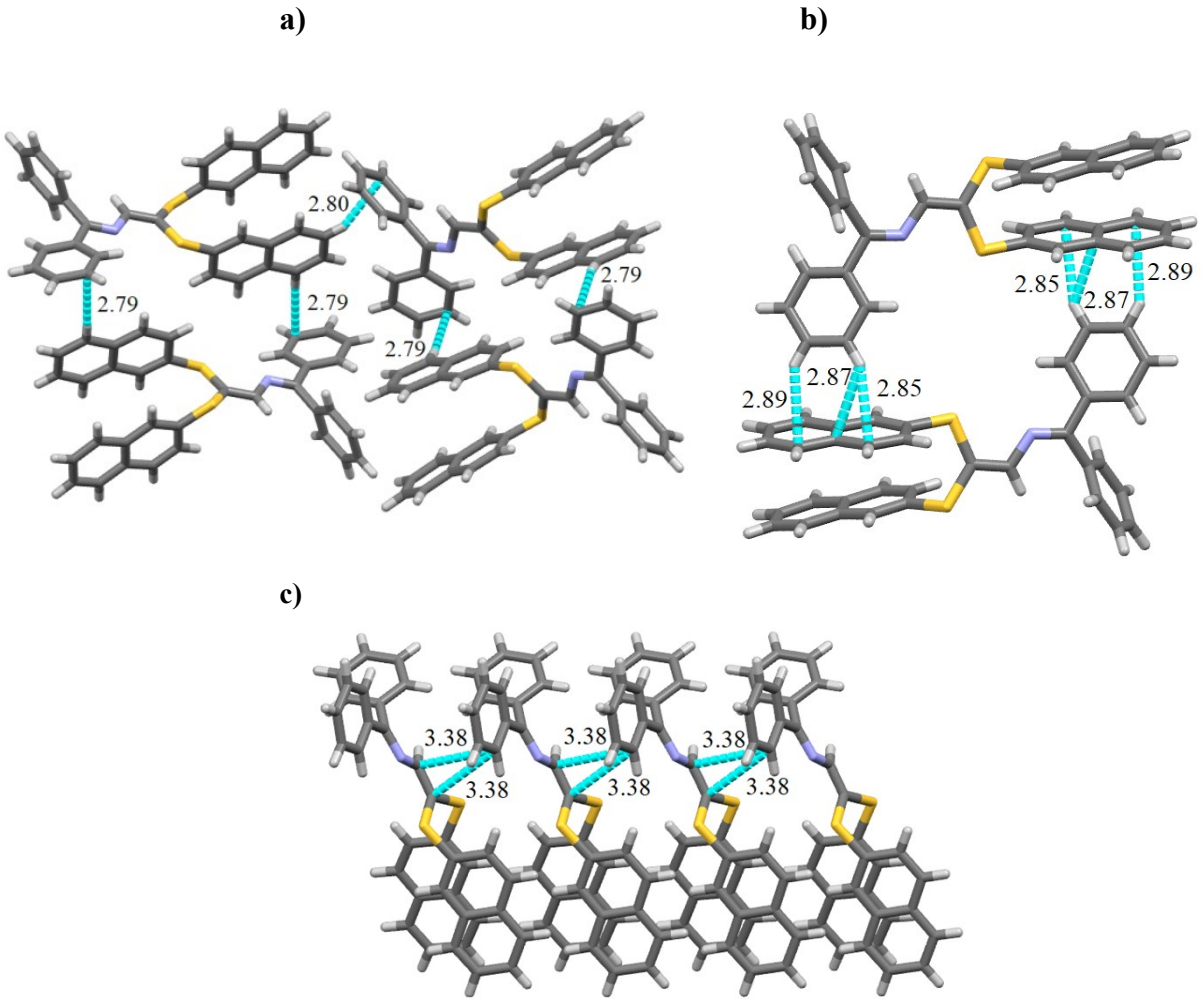

Figure S3. Weak non-covalent interactions in free ligand **L6**; a) CH···C(π)(Napht to Ph, 2.79 and 2.80 Å), b) C-H···C(π)(Ph to Napht, 2.85, 2.87 and 2.89 Å), c) C(π)···C(π) (3.38 Å).

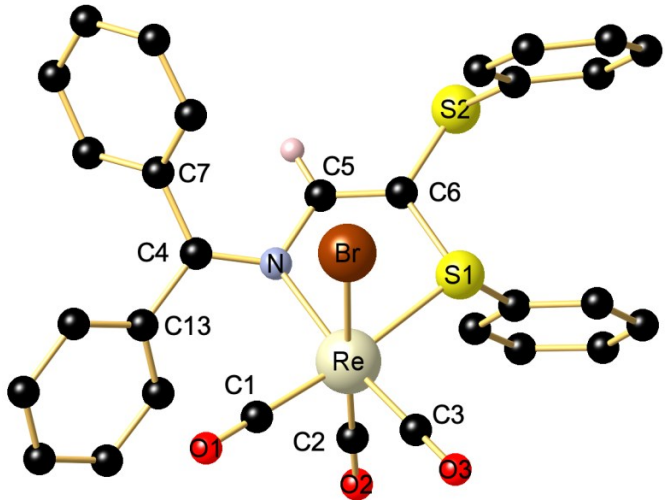

Figure S4. Molecular structure of **1b**. Selected bond lengths [Å] and angles [°]: Re–Br 2.6295(6), Re–N 2.254(4), Re–S1 2.455(13), Re–C1 1.946(6), Re–C2 1.916(6), Re–C3 1.916(6), C4–N 1.321(6), N–C5 1.409(6), C5–C6 1.337(7), C6–S1 1.780(5), C6–S2 1.764(5), S1–C19 1.801(5), S2–C25 1.779(6); N–Re–S1 80.11(11), Br–Re–S1 81.25(3), Br–Re–N 81.62(11), Re–N–C5 115.0(3), S1–C6–S2 8117.3(3).

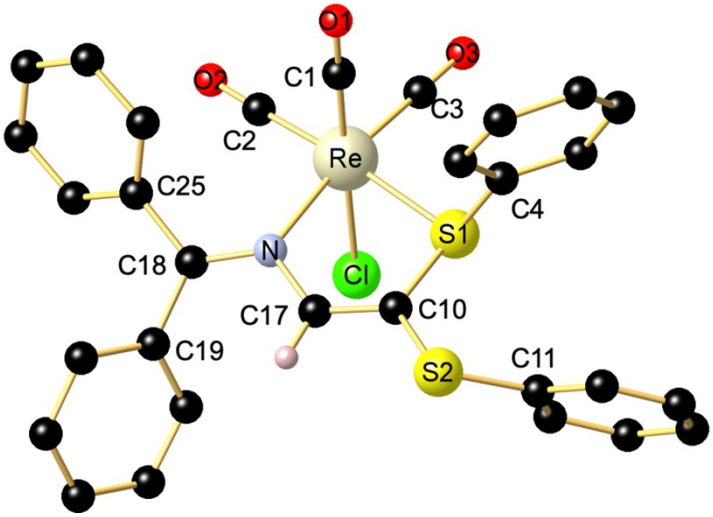

Figure S5. Molecular structure of **1c**. The two $CHCl_3$ solvate molecules are not shown. Selected bond lengths [Å] and angles [°]: Re–Cl 2.4951(17), Re–C1 1.891(7), Re–C2 1.939(6), Re–C3 1.933(6), Re–N 2.247(5), Re–S1 2.4598(15), C18–N 1.321(7), N–C17 1.411(7), C17–C10 1.340(8), C10–S1 1.774(6), C10–S2 1.760(6), S1–C4 1.797(6), S2–C11 1.778(6); N–Re–S1 80.40(12), Cl–Re–S1 81.33(6), Cl–Re–N 80.67(13), Re–N–C18 125.7(4), Re–N–C17 115.4(3), Re–S1–C10 99.52(19), Re–S1–C4 113.5(2), S1–C10–S2 121.4(3).

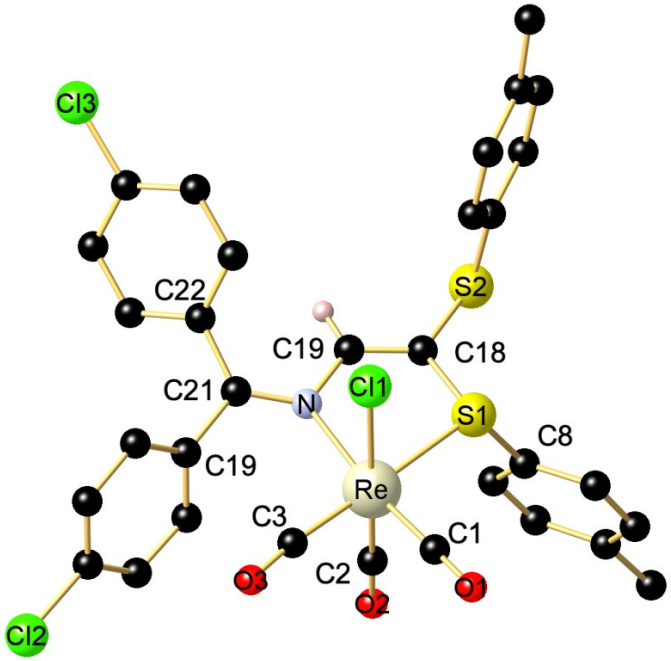

Figure S6. Molecular structure of **1f**. Selected bond lengths [Å] and angles [°]: Re–Cl 2.4803(15), Re–C1 1.904(7), Re–C2 1.912(6), Re–C3 1.933(6), Re–N 2.259(5), Re–S1 2.4640(14), C21–N 1.308(7), N–C19 1.412(7), C19–C18 1.343(9), C18–S1 1.772(6), C(18–S2 1.767(6), S1–C8 1.803(6), S2–C15 1.771(6); N–Re–S1 80.42(12), Cl–Re–S1 81.314(5), Cl–Re–N 79.30(12), Re–N–C21 125.0(4), Re–N-C19 115.5(4), Re-S1–C18 99.4(2), Re–S1–C8 112.32(18), S1–C18–S2 118.3(4).

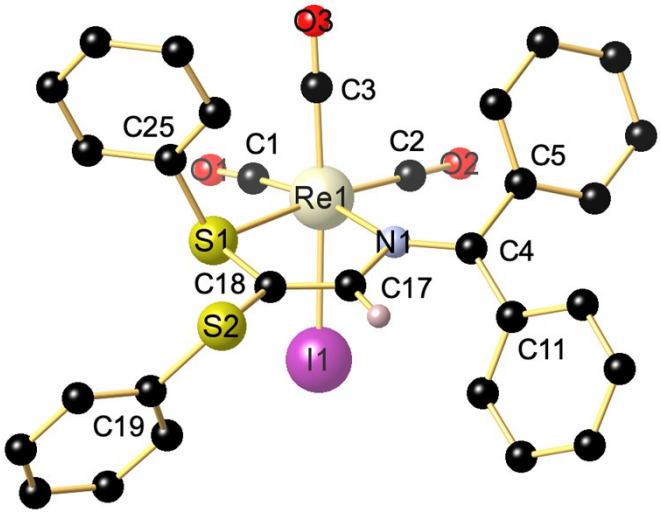

Figure S7. Molecular structure of **1g**. Selected bond lengths [Å] and angles [°]: angles [°]: Re1–I1 2.8167(6), Re1–C1 1.895(9), Re1–C2 1.939(9), Re1–C3 1.915(9), Re1–N1 2.242(7), Re1–S1 2.461(2), C4–N1 1.300(10), N1–C17 1.419(10), C17–C18 1.344(11), C18–S1 1.772(8), C18–S2 1.748(8); I1–Re1-–C1 87.5(3), I1–Re1–C2 92.1(3), I1–R1e–C3 176.5(3), N1–Re1–S1 80.78(17), I1–Re1–S1 82.05(5), I1–R1e–N1 83.65(16), Re1–N1–C4 127.9(5), Re1–N1–C17 114.2(5), Re1–S1–C18 99.2(3), Re1–S1–C25 112.6(3), S1–C18–S2 119.4(4). Only one of the two independent molecules is shown.

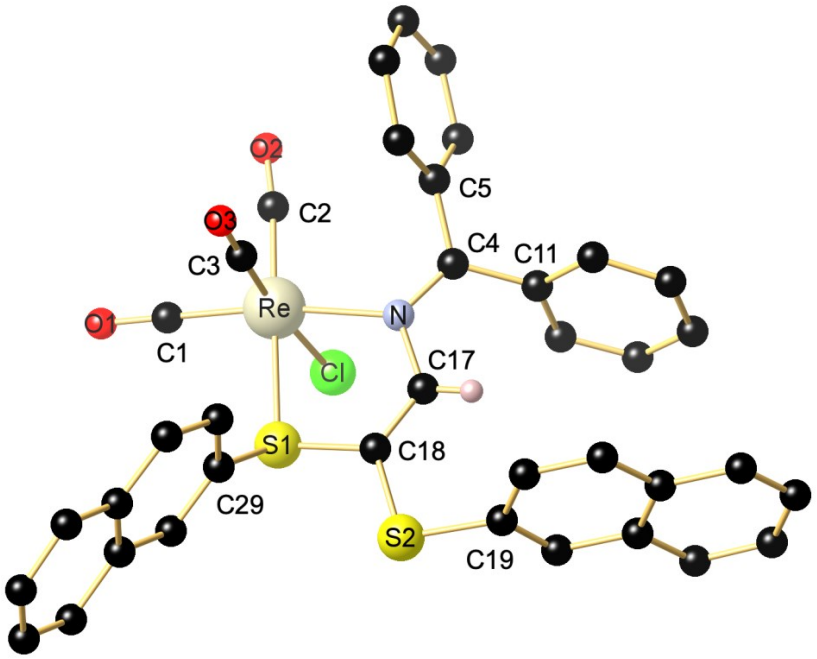

Figure S8. Molecular structure of **1h**. Selected bond lengths [Å] and angles [°]: Selected bond lengths [Å] and angles [°]: Re–Cl 2.4809(10), Re–C1 1.909(4), Re–C2 1.930(4), Re–C3 1.906(4), Re–N 2.223(3), Re–S1 2.4672(9), C4–N 1.308(5), N–C17 1.411(5), C17–C18 1.338(85), C18–S1 1.775(4), C18–S2 1.759(4), S1–C29 1.786(2), S2–C19 1.780(5); N–Re–S1 80.33(9), Cl–Re–S1 78.86(3), Cl–Re–N 79.587(19), Re–N–C4 126.4(3), Re–N–C17 116.1(3), Re–S1–C18 99.37(13), Re–S1–C29 115.38(14), S1–C18–S2 114.7(2).

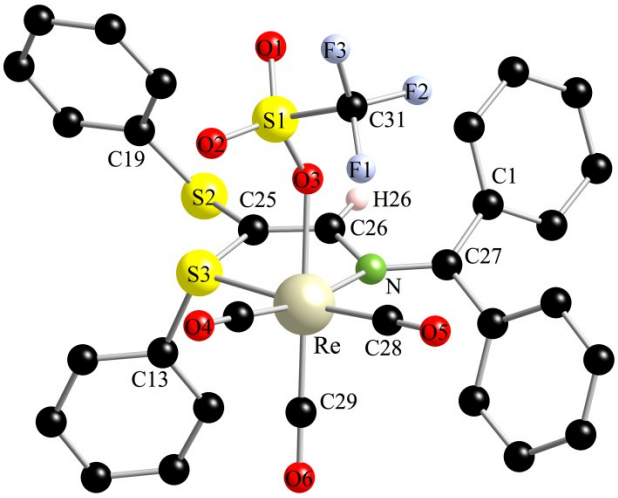

Figure S9. Molecular structure of **1j**. The CH_2Cl_2 solvate molecules are not shown. Selected bond lengths [Å] and angles [°]: Re–C28 1.930(7), Re–C29 1.903(8), Re–C30 1.922(6), Re–O3 2.200(15), Re–N 2.230(5), Re–S3 2.4634(17), C27–N 1.332(8), N–C26 1.421(8), C25–C26 1.340(9), C25–S2 1.7750(7), C25–S3 1.776(7), S2–C19 1.769(8), S3–C13 1.767(68); N–Re–S3 79.90(14), O3–Re–S3 79.48(14), O3–Re–N 74.69(119), Re–N–C27 125.1(4), Re–N–C26 116.5(5), Re–S3–C25 99.0(2), Re–S3–C13 113.8(3), S2–C25–S3 117.7(4).

Table S2. Selected bond lengths (Å) and angles (deg.) for the Re complexes.

	Re–X	Re–S	Re–N	Re–C(CO)	X-Re-CO trans	S–Re–N
1a	2.6293(4)	2.4585(7)	2.249(2)	1.901(3) (a) 1.924(3) (b) 1.908(3) (c)	176.06(8)	79.64(5)
1b	2.6295(6)	2.4538(13)	2.254(4)	1.916(6) (a) 1.946(6) (b) 1.916(6) (c)	177.52(17)	80.61(11)
1c	2.4951(17)	2.4598(15)	2.247(5)	1.891(7) (a) 1.939(6) (b) 1.933(6) (c)	177.17(18)	80.40(12)
1e (mon)	2.4875(11)	2.4557(11)	2.259(4)	1.901(5) (a) 1.936(5) (b) 1.921(5) (c)	176.26(13)	79.81(9)
1e (tricl)	2.4877(6) 2.4770(6)	2.4570(6) 2.4527(6)	2.239(2) 2.245(2)	1.895(3) (a) 1.931(3) (b) 1.916(3) (c) 1.904(3) (a) 1.932(3) (b) 1.919(3) (c)	173.09(8) 173.62(8)	80.60(5) 80.54(5)
1f	2.4803(15)	2.4640(14)	2.259(5)	1.912(6) (a) 1.933(6) (b) 1.904(8) (c)	174.08(19)	80.42(12)
1g **molecule 1** **molecule 2**	**1g**	2.8167(6) 2.8179(6)	2.461(2) 2.464(2)	2.242(7) 2.236(6)	1.772(9) (a) 1.939(9) (b) 1.895(9) (c) 1.890(9) (a) 1.942(9) (b) 1.933(9) (c)	176.5(3) 176.5(3)
1h	2.4809(10)	2.4672(9)	2.223(3)	1.906(4) (a) 1.930(4) (b) 1.909(4) (c)	173.49(13)	80.33(9)
1i	2.6208(4)	2.4763(10)	2.260(3)	1.921(4) (a) 1.944(4) (b) 1.900(4) (c)	175.71(12)	78.28(8)
1j	2.200(5)	2.4634(17)	2.230(5)	1.903(8) (a) 1.930(7) (b) 1.922(6) (c)	174.6(2)	79.90(14)

(a) CO trans to X, (b) CO trans to S, (c) CO trans to N.

Table S3. Torsion and significant dihedral angles (deg.) observed in the structures **1a-c** and **1e-j.** Values for the corresponding azadiene molecules (free ligands) are reported in square brackets.

	C=N–C=C[a)]	C–S···S–C[b)]	Ph1/C=N–C=C[c)]	Ph2/C=N–C=C[d)]
1a **[AzBu(S^{i}Pr)2]**[e)]	179.2() [159.8(4)]	104.5() [107.0(2)]	58.7() [38.8(4)]	63.3() [61.3(2)]
1b **[AzBu(SPh)2]**[f)]	171.8() [177.4(3)]	116.8(2) [65.7(1)]	52.3(5) [21.0(2)]	56.4(2) [77.8(1)]
1c **[AzBu(SPh)2]**[f)]	178.3(6) [177.4(3)]	86.4(3) [65.7(1)]	59.6(5) [21.0(2)]	62.1(3) [77.8(1)]
1e(mono) [viscous oil]	178.6(5)	109.1(2)	49.3(4)	57.7(2)
1e(tricl) **R** **S** [viscous oil]	170.6(2) 168.9(3)	125.1(1) 119.6(1)	59.2(2) 61.6(2	61.5(1) 52.0(1)
1f [not known]	169.7(6)	137.4(3)	65.2(5)	52.5(3)
1g molecule 1 molecule 2 **[AzBu(SPh)2]**[f)]	180.0(8) 178.8(8) [177.4(3)]	113.3(5) 116.2(5) [65.7(1)]	54.2(7) 53.2(7) [21.0(2)]	53.4(3) 53.8(4) [77.8(1)]
1h **[AzBu(Snaft)2]**[g)]	177.6(4) [175.7(2)]	133.1(2) [62.6(2)]	69.9(3) [25.3(2)]	71.7(2) [65.5(1)]
1i **[AzBu(S^{t}Bu)2]**[h)]	148.4(4) [111.6(3)]	28.9(2) [87.8(2)]	68.5(4)[i)] [15.0(3)]	48.3(2) [i)] [72.4(1)]
1j **[AzBu(SPh)2]**[f)]	178.7(6) [177.4(3)]	118.5(4) [65.7(1)]	58.0(5) [21.0(2)]	59.1(3) [77.8(1)]

[a)] torsion angle (measure of electron delocalization), [b)] torsion angle (measure of conformation of SR groups) [c)]dihedral angle, Ph1 is the ring on the side of N lone pair in free ligand, [d)] Ph2 is the second phenyl ring in imine part, [e)] see ref. 1, [f)] see ref. 2, [g)] this work, [h)] see ref. 3, [i)] because of the broken conjugation in the main azadienic chain C=N-C=C only its imine part C=N-C is taken as reference plane.

Table S4. Types of intermolecular non-covalent interactions observed in the structures **1a-c** and **1e-j** (per one molecule of the complex).

	1a	**1b**	**1c**	**1e (mono)**	**1e (tricl)**	**1f**	**1g**	**1h**	**1i**	**1j**
CH–XRe	2	2	2	1	2	2		2		
CH–π(Ph)			5	1	1	7	6	4		4
CO–π(Ph)	1	1			1					
CO–πazBu					1					2
CO–π(CO)								1		
CH–S		2		2	1		2		2	
CH–O		1	1	4	2	3		1		
CH–π(CO)									1	
CCl–OC			139.2 [a)] 165.0 [a)]			154.4 [a)]				
CCl–HalC										167.4 [b)] 168.2 [b)]
CCl–π(Ph)			1							
ReCl–πazBu								1		

[a)] C-Cl···O angle (°), [b)] C-Cl···F angle (°).

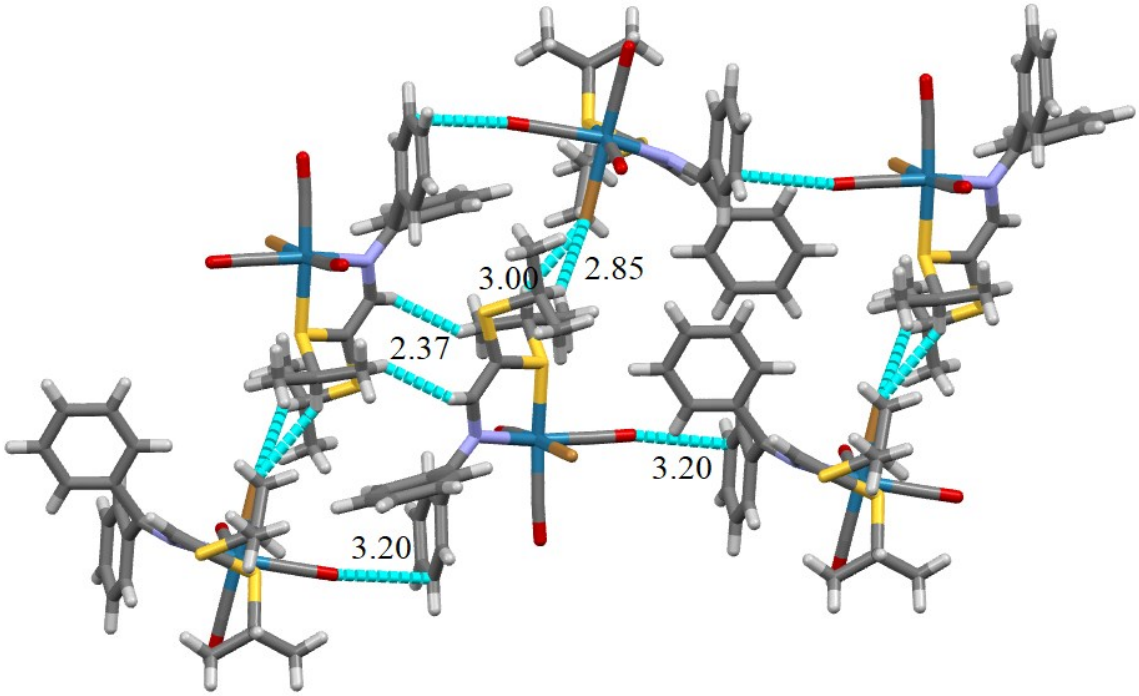

Figure S10. Illustration of the CH···Br-Re (2.85 Å, 3.00 Å), CO···π(Ph) (3.20 Å) intermolecular interactions and van der Waals H···H (2.37 Å) contacts in complex **1a**.

a) **b)**

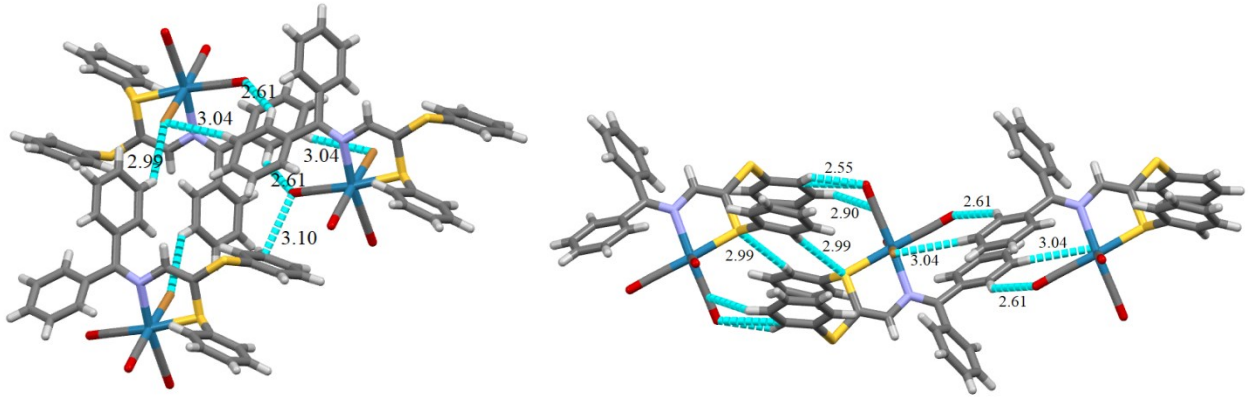

Figure S11. Illustration of a) CH···BrRe (2.99, 3.04 Å), CH···O (2.61 Å), and CO···π(Ph) (3.10 Å), b) CH···πCO (2.55(O) Å, 2.90(C) Å), CH···O (2.60 Å) and CH···S (2.99 Å) intermolecular interactions in complex **1b**.

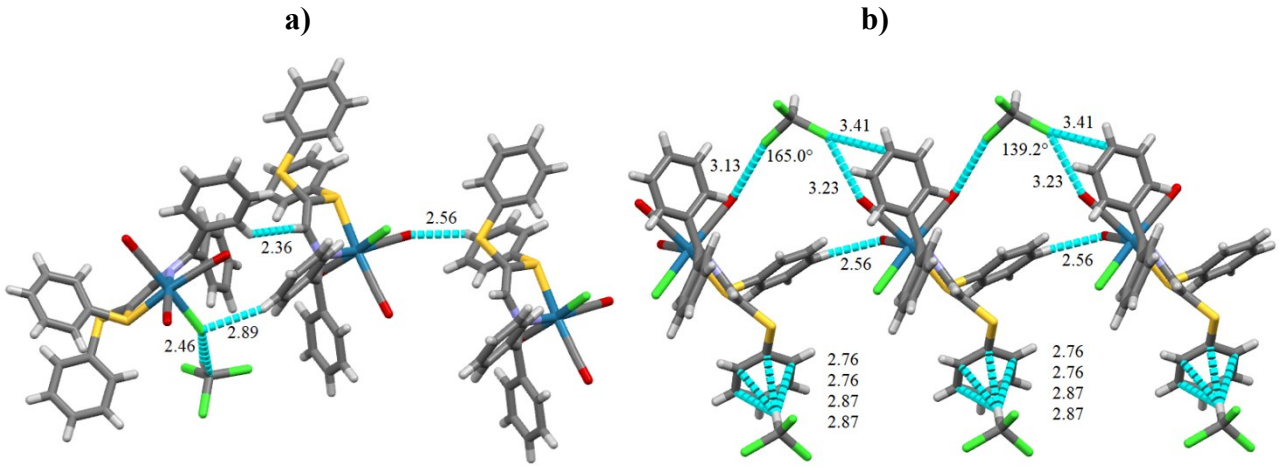

Figure S12. Illustration of a) ReCl···HC (2.46 Å, 2.89 Å), CH···O (2.56 Å) and CH(Ph)···HC(aza) (2.36 Å), b) $CH(CHCl_3)$ ···π(Ph) (2.76, 2.76, 2.87, 2.87 Å), $CCl(CHCl_3)$···O (3.13 Å, 3.23 Å) and $CCl(CHCl_3)$···π(Ph) (3.41) interactions in complex **1c**.

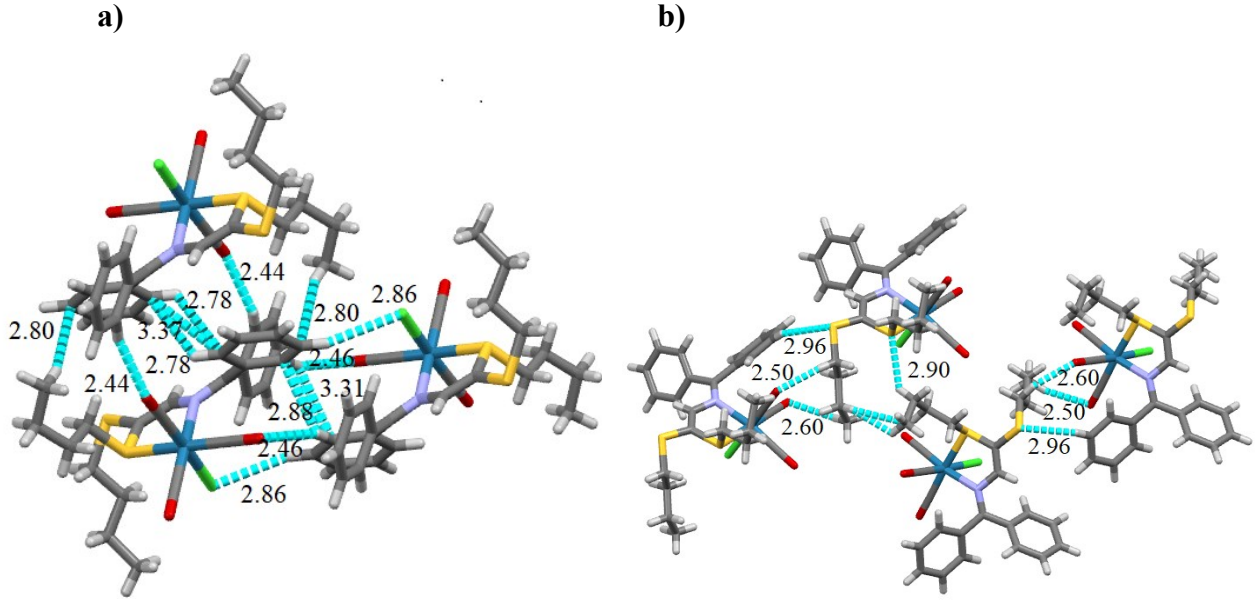

Figure S13. Illustration of a) CH···ClRe (2.86 Å), CH···O (2.46, 2.44 Å), CH···π(Ph) (2.80 Å) interactions and CH(Ph)bond···CH(Ph)bond (2.88 and 2.78 (H-C), 3.31 and 3.37 (C-C)) overlaps, b) CH···S (2.90, 2.96 Å) and CH···O (2.50, 2.60 Å) interactions in complex **1e(mono)**.

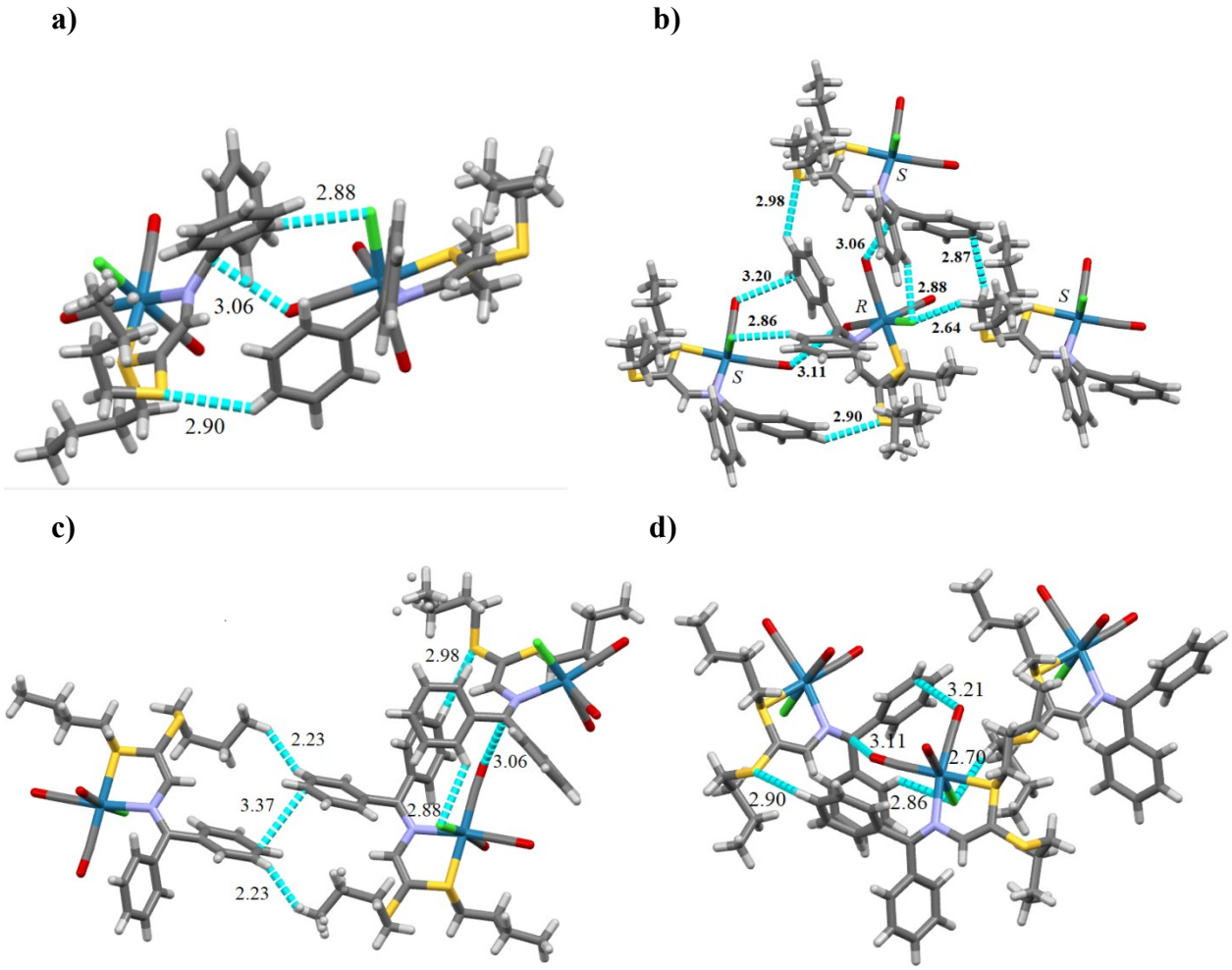

Figure S14. Illustration of a) connectivity between R and S isomers present in the assymetric unit (CH···ClRe (2.88 Å), CH-S (2.90 Å) and CO···πC(C atom from imine part of AzBu ligand, 3.06 Å), b) CH···ClRe (2.88, 2.64 and 2.86 Å), CH···πC(Ph, 2.87 Å), CO···πC(Ph, 3.20 Å), CO-πC(C atom from imine part of AzBu ligand, 3.06 and 3.11 Å) and CH···S (2.90 and 2.98 Å) interactions, c) πC(Ph)-πC(Ph) 3.37 Å, CH-ClRe (2.88 Å), CO-πC (3.06 Å), CH-S (2.98 Å) and H···H (2.23 Å) interactions and d) CH···ClRe (2.70 and 2.86 Å), CO-πC(3.11 and 3.21 Å) and CH···S (2.90 Å) interactions in complex **1e(tricl)**.

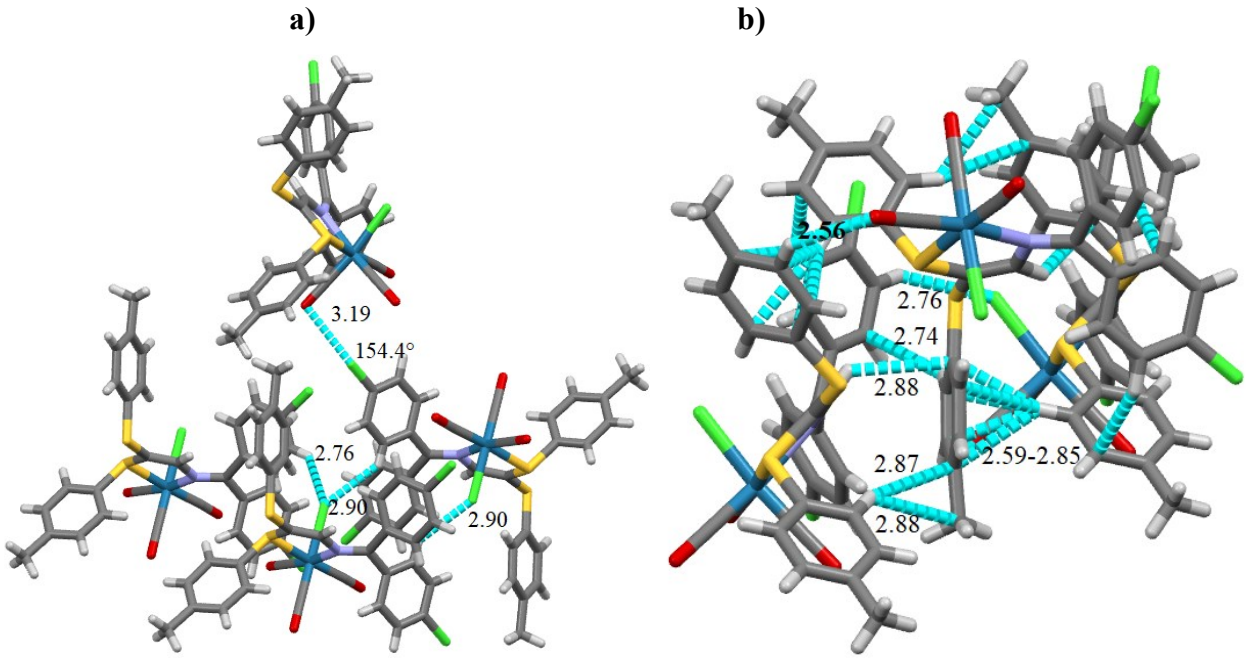

Figure S15. Illustration of a) CH···ClRe and CCl···O (154.4°), b) CH···π interactions in complex **1f**.

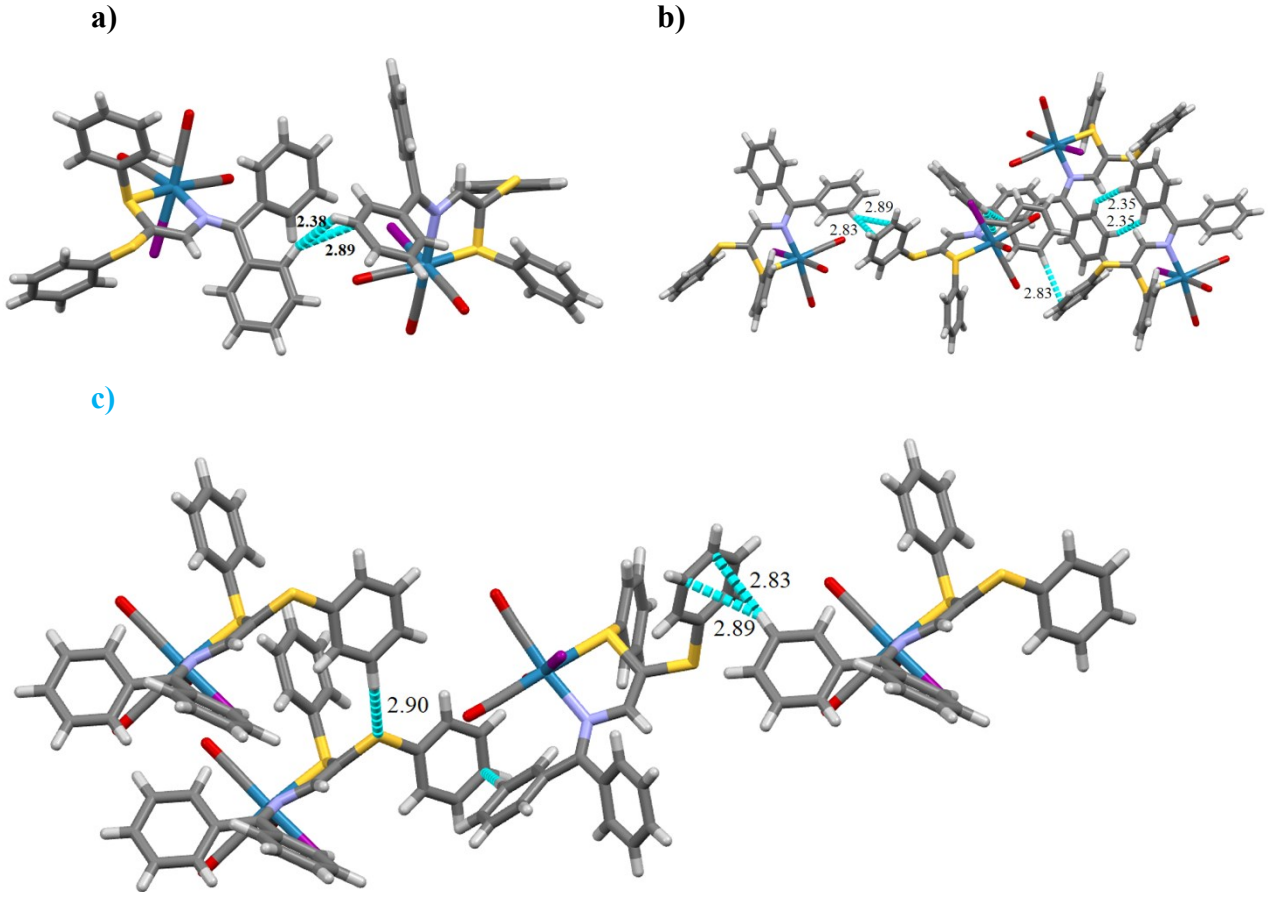

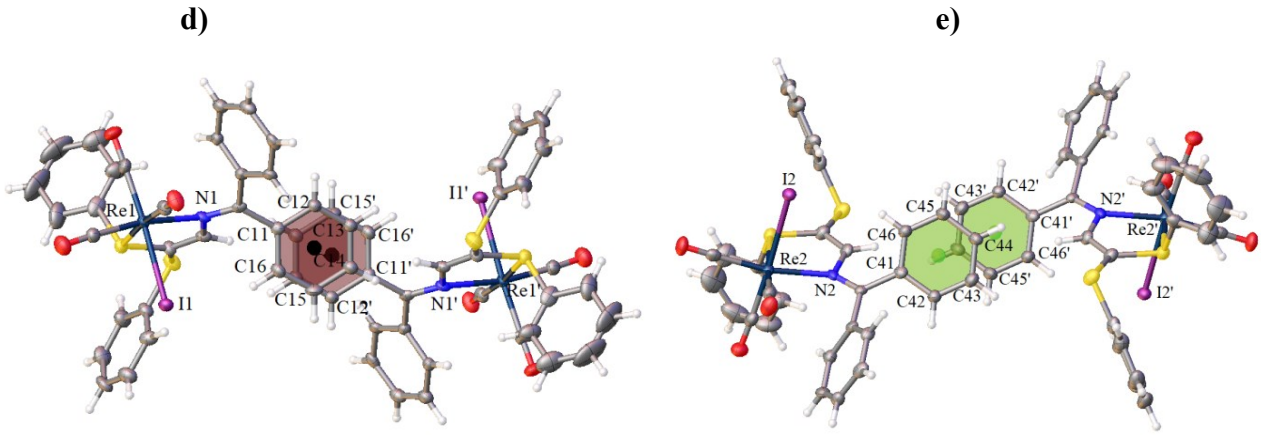

Figure S16. Complex **1g.** Two molecules in the asymmetric unit linked through side CH···CH (2.38 Å (H···H), 2.89 Å (C···H)) interactions; b) Point-to-point CH···CH (2.35 Å) and CH–π (2.83, 2.89 and 2.83 Å) interactions; c) CH···S (2.90 Å) and CH···π (2.83 and 2.89 Å) interactions; d) π–π stacking involving molecules built over the Re1 atoms; e) π–π stacking involving molecules built over the Re2 atoms.

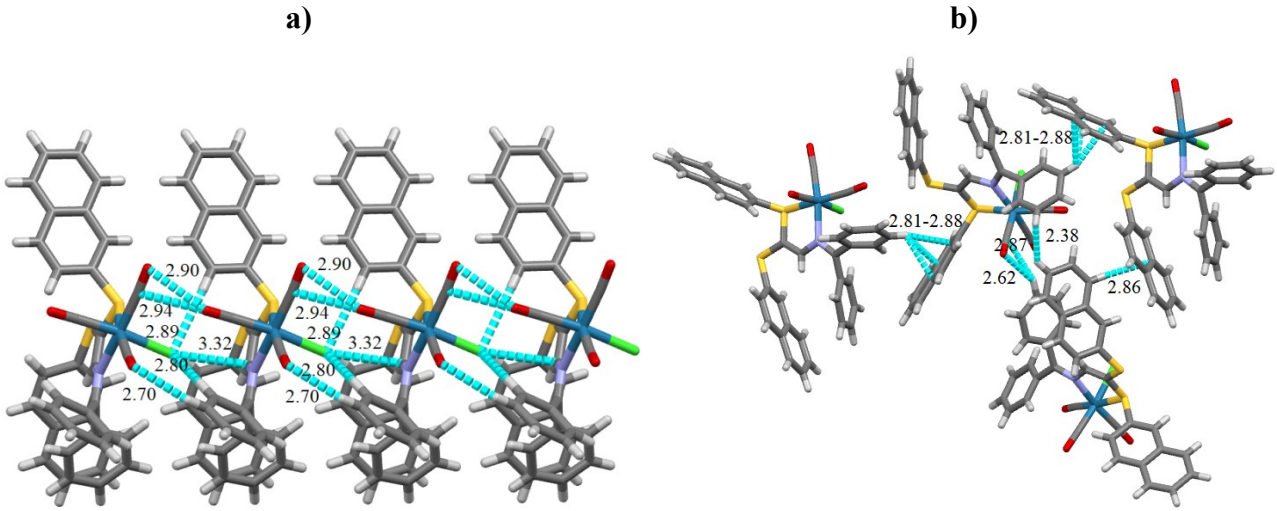

Figure S17. Illustration of a) CH···ClRe (2.80 Å), ReCl–π(C atom from ethylene part of the AzBu ligand 3.32 Å), CH···O (2.70 Å) and CO–π(CO) (2.94 (C···O), 2.90 Å (O···O)), b) CH–π (2.81 – 2.88 Å) interactions in complex **1h**.

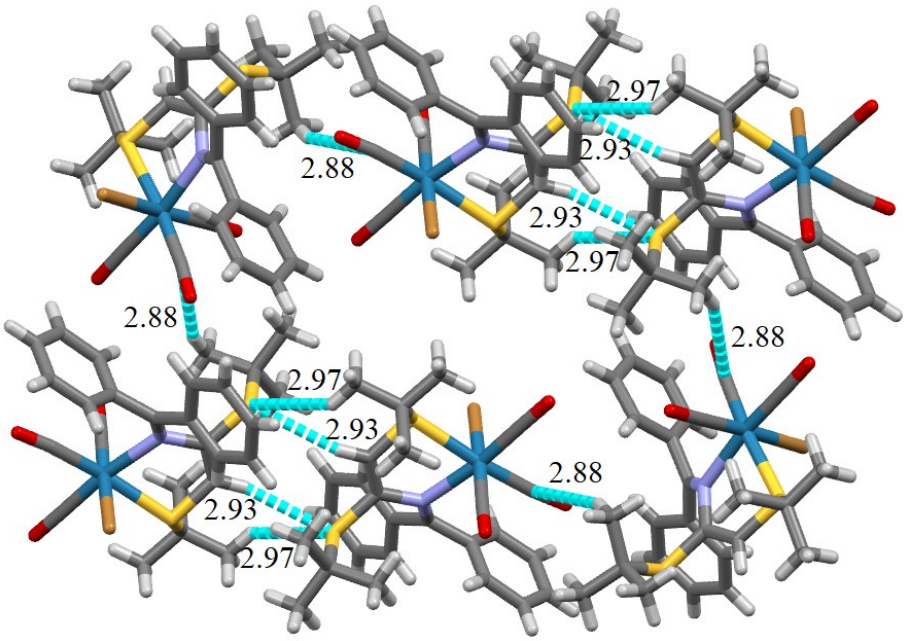

Figure S18. Illustration of CH···S (2.93 and 2.97 Å) and CH–πC(CO) (2.88 Å) interactions in complex **1i**.

a) **b)**

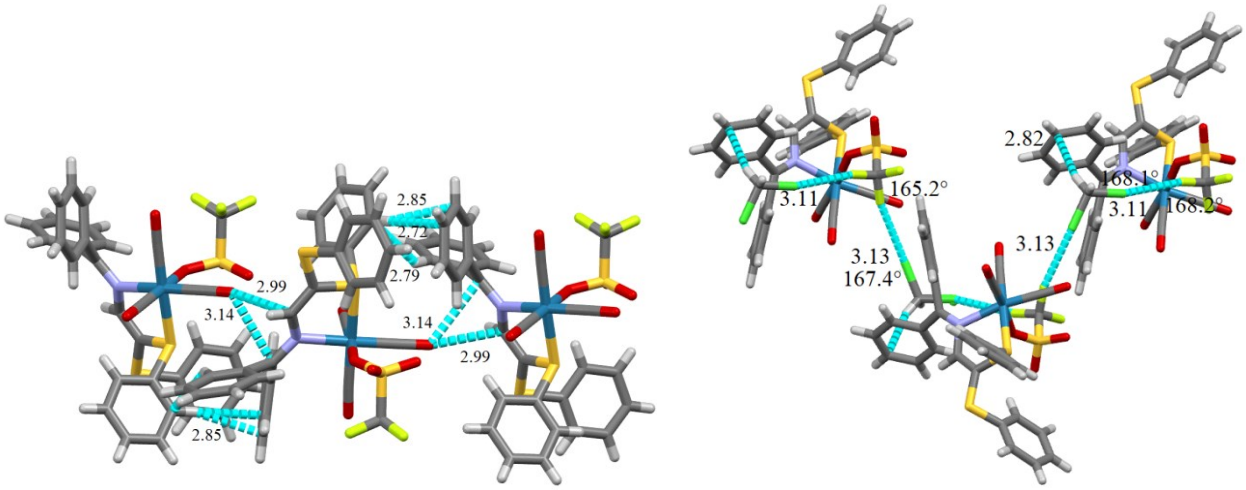

Figure S19. Illustration of a) CH(Ph)···π(Ph) (2.72, 2.79, 2.85 Å), and CO···π(AzBu) (2.99 C-ethylene; 3.14 Å C-imine), b) suggested halogen-type bonding and $CCl(CHCl_3)$ ···π(Ph) (2.82 Å) interactions in complex **1j**.

Table S5. Crystallographic and refinement data for **L6**.

Compound	**L6**
Empirical formula	$C_{35}H_{25}NS_2$
Formula weight	523.68
Temperature	115(2) K
Wavelength	0.71073 Å
Crystal system	monoclinic
Space group	P21/c
Unit cell dimensions	a = 20.4381(7)Å, b = 5.9114(2)Å, c = 28.7530(8)Å, β = 130.941(2)°, γ = 90.
Volume	2624.11(15) $Å^3$
Z	4
Density (calculated)	1.326 g/cm^3
Absorption coefficient	0.229 mm^{-1}
F(000)	1096
Crystal size (mm^3)	0.25 x 0.12 x 0.10
Theta range for data collection	1.88 to 27.56°
Index ranges	-26≤h≤26, -7≤k≤6, -37≤l≤36
Reflections collected	10402
Independent reflections	5999[R(int)=0.1025]
Refinement method	Full-matrix least-squares on F^2
Data / restraints / parameters	5627 / 0 / 370
Goodness-of-fit on F^2	0.905
Final R indices [I>2sigma(I)]	R1 = 0.0556, wR2 = 0.0941
R indices (all data)	R1 = 0.1731, wR2 = 0.1223
Largest diff. peak and hole	0.339 and -0.368 $e.Å^{-3}$

Table S6. Crystallographic and refinement data for compounds **1a-c**, **1e(mono)** and **1e(tricl)**.

Comp.	**1a**	**1b**	**1c**	**1e (mono)**	**1e (tricl)**
Empirical formula	$C_{24}H_{25}BrNO_3ReS_2$	$C_{33}H_{28}BrNO_3ReS_2$	$C_{32}H_{23}Cl_7NO_3ReS_2$	$C_{26}H_{29}ClNO_3ReS_2$	$C_{26}H_{29}ClNO_3ReS_2$
Formula weight	705.68	822.84	967.98	689.27	689.27
Temperature	173(2) K	115(2) K	173(2) K	115(2) K	115(2) K
Wavelength	0.71073 Å	0.71073 Å	0.71073 Å	0.71069 Å	0.71073 Å
Crystal system	monoclinic	triclinic	monoclinic	monoclinic	Triclinic
Space group	P21/n	P-1	P21/n	P21/n	P -1
Unit cell dimensions	a = 13.812(3) Å, b = 18.927(3) Å, c = 19.852(3) Å, α = 90° β = 90° γ = 90°	a = 10.7007(4) Å, b = 10.9549(4) Å, c = 12.8192(6) Å, α = 83.524(2)° β = 80.524(2)° γ = 87.817(2)°	a = 16.739(8) Å, b = 9.579(5) Å, c = 22.898(9) Å, α = 90° β = 94.956(11)° γ = 90°	a = 10.4796(2)Å, b = 10.1519(2)Å, c = 25.1136(5) Å, α = 90° β = 93.7940(10)° γ = 90°	a = 11.9182(2) Å b = 12.5778(3) Å, c = 18.4701(2) Å, α= 91.6840(10)° β= 98.8550(10)° γ = 90.2710(10)°.
Volume	5189.5(15) $Å^3$	1472.48(10) $Å^3$	3658(3) $Å^3$	2665.93(9) $Å^3$	2734.45(9) $Å^3$
Z	8	2	4	4	4
Density (calculated)	1.806 g/cm^3	1.856 g/cm^3	1.758 g/cm^3	1.717 g/cm^{-3}	1.674 g/cm^3
Absorption coefficient	6.409 mm^{-1}	5.662 mm^{-1}	3.982 mm^{-1}	4.843 mm^{-1}	4.721 mm^{-1}
F(000)	2736	804	1888	1360	1360
Crystal size (mm^3)	0.30 x 0.30 x 0.20	0.15 x 0.12 x 0.1	0.40 x 0.40 x 0.40	0.25 x 0.20 x 0.10	0.35 x 0.27 x 0.25
Theta range for data collection	2.05 to 27.00°	2.66 to 27.58°	1.45 to 25.00°	2.58 to 27.48°	2.00 to 27.52°
Index ranges	-17≤h≤17, -24≤k<=24, -25≤l≤25	-13≤h≤12, -14≤k≤12, -16≤l≤15	-19≤h≤19, -11≤k≤6, -24≤l≤20	-13≤h≤13, -13≤k≤9, -32≤l≤22	-15≤h≤15, -16≤k≤16, -23≤l≤23
Reflections collected	42399	9335	11875	16297	85374
Independent reflections	5655[R(int)=0.0337]	6679[R(int)=0.0357]	6010[R(int)=0.0297]	6065[R(int)=0.0627]	12574[R(int)=0.0477]
Refinement method	Full-matrix least-squares on F^2	Full-matrix least-squares on F^2	Full-matrix least-squares on F^2	Full-matrix least-squares on F^2	Full-matrix least-squares on F^2
Data / restraints / parameters	5655/0/293	6679/0/343	6010/0/415	6065/0/307	12574 / 8 / 615
Goodness-of-fit on F^2	1.039	0.948	1.025	1.041	1.128
Final R indices [I>2sigma(I)]	R1 = 0.0189, wR2 = 0.0458	R1 = 0.0370, wR2 = 0.0922	R1 = 0.0364, wR2 = 0.0925	R1 = 0.0358, wR2 = 0.0814	R1 = 0.0205, wR2 = 0.0473
R indices (all data)	R1 = 0.0239, wR2 = 0.0474	R1 = 0.0483, wR2 = 0.0985	R1 = 0.0488 wR2 = 0.1039	R1 = 0.0519, wR2 = 0.0870	R1 = 0.0223, wR2 = 0.0482
Largest diff. peak and hole	0.763 and –0.548 $e.Å^{-3}$	0.955 and -1.212 $e.Å^{-3}$	1.120 and -0.771 $e.Å^{-3}$	0.867 and -3.493 $e.Å^{-3}$	0.747 and -1.354 $e.Å^{-3}$

Table S7. Crystallographic and refinement data for compounds **1f-j**.

Comp.	**1f**	**1g**	**1h**	**1i**	**1j**
Empirical formula	$C_{32}H_{23}Cl_3NO_3ReS_2$	$C_{30}H_{21}INO_3ReS_2$	$C_{38}H_{28}ClNO_3ReS_2$	$C_{26}H_{29}BrNO_3ReS_2$	$C_{31}H_{21}F_3NO_6ReS_3$
Formula weight	826.18	820.7	829.36	733.77	842.9
Temperature	115(2) K	100 K	100 K	120(2) K	115(2) K
Wavelength	0.71073 Å	0.71073	0.71073	0.71073 Å	0.71073 Å
Crystal system	monoclinic	triclinic	orthorhombic	monoclinic	monoclinic
Space group	P21/n	P-1	Pna21	P21/c	P21/c
Unit cell dimensions	a = 18.0038(5) Å, b = 9.5728(3) Å, c = 18.2867(6) Å, α = 90° β = 95.357(2)° γ = 90°	a = 7.3829(9) Å b = 21.931(3) Å c = 22.433(3) Å α = 61.691(2)° β = 88.620(2)° γ = 88.971(2) °	a = 23.3652(8) Å b = 21.7884(7) Å c = 6.1889(2) Å α = 90° β = 90° γ = 90°	a = 9.6675(2) Å b = 23.3392(4) Å c = 12.9169(2) Å α = 90° β = 111.1467(9)° γ = 90°	a = 11.9898(3) Å b = 14.9435(4) Å c = 22.7467(5) Å α = 90° β = 110.2660(10)° γ = 90°
Volume	3137.89(17) $Å^3$	3196.7(7) $Å^3$	3150.71(18) $Å^3$	2718.20(8) $Å^3$	1206.3(4) $Å^3$
Z	4	4	4	4	2
Density (calculated)	1.749 g/cm^3	1.705 g/cm^3	1.748 g/cm^3	1.793 g/cm^3	1.686 g/cm^3
Absorption coefficient	4.296 mm^{-1}	4.926 mm^{-1}	4.115 mm^{-1}	6.121 mm^{-1}	3.608 mm^{-1}
F(000)	1616	1568	1632	1432	1900
Crystal size (mm^3)	0.15 x 0.07 x 0.04	0.21 x 0.10 x 0.04	1.42 x 0.20x 0.04	0.2 x 0.1 x 0.1	0.15 x 0.15 x 0.10
Theta range for data collection	1.52 to 27.48	2.14 to 28.00°	2.56 to 36.60°	1.75 to 27.49°	1.91 to 27.48°
Index ranges	-22≤h≤231, -11≤k≤12, -23≤l≤23	-9≤h≤9 -28≤k≤28 -29≤l≤26	-37≤h<=37 -35≤k≤35 -9≤l≤9	-12≤h≤12 -28≤k≤30 -16≤l≤16	-13≤h≤15 -19≤k≤19 -29≤l≤27
Reflections collected	24635	55879	9884	11126	27486
Independent reflections	7192[R(int)=0.0723]	15405[R(int)=0.0552]	11854 [R(int)= 0.030]	6195[R(int)=0.0326]	8745[R(int)=0.0750]
Refinement method	Full-matrix least-squares on F^2	Full-matrix least-squares on F^2	Full-matrix least-squares on F^2	Full-matrix least-squares on F^2	Full-matrix least-squares on F^2
Data / restraints / parameters	7192/0/381	15405/0/685	13827/1/420	6195/0/311	8745 / 0 / 473
Goodness-of-fit on F^2	1.103	1.041	1.069	1.056	1.071
Final R indices [I>2sigma(I)]	R1 = 0.0465, wR2 = 0.0844	R1 = 0.0575 wR2 = 0.1385	R1 = 0.03004 wR2 = 0.0532	R1 = 0.0312 wR2 = 0.0653	R1 = 0.0533, wR2 = 0.1124
R indices (all data)	R1 = 0.0644, wR2 = 0.0920	R1 = 0.0722 wR2 = 0.1473	R1 = 0.0419 wR2 = 0.0577	R1 = 0.0442, wR2 = 0.0694	R1 = 0.0730, wR2 = 0.1230
Largest diff. peak and hole	1.084 and –1.214 $e.Å^{-3}$	9.48 and -2.15 $e.Å^{-3}$	1.49 and -2.12 $e.Å^{-3}$	0.817 and -1.372 $e.Å^{-3}$	1.976 and -0.877 $e.Å^{-3}$

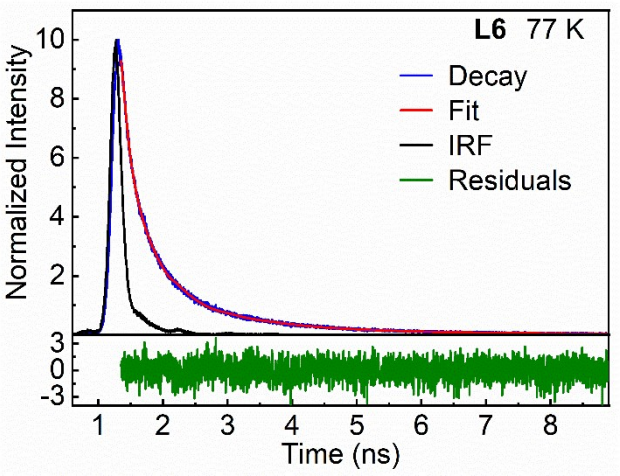

Figure S20. Emission decay (blue), residuals (green), IRF (black) and best fit (red) of **L6** in 2-MeTHF at 77 K. Multi-exponential analysis yields τ = 0.11ns (31), 0.44ns (36%), 1.68ns (33), χ^2 = 1.044.

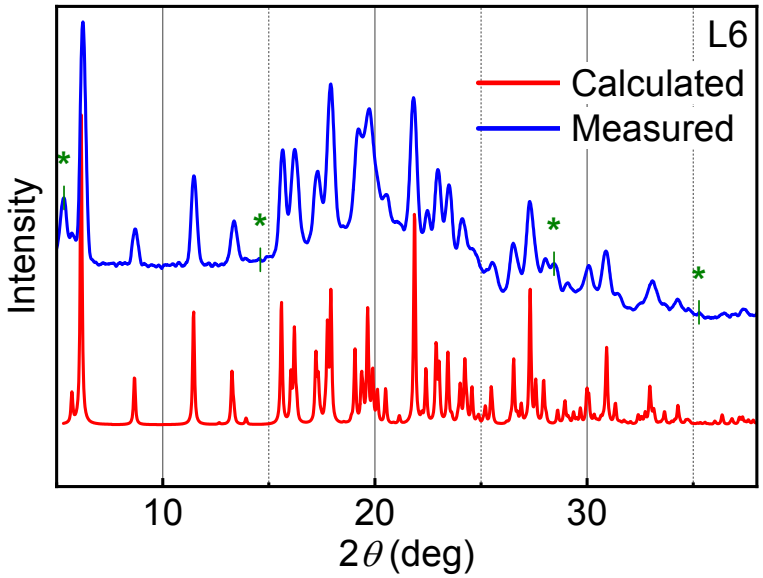

Figure S21. Powder X-ray diffraction patterns for **L6** calculated (red) and experimental (blue) at 115 K. 2θ = [5° – 38°] (* = notable peaks difference).

Ligand L6 (singlet state)

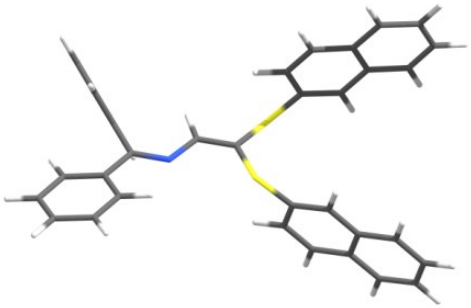

Figure S22. Optimized geometry for **L6** applying a THF solvent field.

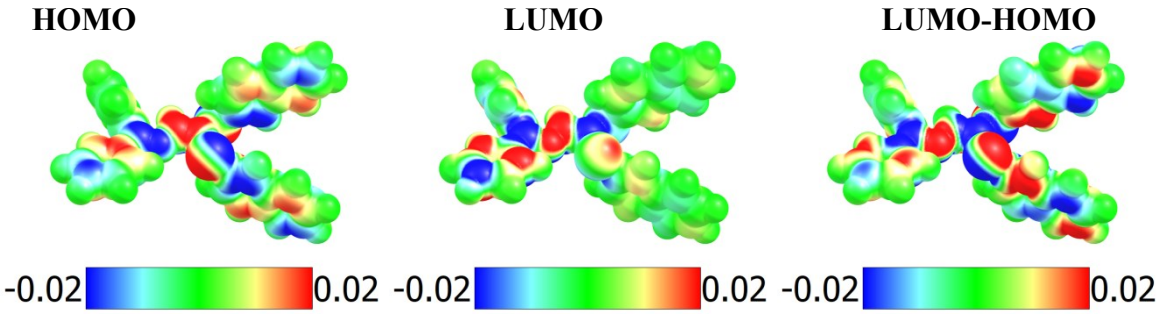

Figure S23. Electron-density map of the HOMO and LUMO; Electron-density difference (LUMO-HOMO)

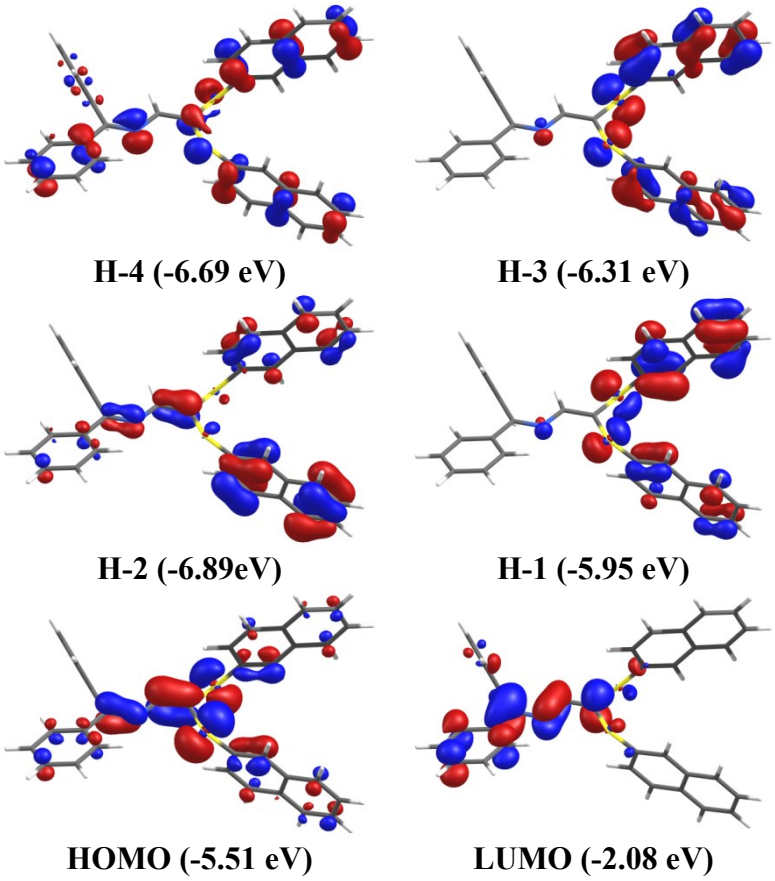

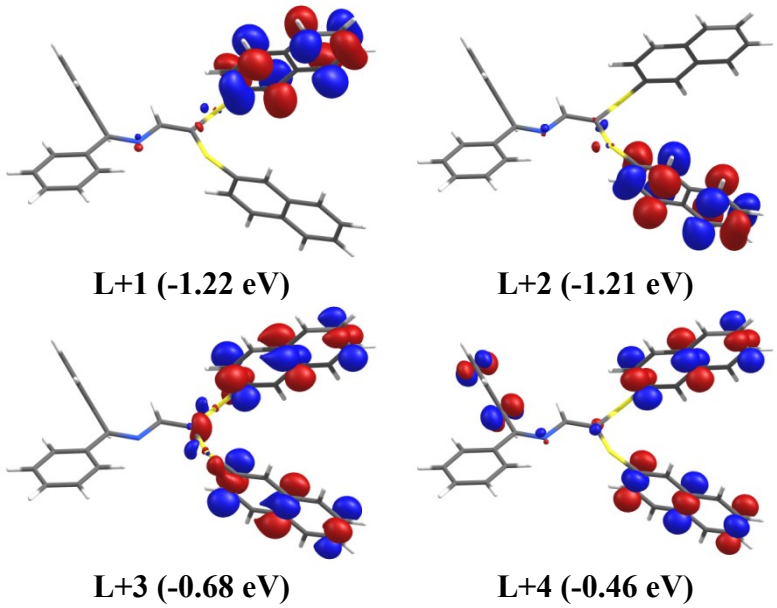

Figure S24. Representations of the frontier MOs for **L6** (optimized) applying a THF solvent field.

Table S8. Relative atomic contributions (%) of the various fragments to the frontier MOs of **L6**. [a]

Fragments	H-4	H-3	H-2	H-1	HOMO	LUMO	L+1	L+2	L+3	L+4
Phenyls	19%	1%	8%	1%	9%	33%	2%	2%	0%	18%
Core (C=N-(H)C=C)	11%	4%	13%	11%	23%	**44%**	14%	5%	23%	11%
Thionaphthyls	**70%**	**95%**	**79%**	**89%**	**68%**	23%	**85%**	**94%**	**76%**	**71%**

[a]H = HOMO, L = LUMO; the values in bold represent the largest contributions.

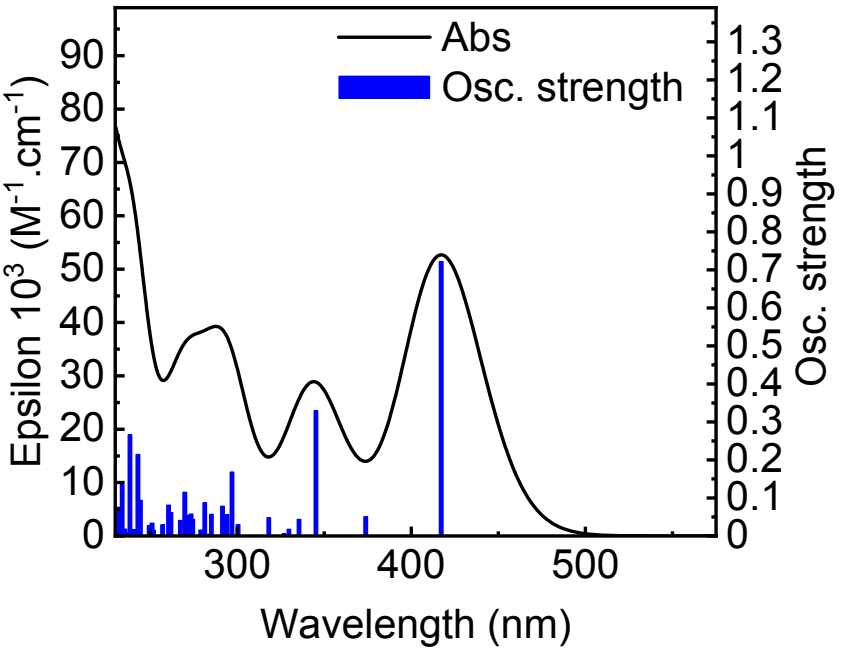

Figure S25. Simulated absorption spectrum for **L6** by TDDFT computations. Bar graph reporting the calculated oscillator strength and calculated position of the 100st electronic transitions calculated by TDDFT for **L6** (bar graph; f = computed oscillator strength).

Table S9. Calculated position, oscillator strength (f) and major contributions (%) of the first 100 singlet-singlet electronic transitions for **L6**.

No.	λ (nm)	f	Major contributions (%)
1	417.2	0.7222	HOMO→LUMO (97%)
2	373.8	0.0507	H-1→LUMO (86%)
3	345.2	0.3298	H-2→LUMO (95%)
4	335.6	0.0439	H-3→LUMO (70%), H-1→LUMO (11%)
5	329.7	0.0178	HOMO→L+1 (23%), HOMO→L+2 (65%)
6	326.9	0.006	HOMO→L+1 (65%), HOMO→L+2 (25%)
7	318.2	0.0483	H-9→LUMO (19%), H-6→LUMO (31%), H-4→LUMO (22%), H-3→LUMO (12%)
8	300.5	0.0301	H-1→L+2 (10%), HOMO→L+3 (51%)
9	297.0	0.1684	H-9→LUMO (12%), H-4→LUMO (54%)
10	294.2	0.0565	H-1→L+1 (31%), H-1→L+2 (24%)
11	293.6	0.0226	H-5→LUMO (81%)
12	292.2	0.0427	H-1→L+1 (24%), H-1→L+2 (38%), HOMO→L+3 (27%)
13	291.6	0.0786	H-7→LUMO (56%), H-6→LUMO (25%)
14	285.2	0.0569	H-8→LUMO (11%), H-1→L+1 (15%)
15	283.6	0.0049	H-8→LUMO (25%), H-7→LUMO (19%), H-6→LUMO (13%)
16	281.4	0.0869	H-2→L+1 (47%), H-2→L+2 (36%)
17	279.1	0.0157	H-2→L+1 (33%), H-2→L+2 (42%)
18	274.5	0.0438	H-3→L+1 (24%), H-3→L+2 (16%), HOMO→L+4 (13%)
19	273.5	0.0578	H-3→L+2 (12%), HOMO→L+4 (20%), HOMO→L+5 (46%)
20	271.7	0.0548	H-9→LUMO (12%), H-8→LUMO (13%), HOMO→L+4 (25%), HOMO→L+5 (18%)
21	269.9	0.1153	H-9→LUMO (14%), H-8→LUMO (29%), HOMO→L+5 (15%), HOMO→L+6 (10%)
22	267.4	0.0409	H-8→LUMO (12%), HOMO→L+6 (73%)
23	262.0	0.0612	H-10→LUMO (37%), H-3→L+1 (21%)
24	260.6	0.0815	H-4→L+2 (10%), H-3→L+1 (10%), H-3→L+2 (24%), H-1→L+3 (32%)
25	257.1	0.0291	H-10→LUMO (44%), H-4→L+2 (12%), H-2→L+3 (11%)
26	252.1	0.015	H-4→L+1 (23%), H-3→L+3 (10%), H-1→L+3 (14%), H-1→L+4 (17%)
27	251.2	0.0339	HOMO→L+7 (79%)
28	249.5	0.0265	H-2→L+3 (34%), H-1→L+4 (27%)
29	244.4	0.0937	H-11→LUMO (26%), H-4→L+2 (10%), HOMO→L+8 (32%)
30	243.0	0.2149	H-4→L+1 (13%), H-4→L+2 (18%), H-1→L+4 (17%), HOMO→L+8 (12%)
31	241.5	0.0065	H-1→L+5 (79%)
32	240.8	0.0159	H-3→L+3 (38%), H-2→L+4 (39%)
33	238.5	0.2666	H-6→L+2 (15%), H-4→L+1 (18%), H-4→L+2 (12%), H-3→L+3 (18%)
34	238.1	0.0083	H-1→L+6 (86%)
35	235.6	0.0181	H-2→L+4 (11%), H-2→L+5 (76%)
36	234.0	0.1344	H-11→LUMO (24%), H-2→L+6 (17%), HOMO→L+8 (14%)
37	233.6	0.0085	H-3→L+4 (26%), HOMO→L+9 (18%)
38	232.8	0.0307	H-2→L+6 (56%)
39	231.6	0.0756	H-11→LUMO (18%), HOMO→L+8 (19%), HOMO→L+9 (25%)
40	230.2	0.0667	H-6→L+1 (66%), H-3→L+4 (12%)
41	228.7	2E-4	H-5→L+1 (22%), H-5→L+2 (58%)
42	228.1	0.0068	H-12→LUMO (89%)
43	227.7	0.0027	H-5→L+1 (59%), H-5→L+2 (33%)

44	226.9	0.1845	H-6→L+2 (31%)
45	226.7	0.0694	H-13→LUMO (55%), H-1→L+7 (17%)
46	226.3	0.0278	H-13→LUMO (12%), H-7→L+1 (13%), H-6→L+2 (12%), H-1→L+7 (21%)
47	226.2	0.0118	H-7→L+1 (10%), H-1→L+7 (26%)
48	225.6	0.0146	H-3→L+4 (10%), H-3→L+5 (77%)
49	225.4	0.0101	H-7→L+1 (65%)
50	224.9	0.0774	H-7→L+2 (62%), H-4→L+3 (11%)
51	223.1	0.049	H-10→L+2 (14%), H-9→L+2 (24%), H-7→L+2 (10%), H-4→L+3 (23%)
52	222.5	0.0308	H-9→L+2 (13%), H-3→L+6 (66%)
53	222.3	0.0596	H-9→L+2 (46%), H-4→L+3 (10%), H-3→L+6 (16%)
54	221.0	0.0704	H-10→L+1 (13%), H-9→L+1 (21%), H-8→L+1 (35%), H-2→L+7 (12%)
55	220.7	0.0333	H-2→L+7 (38%)
56	220.6	0.0245	HOMO→L+10 (48%)
57	220.2	0.0346	H-2→L+7 (21%), H-1→L+7 (10%), H-1→L+8 (19%), HOMO→L+11 (12%)
58	219.8	0.0448	H-9→L+1 (22%), H-8→L+1 (49%)
59	218.8	0.0013	H-10→L+2 (21%), H-8→L+2 (57%)
60	217.9	0.0032	H-1→L+8 (38%), HOMO→L+11 (32%)
61	217.0	0.4451	H-10→L+1 (17%), H-10→L+2 (13%), H-4→L+4 (17%), HOMO→L+10 (10%)
62	215.4	0.0938	H-10→L+1 (10%), H-10→L+2 (10%), H-4→L+3 (13%), H-4→L+5 (18%)
63	215.2	0.0255	H-10→L+2 (12%), H-4→L+5 (29%)
64	212.9	0.0197	H-4→L+4 (25%), H-3→L+7 (34%)
65	212.7	0.0049	H-4→L+4 (12%), H-4→L+5 (13%), H-3→L+7 (17%), H-2→L+8 (18%), H-1→L+9 (16%)
66	212.0	0.2022	H-4→L+4 (11%), H-3→L+7 (13%), H-2→L+8 (45%)
67	211.2	0.0094	H-4→L+6 (49%)
68	210.2	0.2519	H-6→L+3 (46%)
69	209.7	0.2984	H-1→L+10 (13%), H-1→L+11 (14%)
70	209.1	0.0217	H-5→L+5 (26%)
71	208.8	0.1758	H-6→L+3 (18%)
72	208.6	0.0793	H-11→L+2 (16%)
73	208.1	0.0449	H-9→L+5 (23%), H-6→L+4 (10%), H-6→L+5 (19%), H-4→L+5 (11%)
74	207.8	0.0014	H-5→L+3 (94%)
75	205.9	0.0065	H-7→L+3 (79%)
76	205.6	0.0013	H-7→L+3 (11%), H-3→L+8 (57%)
77	205.1	0.0221	H-9→L+3 (14%), H-9→L+6 (10%), H-6→L+6 (18%), H-5→L+6 (16%)
78	204.7	0.0319	H-9→L+3 (19%)
79	204.2	0.0098	H-11→L+1 (12%), H-5→L+6 (18%)
80	203.9	0.0104	H-5→L+6 (18%), H-1→L+11 (10%)
81	203.4	0.0053	H-9→L+3 (17%), H-4→L+7 (21%)
82	203.2	0.0087	H-11→L+1 (23%), H-9→L+3 (18%), H-1→L+10 (10%)
83	202.4	0.0155	H-11→L+1 (14%), H-2→L+9 (14%)
84	202.1	0.0238	H-14→LUMO (11%), H-12→L+2 (10%), H-11→L+2 (28%)
85	202.0	0.006	H-14→LUMO (16%), H-8→L+3 (12%), H-6→L+4 (15%), H-6→L+5 (12%)
86	201.7	0.0813	H-8→L+5 (10%), H-7→L+6 (14%), H-6→L+4 (11%)
87	201.1	0.0349	H-14→LUMO (11%), H-8→L+3 (15%), H-5→L+4 (12%)
88	200.9	0.016	H-8→L+3 (47%)
89	200.4	0.0125	H-14→LUMO (11%), H-6→L+7 (11%), H-5→L+4 (21%)

90	199.9	0.0092	H-2→L+9 (17%), H-2→L+11 (28%)
91	198.9	0.0061	H-10→L+3 (38%)
92	198.7	0.0216	H-5→L+4 (21%), H-5→L+5 (15%)
93	198.5	0.0103	H-9→L+5 (14%), H-7→L+4 (35%), H-6→L+5 (13%)
94	198.1	0.0147	H-7→L+4 (20%), H-7→L+5 (10%), H-7→L+6 (25%)
95	197.8	0.0145	H-6→L+8 (10%)
96	197.3	0.123	H-3→L+9 (22%)
97	196.8	0.0394	H-13→L+1 (40%), H-12→L+1 (28%)
98	196.4	0.0268	H-13→L+2 (24%), H-12→L+2 (16%), H-9→L+4 (11%), H-4→L+8 (11%)
99	196.3	9E-4	H-13→L+2 (23%), H-12→L+2 (15%), H-9→L+4 (11%), HOMO→L+12 (11%)
100	195.8	0.002	H-20→LUMO (21%), H-4→L+8 (11%), HOMO→L+12 (12%)

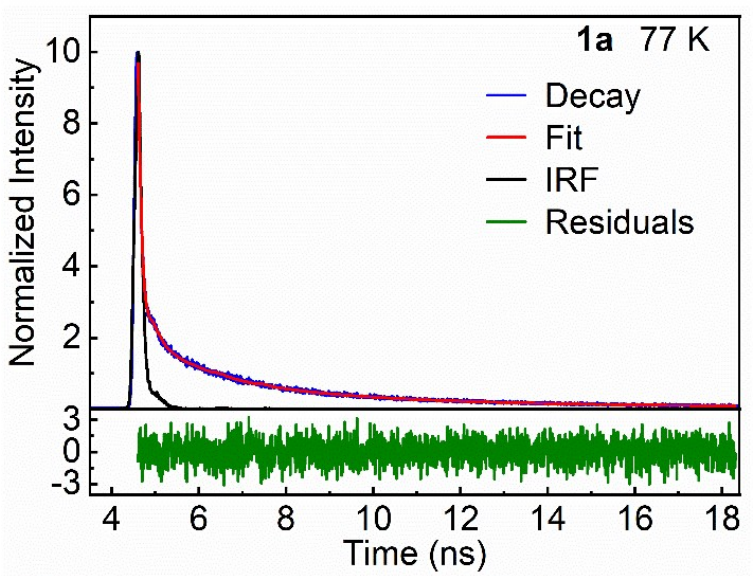

Figure S26. Emission decay (blue), residuals (green), IRF (black) and best fit (red) of **1a** in 2-MeTHF at 77 K. Multi-exponential analysis yields τ = 1.70ns (24%), 5.34ns (38%), χ^2 = 1.051. Note that the sum of the f % values is not equal to 100% because the remainder is close to the lamp profile (*i.e.* approaching or smaller than 100 ps) and cannot be extracted accurately.

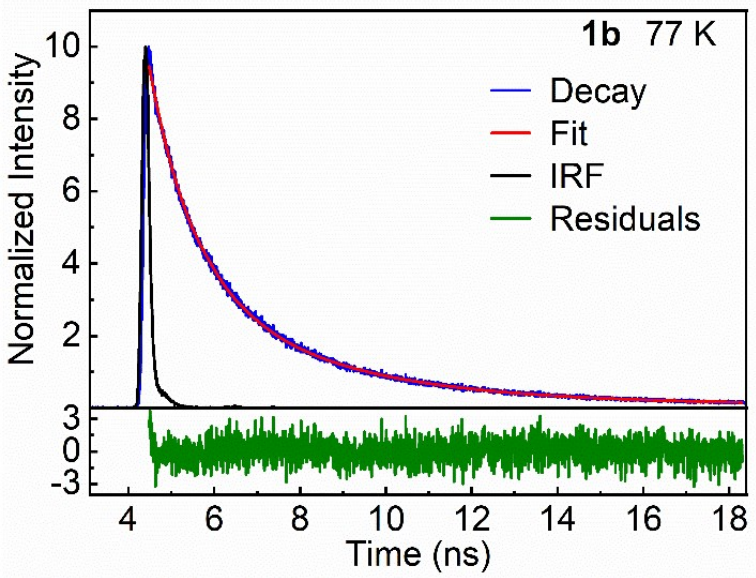

Figure S27. Emission decay (blue), residuals (green), IRF (black) and best fit (red) of **1b** in 2-MeTHF at 77 K. Multi-exponential analysis yields τ = 1.38ns (41%), 4.60ns (51%), χ^2 = 1.003. Note that the sum of the f % values is not equal to 100% because the remainder is close to the lamp profile (*i.e.* approaching or smaller than 100 ps) and cannot be extracted accurately.

Complex 1c (photophysical properties)

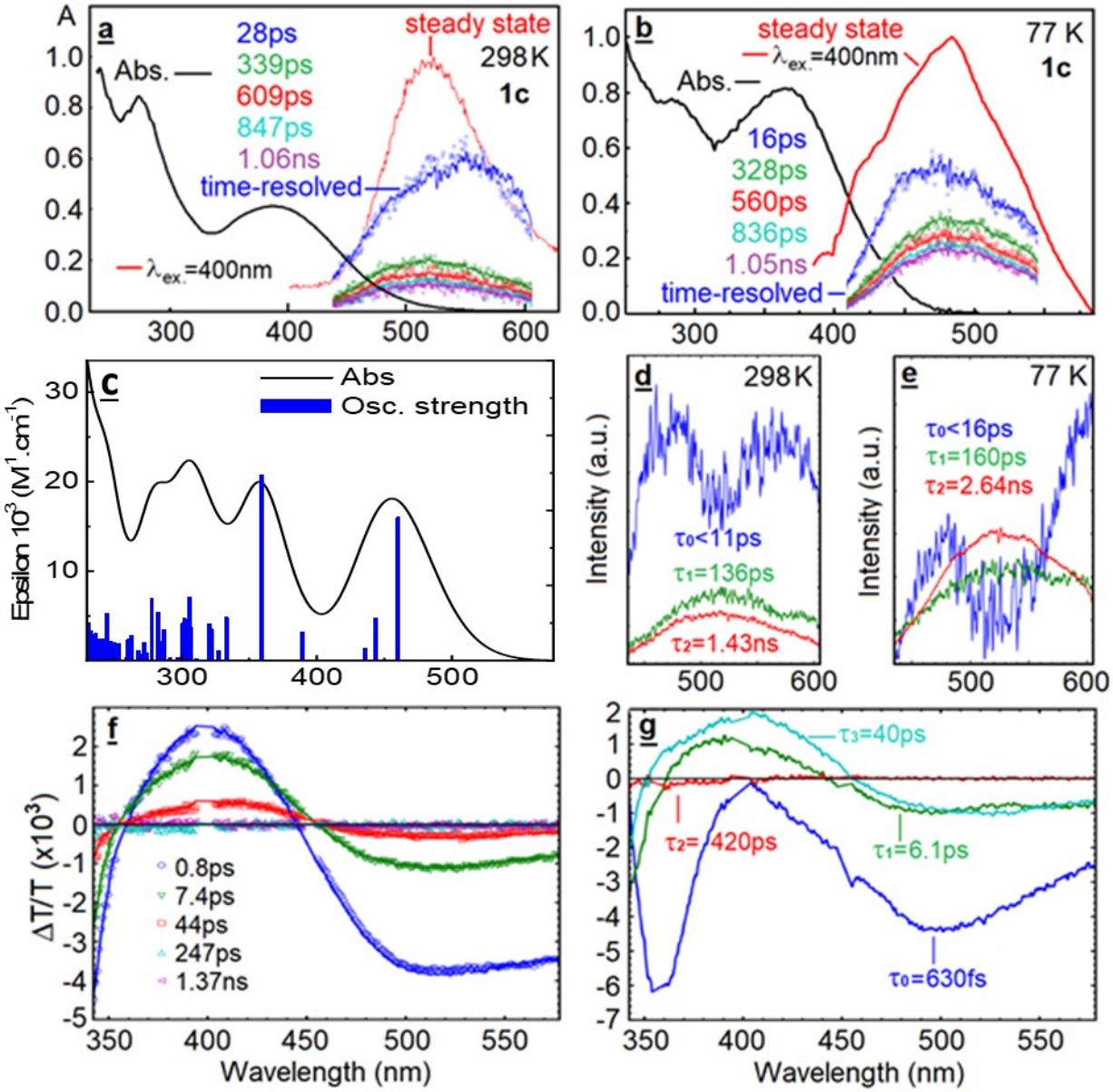

Figure S28. **a** and **b**: Steady state absorption (black) and emission (red) spectra of **1c** in 2-MeTHF at 298 and 77 K, respectively. The time-resolved emission spectra of **1c** in 2MeTHF are shown in different colors. **c**: simulated absorption spectrum of **1c** (TDDFT, applying a THF solvent field); the bar graph (blue) reports the calculated oscillator strengths (f) and positions of the 100st electronic transitions. An arbitrary thickness of 3000 cm^{-1} is assigned to each bar for the spectra simulation. **d** (298 K) and **e** (77 K): decay associated spectra of **1c** in 2-MeTHF (Streak camera; λ_{exc} = 397 nm, note that the spectra are not corrected for the PMT response and the spectra of short-lived species (*i.e.* τ_F < IRF, blue traces) are severely distorted. **f**: Time evolution of the fs-TAS of **1c** in 2MeTHF at 298 K (λ_{exc} = 397 nm). The bleach and transient signals are positive and negative signals, respectively. The delay times are indicated. **g**: Decay associated spectra of the fs-TAS of **1c**. Note that the positive and negative responses represent the bleached and transient signals, respectively.

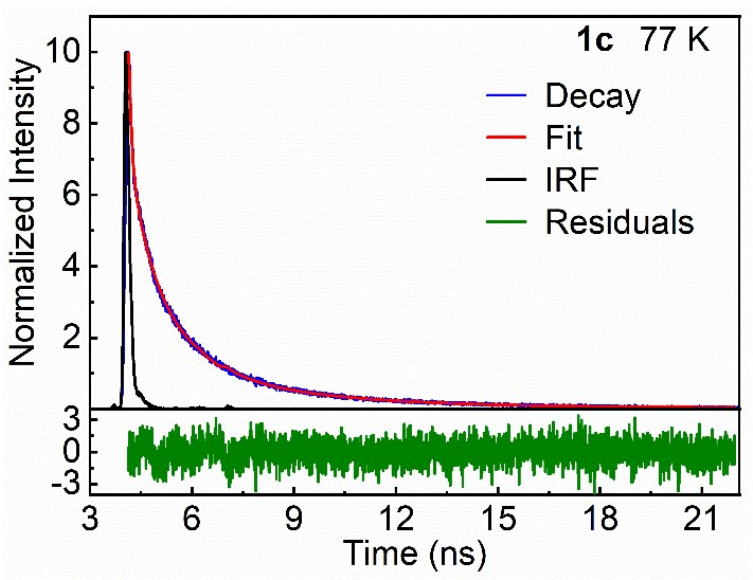

Figure S29. Emission decay (blue), residuals (green), IRF (black) and best fit (red) of **1c** in 2-MeTHF at 77 K. Multi-exponential analysis yields τ = 1.15ns (42%), 4.09ns (40%), χ^2 = 1.038. Note that the sum of the f % values is not equal to 100% because the remainder is close to the lamp profile (*i.e.* approaching or smaller than 100 ps) and cannot be extracted accurately.

Complex 1d (photophysical properties)

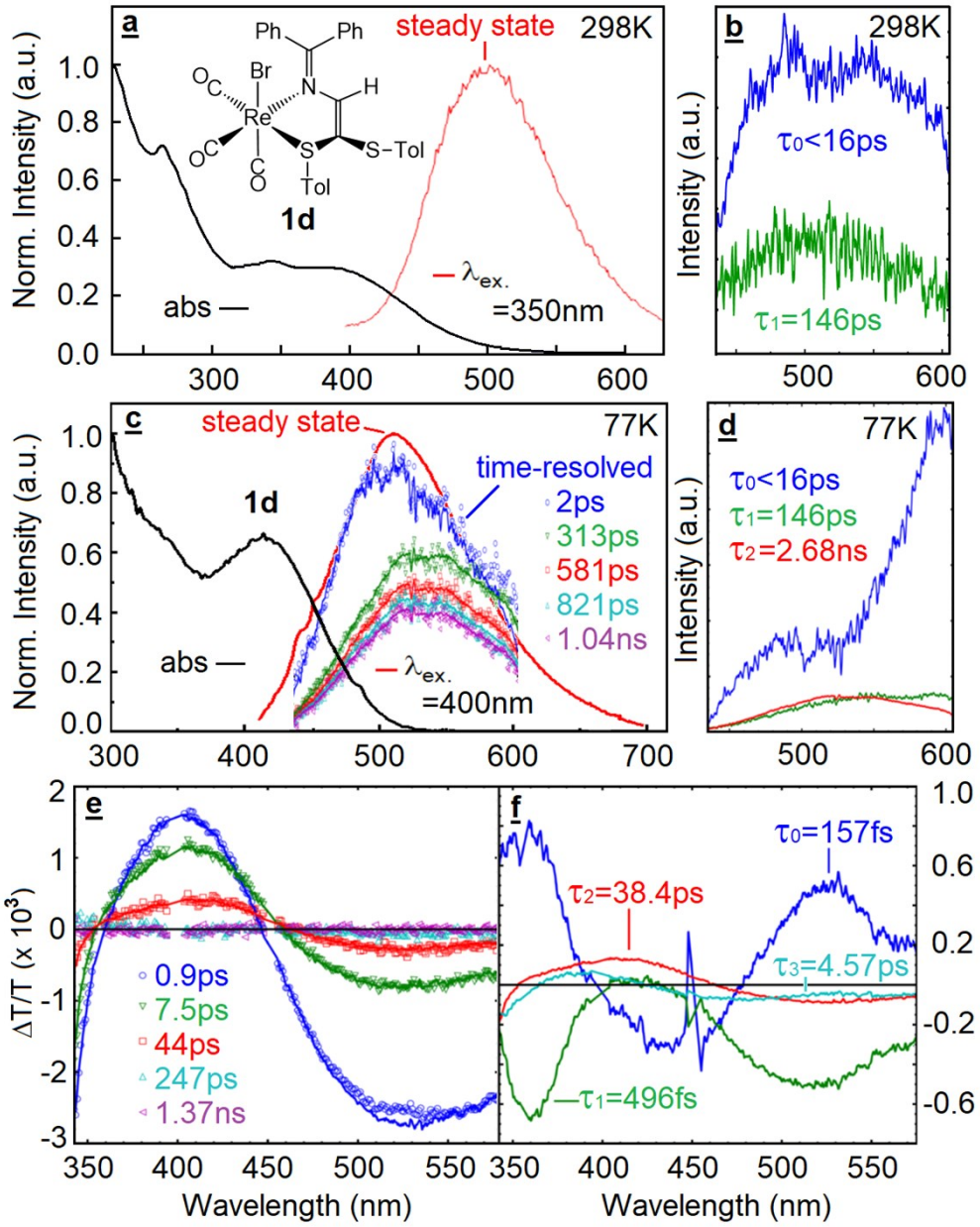

Figure S30. **a** and **c**: Steady state absorption (black) and emission (red) spectra of **1d** in 2-MeTHF at 298 and 77 K, respectively. The time-resolved emission spectra of **1d** in 2-MeTHF are shown in different colors. **b** (298 K) and **d** (77 K): decay associated spectra of **1d** in 2-MeTHF (Streak camera; λ_{exc} = 397 nm, note that the spectra are not corrected for the PMT response and the spectra of short-lived species (i.e. τ_F < IRF, blue traces) are severely distorted. **e**: Time evolution of the fs-TAS of **1d** in 2-MeTHF at 298 K (λ_{exc} = 397 nm). The bleach and transient signals are positive and negative signals, respectively. The delay times are indicated. **f**: Decay associated spectra of the fs-TAS of **1d**. Note that no TDDFT computations was performed for **1d** since no X-ray structure was available. Note that the positive and negative responses represent the bleached and transient signals, respectively.

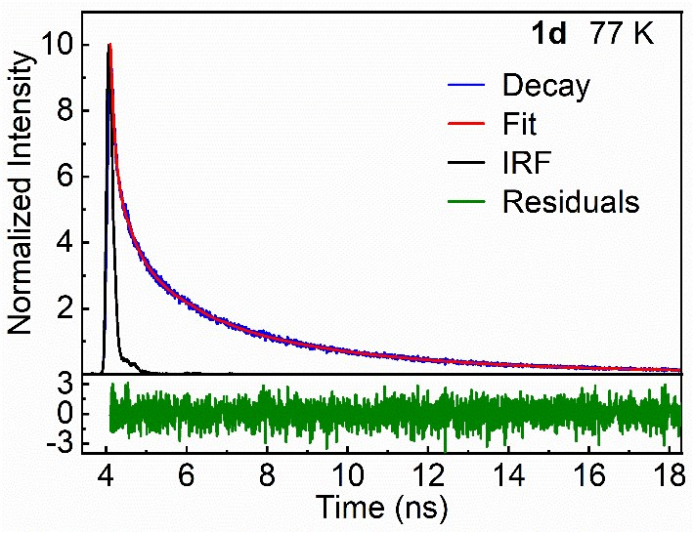

Figure S31. Emission decay (blue), residuals (green), IRF (black) and best fit (red) of **1d** in 2-MeTHF at 77 K. Multi-exponential analysis yields τ = 1.29ns (22%), 4.70ns (61%), χ^2 = 1.061. Note that the sum of the f % values is not equal to 100% because the remainder is close to the lamp profile (*i.e.* approaching or smaller than 100 ps) and cannot be extracted accurately.

Complex 1e (photophysical properties)

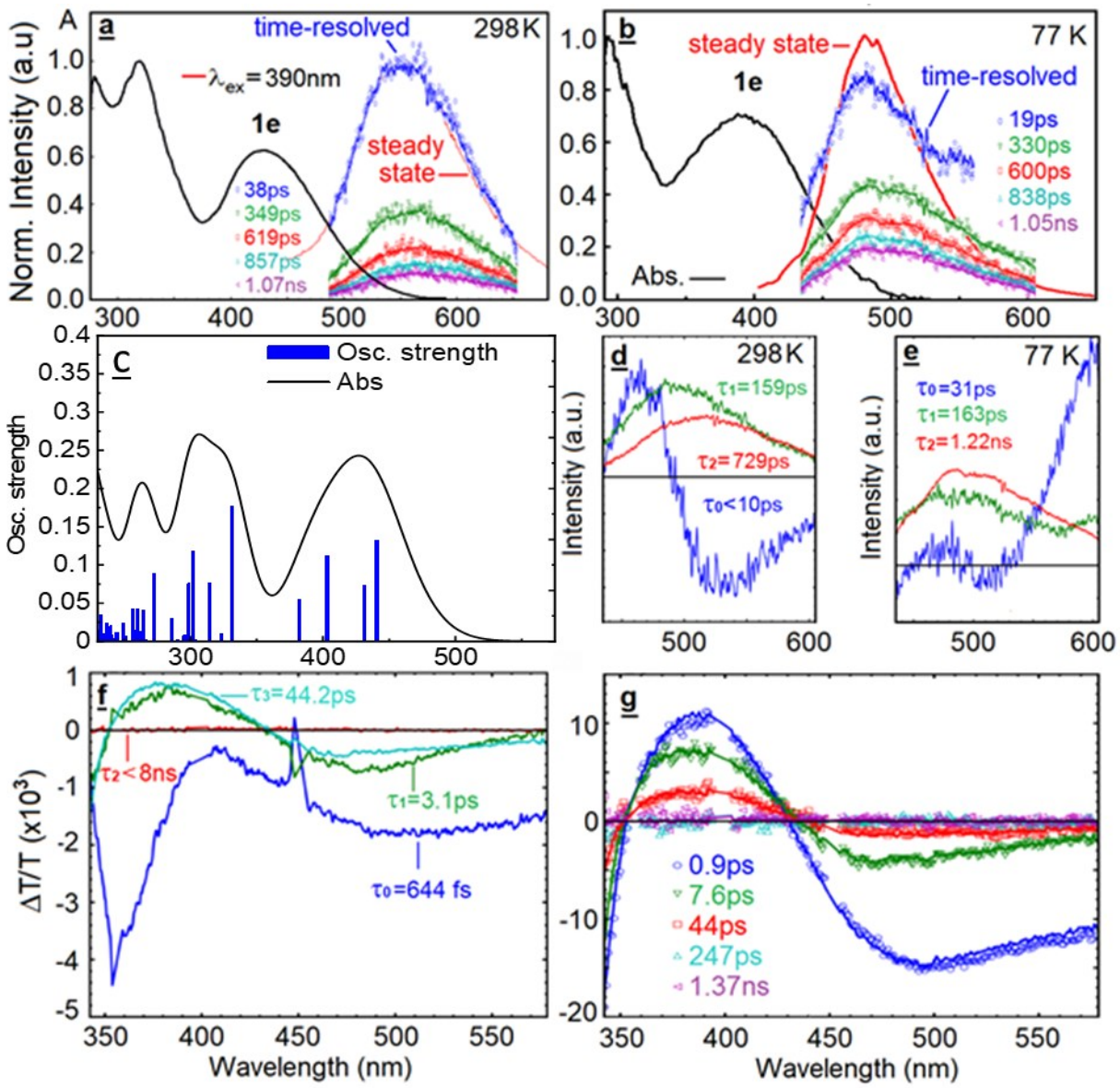

Figure S32. **a** and **b**: Steady state absorption (black) and emission (red) spectra of **1e** in 2-MeTHF at 298 and 77 K, respectively. The time-resolved emission spectra of **1e** in 2-MeTHF are shown in different colors. **c**: simulated absorption spectrum of **1e** (TDDFT, applying a THF solvent field); the bar graph (blue) reports the calculated oscillator strengths (f) and positions of the 100st electronic transitions. An arbitrary thickness of 3000 cm^{-1} is assigned to each bar for the spectra simulation. **d** (298 K) and **e** (77 K): decay associated spectra of **1e** in 2-MeTHF (Streak camera; λ_{exc} = 397 nm, note that the spectra are not corrected for the PMT response and the spectra of short-lived species (*i.e.* τ_F < IRF or near the IRF, blue traces) are severely distorted. **f**: Time evolution of the fs-TAS of **1e** in 2-MeTHF at 298 K (λ_{exc} = 397 nm). The bleach and transient signals are positive and negative signals, respectively. The delay times are indicated. **g**: Decay associated spectra of the fs-TAS of **1e**. Note that the positive and negative responses represent the bleached and transient signals, respectively.

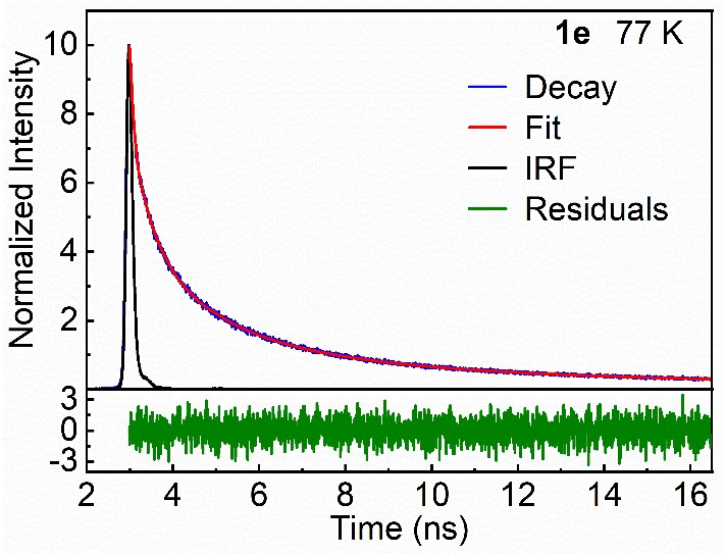

Figure S33. Emission decay (blue), residuals (green), IRF (black) and best fit (red) of **1e** in 2-MeTHF at 77 K. Multi-exponential analysis yields τ = 1.85ns (42%), 6.94ns (52%), χ^2 = 1.029. Note that the sum of the f % values is not equal to 100% because the remainder is close to the lamp profile (*i.e.* approaching or smaller than 100 ps) and cannot be extracted accurately.

Complex 1f (photophysical properties)

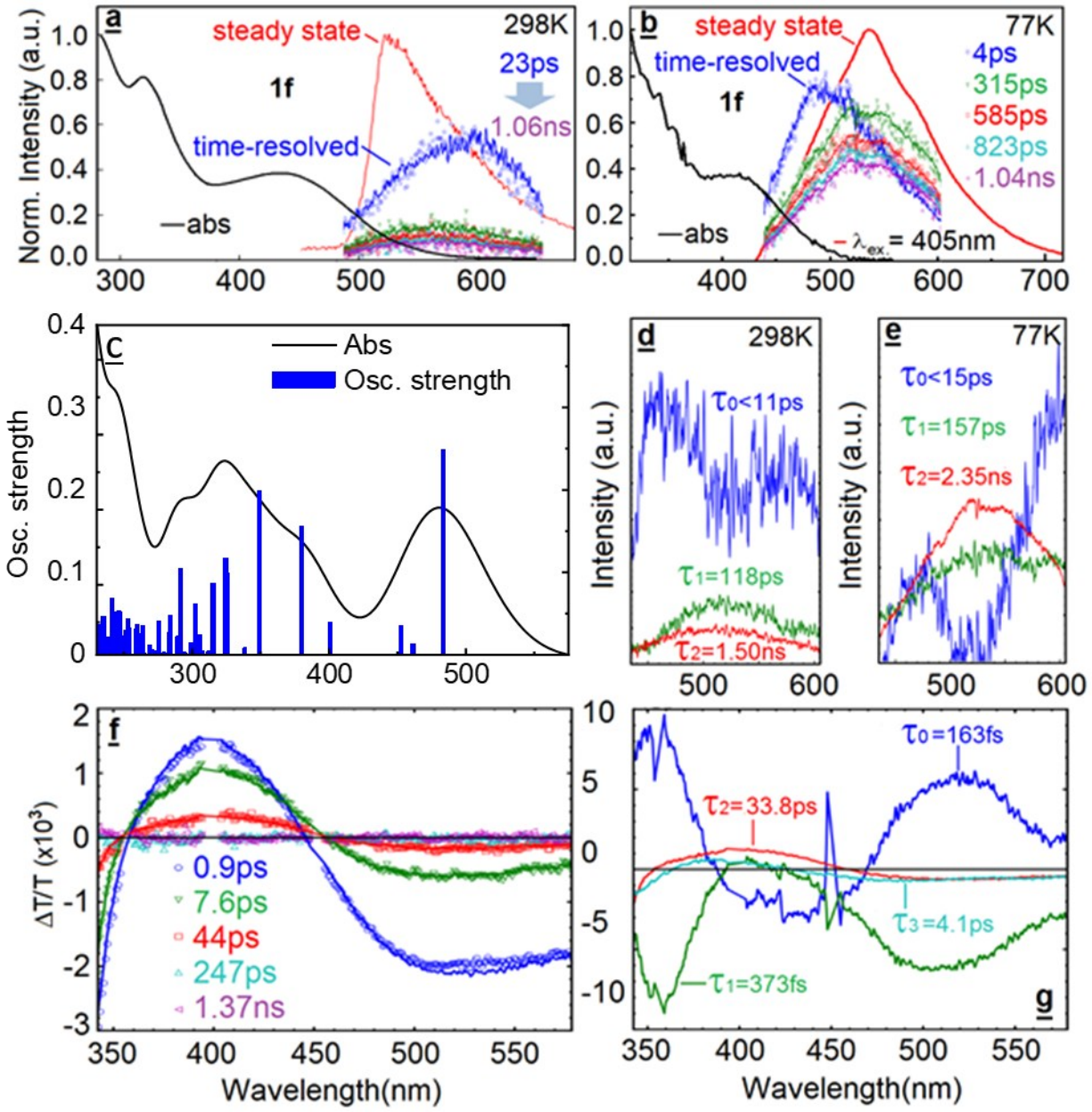

Figure S34. **a** and **b**: Steady state absorption (black) and emission (red) spectra of **1f** in 2-MeTHF at 298 and 77 K, respectively. The time-resolved emission spectra of **1f** in 2-MeTHF are shown in different colors. **c**: simulated absorption spectrum of **1f** (TDDFT, applying a THF solvent field); the bar graph (blue) reports the calculated oscillator strengths (f) and positions of the 100st electronic transitions. An arbitrary thickness of 3000 cm^{-1} is assigned to each bar for the spectra simulation. **d** (298 K) and **e** (77 K): decay associated spectra of **1f** in 2-MeTHF (Streak camera; λ_{exc} = 397 nm, note that the spectra are not corrected for the PMT response and the spectra of short-lived species (*i.e.* τ_F < IRF, blue traces) are severely distorted. **f**: Time evolution of the fs-TAS of **1f** in 2-MeTHF at 298 K (λ_{exc} = 397 nm). The bleach and transient signals are positive and negative signals, respectively. The delay times are indicated. **g**: Decay associated spectra of the fs-TAS of **1f**. Note that the positive and negative responses represent the bleached and transient signals, respectively.

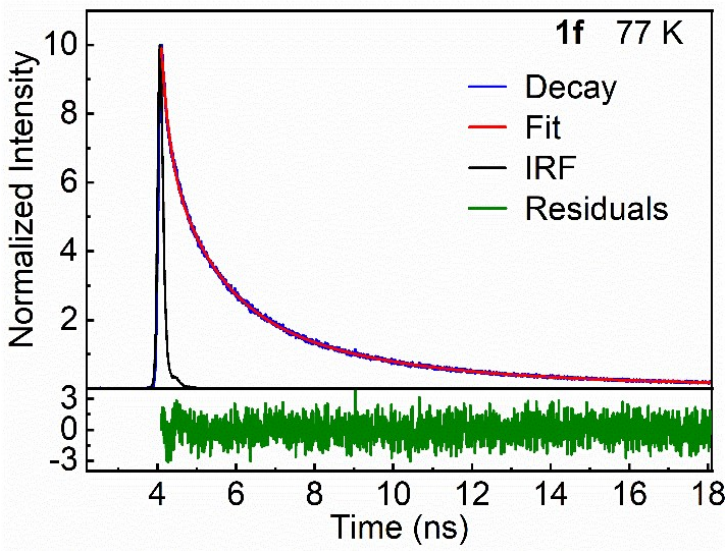

Figure S35. Emission decay (blue), residuals (green), IRF (black) and best fit (red) of **1f** in 2-MeTHF at 77 K. Multi-exponential analysis yields τ = 1.76ns (39%), 5.36ns (53%), χ^2 = 1.040. Note that the sum of the f % values is not equal to 100% because the remainder is close to the lamp profile (*i.e.* approaching or smaller than 100 ps) and cannot be extracted accurately.

Complex 1g (photophysical properties)

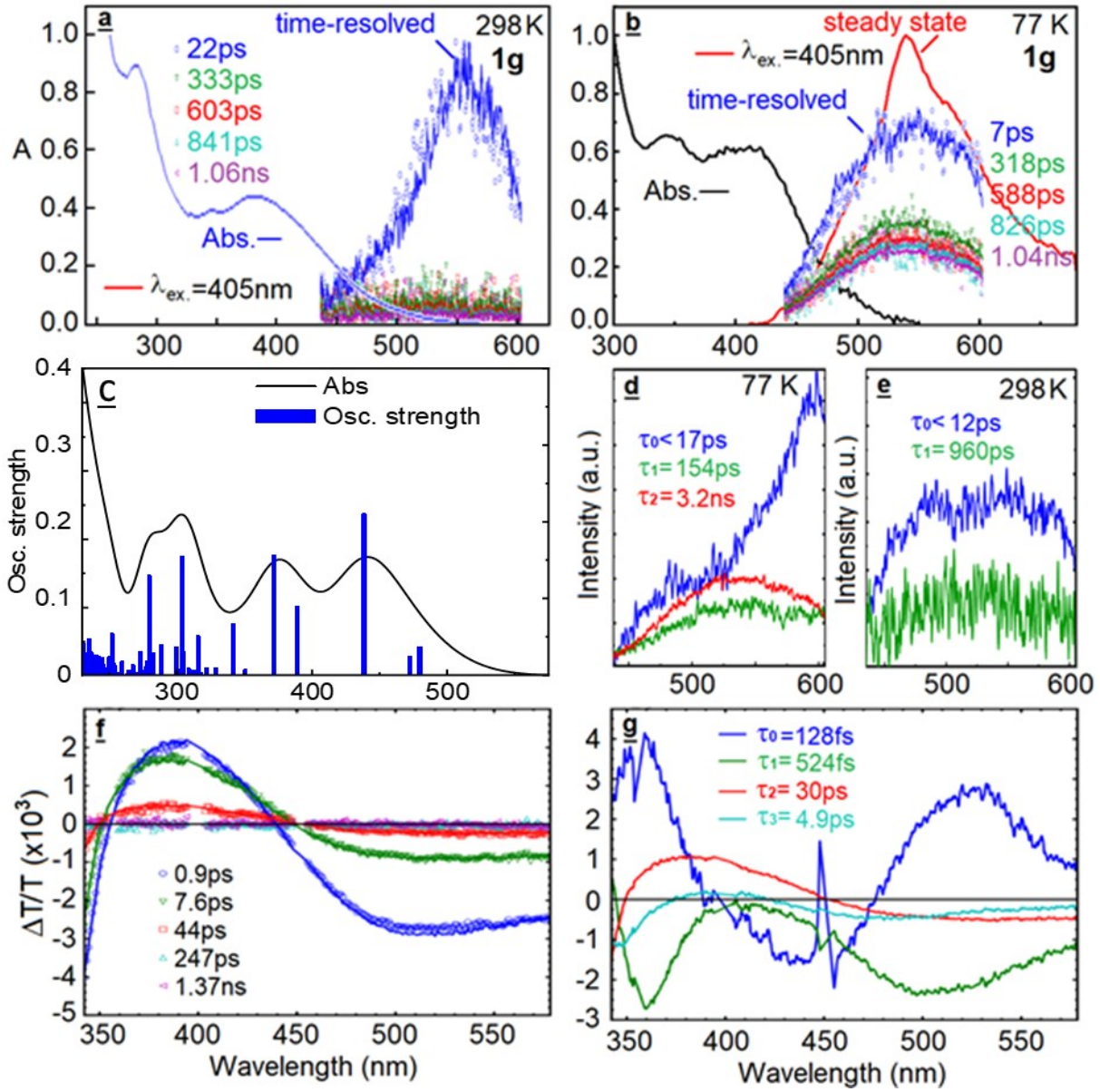

Figure S36. **a** and **b**: Steady state absorption (black) and emission (red) spectra of **1g** in 2-MeTHF at 298 and 77 K, respectively. The time-resolved emission spectra of **1g** in 2-MeTHF are shown in different colors. **c**: simulated absorption spectrum of **1g** (TDDFT, applying a THF solvent field); the bar graph (blue) reports the calculated oscillator strengths (f) and positions of the 100st electronic transitions. An arbitrary thickness of 3000 cm^{-1} is assigned to each bar for the spectra simulation. **d** (298 K) and **e** (77 K): decay associated spectra of **1g** in 2-MeTHF (Streak camera; λ_{exc} = 397 nm, note that the spectra are not corrected for the PMT response and the spectra of short-lived species (*i.e.* τ_F < IRF, blue traces) are severely distorted. **f**: Time evolution of the fs-TAS of **1g** in 2-MeTHF at 298 K (λ_{exc} = 397 nm). The bleach and transient signals are positive and negative signals, respectively. The delay times are indicated. **g**: Decay associated spectra of the fs-TAS of **1g**. Note that the positive and negative responses represent the bleached and transient signals, respectively.

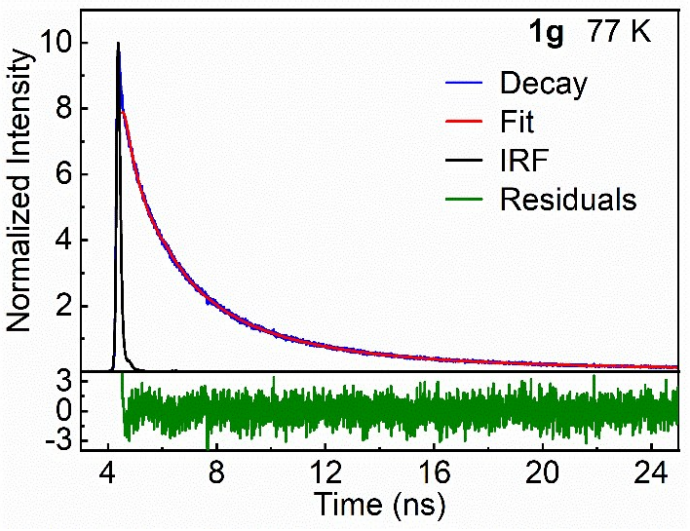

Figure S37. Emission decay (blue), residuals (green), IRF (black) and best fit (red) of **1g** in 2-MeTHF at 77 K. Multi-exponential analysis yields τ = 1.92ns (42%), 5.86ns (54%), χ^2 = 1.001. Note that the sum of the f % values is not equal to 100% because the remainder is close to the lamp profile (*i.e.* approaching or smaller than 100 ps) and cannot be extracted accurately.

Complex 1h (photophysical properties)

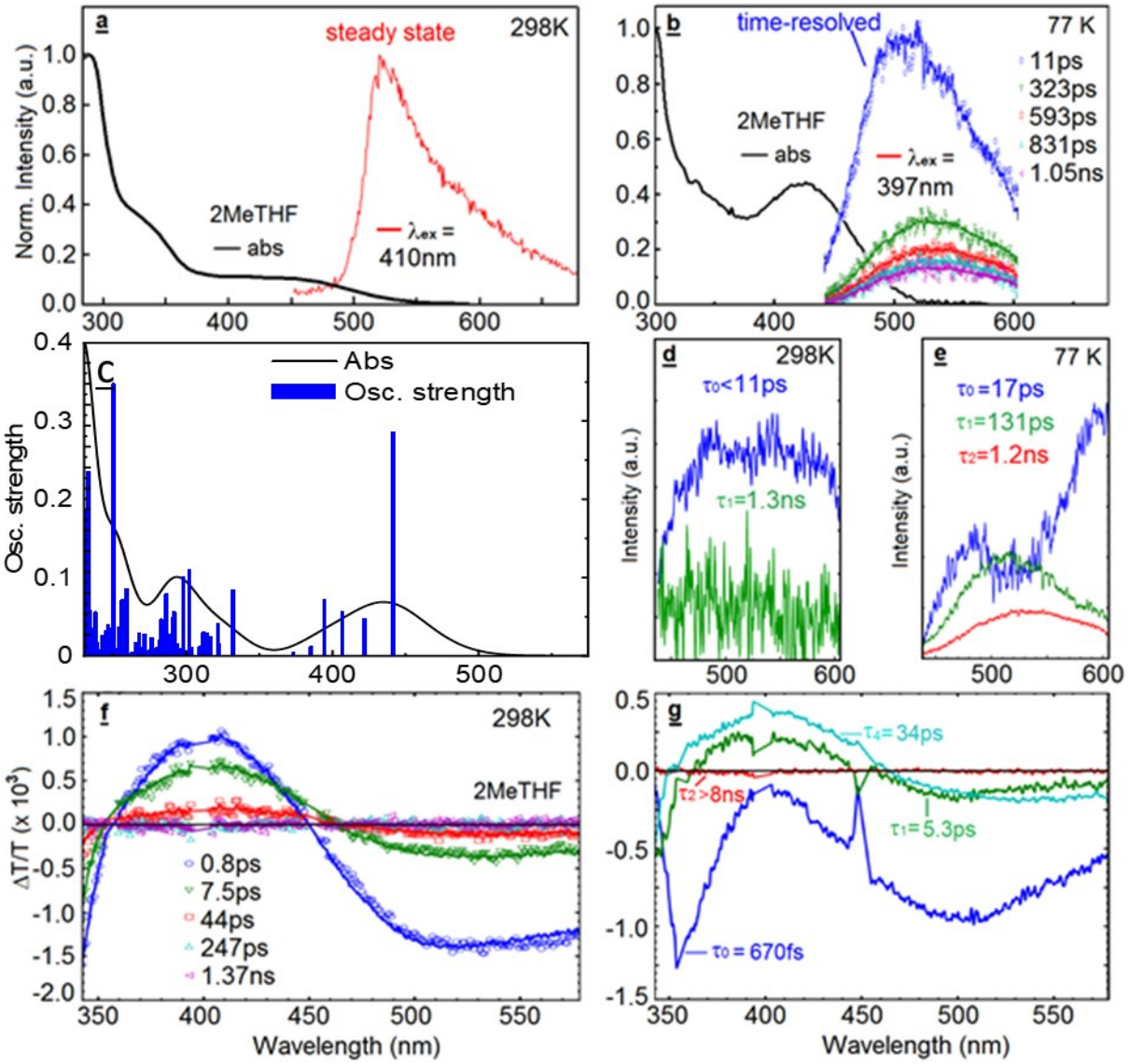

Figure S38. **a** and **b**: Steady state absorption (black) and emission (red) spectra of **1h** in 2-MeTHF at 298 and 77 K, respectively. The time-resolved emission spectra of **1h** in 2-MeTHF are shown in different colors. **c**: simulated absorption spectrum of **1h** (TDDFT, applying a THF solvent field); the bar graph (blue) reports the calculated oscillator strengths (f) and positions of the 100st electronic transitions. An arbitrary thickness of 3000 cm^{-1} is assigned to each bar for the spectra simulation. **d** (298 K) and **e** (77 K): decay associated spectra of **1h** in 2-MeTHF (Streak camera; λ_{exc} = 397 nm, note that the spectra are not corrected for the PMT response and the spectra of short-lived species (*i.e.* τ_F < IRF, blue traces) are severely distorted. **f**: Time evolution of the fs-TAS of **1h** in 2-MeTHF at 298 K (λ_{exc} = 397 nm). The bleach and transient signals are positive and negative signals, respectively. The delay times are indicated. **g**: Decay associated spectra of the fs-TAS of **1h**. Note that the positive and negative responses represent the bleached and transient signals, respectively.

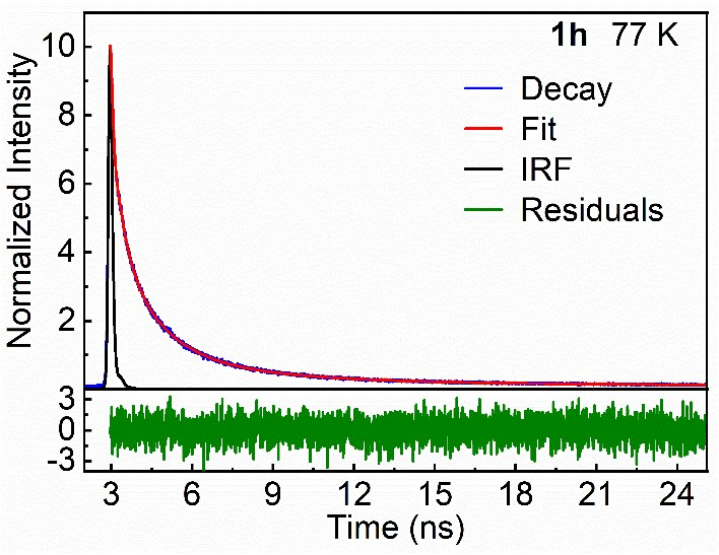

Figure S39. Emission decay (blue), residuals (green), IRF (black) and best fit (red) of **1h** in 2-MeTHF at 77 K. Multi-exponential analysis yields τ = 1.41ns (42%), 5.22ns (39%), χ^2 = 1.000. Note that the sum of the f % values is not equal to 100% because the remainder is close to the lamp profile (*i.e.* approaching or smaller than 100 ps) and cannot be extracted accurately.

Complex 1i (photophysical properties)

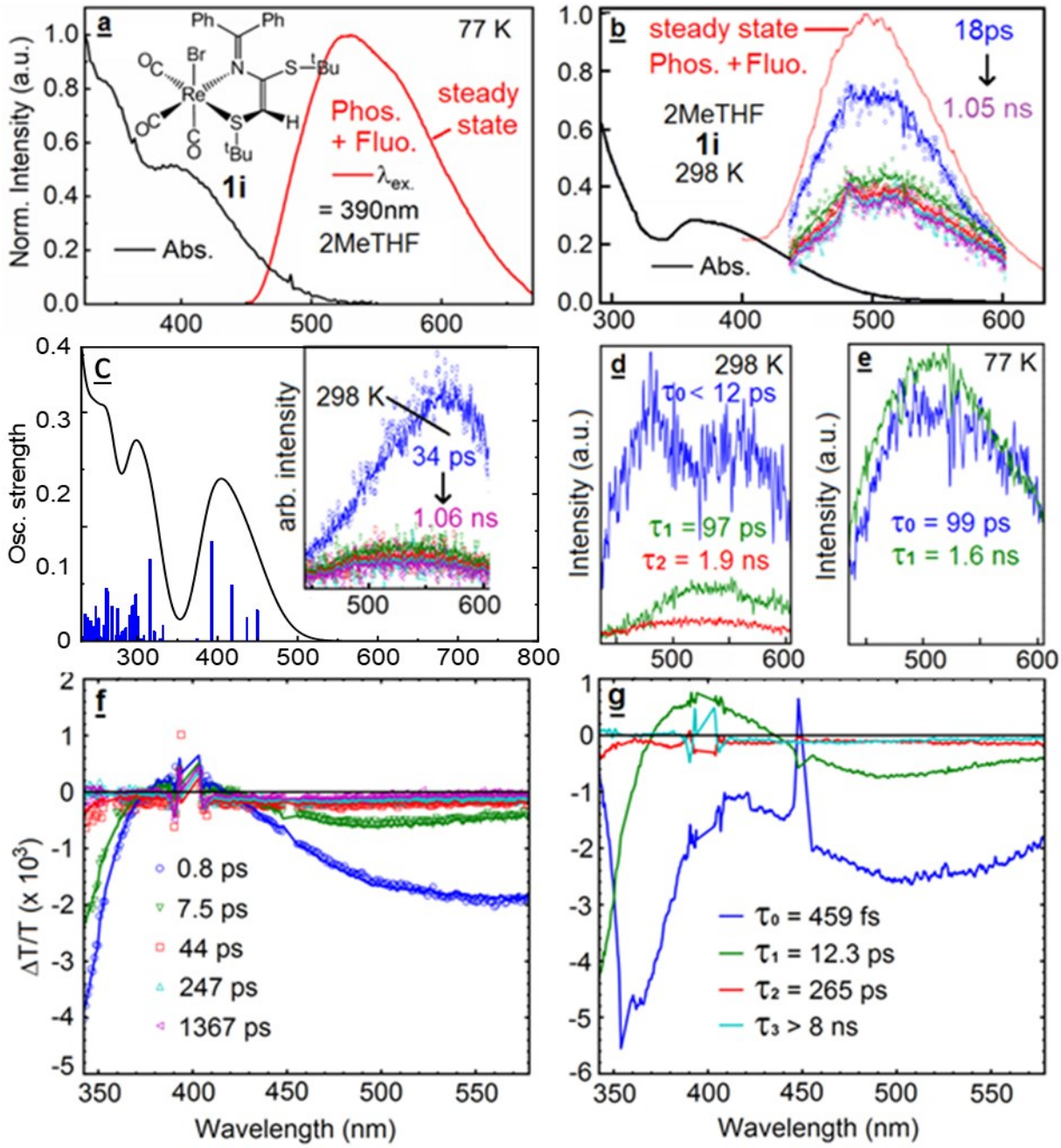

Figure S40. **a** and **b**: Steady state absorption (black) and emission (red) spectra of **1i** in 2-MeTHF at 298 and 77 K, respectively. The time-resolved emission spectra of **1i** in 2-MeTHF are shown in different colors. **c**: simulated absorption spectrum of **1i** (TDDFT, applying a THF solvent field); the bar graph (blue) reports the calculated oscillator strengths (f) and positions of the 100st electronic transitions. An arbitrary thickness of 3000 cm^{-1} is assigned to each bar for the spectra simulation. **d** (298 K) and **e** (77 K): decay associated spectra of **1i** in 2-MeTHF (Streak camera; λ_{exc} = 397 nm, note that the spectra are not corrected for the PMT response and the spectra of short-lived species (*i.e.* τ_F < IRF, blue traces) are severely distorted. **f**: Time evolution of the fs-TAS of **1i** in 2-MeTHF at 298 K (λ_{exc} = 397 nm). The bleach and transient signals are positive and negative signals, respectively. The delay times are indicated. **g**: Decay associated spectra of the fs-TAS of **1i**. Note that the positive and negative responses represent the bleached and transient signals, respectively.

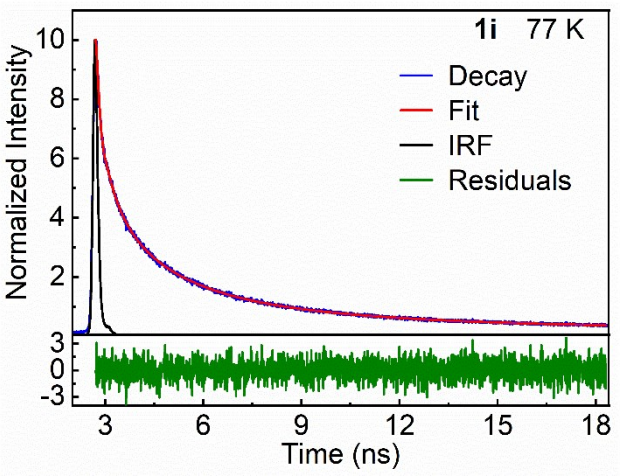

Figure S41. Emission decay (blue), residuals (green), IRF (black) and best fit (red) of **1i** in 2-MeTHF at 77 K. Multi-exponential analysis yields τ = 1.68ns (29%), 5.80ns (57%), χ^2 = 1.030. Note that the sum of the f % values is not equal to 100% because the remainder is close to the lamp profile (*i.e.* approaching or smaller than 100 ps) and cannot be extracted accurately.

Complex 1j (photophysical properties)

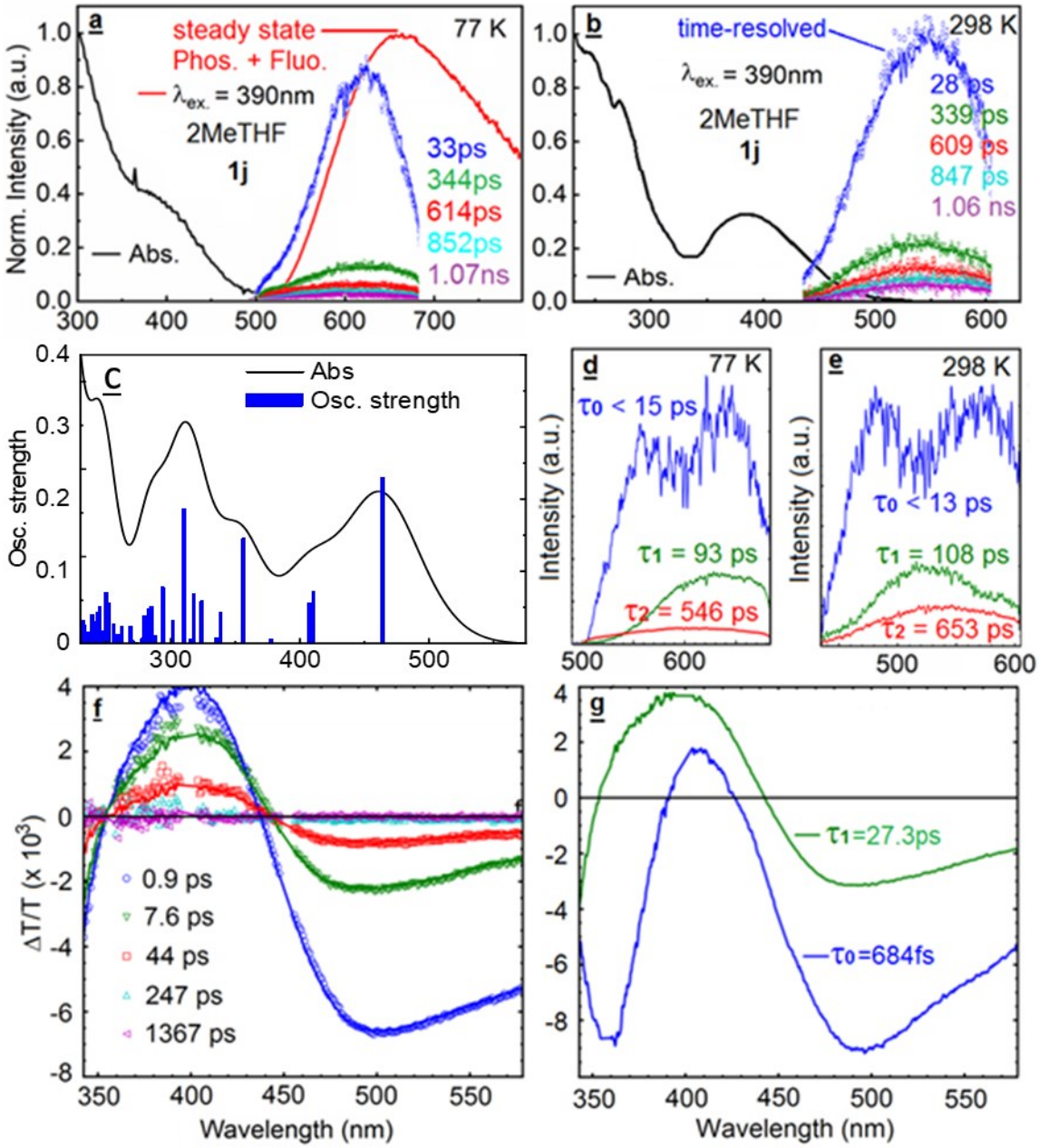

Figure S42. **a** and **b**: Steady state absorption (black) and emission (red) spectra of **1j** in 2-MeTHF at 298 and 77 K, respectively. The time-resolved emission spectra of **1j** in 2-MeTHF are shown in different colors. **c**: simulated absorption spectrum of **1j** (TDDFT, applying a THF solvent field); the bar graph (blue) reports the calculated oscillator strengths (f) and positions of the 100st electronic transitions. An arbitrary thickness of 3000 cm^{-1} is assigned to each bar for the spectra simulation. **d** (77 K) and **e** (298 K): decay associated spectra of **1j** in 2-MeTHF (Streak camera; λ_{exc} = 397 nm, note that the spectra are not corrected for the PMT response and the spectra of short-lived species (*i.e.* τ_F < IRF, blue traces) are severely distorted. **f**: Time evolution of the fs-TAS of **1j** in 2-MeTHF at 298 K (λ_{exc} = 397 nm). The bleach and transient signals are positive and negative signals, respectively. The delay times are indicated. **g**: Decay associated spectra of the fs-TAS of **1j**. Note that the positive and negative responses represent the bleached and transient signals, respectively.

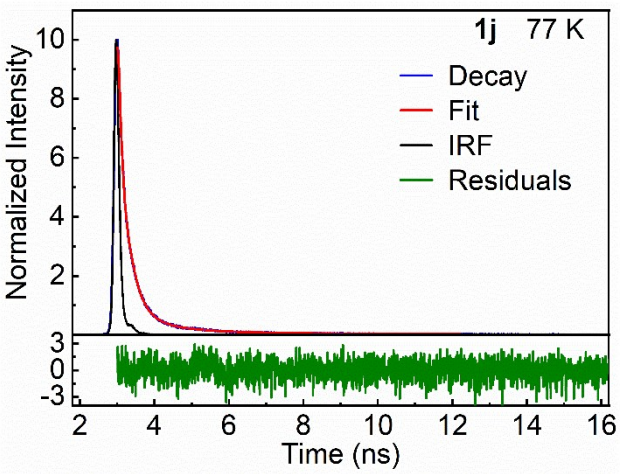

Figure S43. Emission decay (blue), residuals (green), IRF (black) and best fit (red) of **1j** in 2-MeTHF at 77 K. Multi-exponential analysis yields τ = 1.40ns (33%), 4.74ns (42%), χ^2 = 1.183. Note that the sum of the f % values is not equal to 100% because the remainder is close to the lamp profile (*i.e.* approaching or smaller than 100 ps) and cannot be extracted accurately.

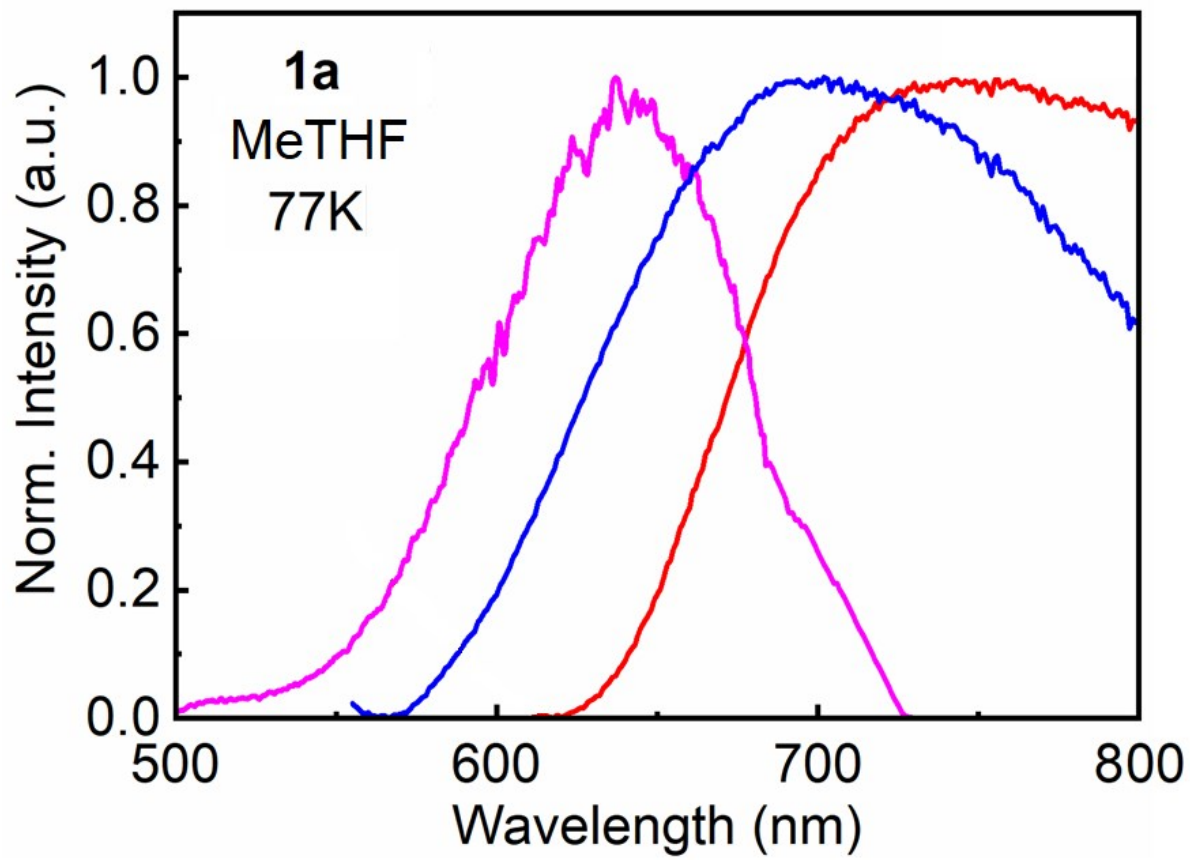

Figure S44. Spectrum recorded with the Streak camera (purple, delay time = 28ps), steady state spectrum (blue), and resulting spectrum (*i.e.* phosphorescence) from the spectrum recorded with the Streak camera subtracted from that of the steady state (red) of **1a** in 2-MeTHF at 77 K. Note that the Streak camera spectra are not corrected for the PMT response. Consequently, the resulting spectrum above 725 nm should be considered qualitative. Nonetheless, the conclusion that the phosphorescence spectrum of 1a extends well in the near-IR region (*i.e.* > 750 nm) stands.

Complex 1a (singlet state)

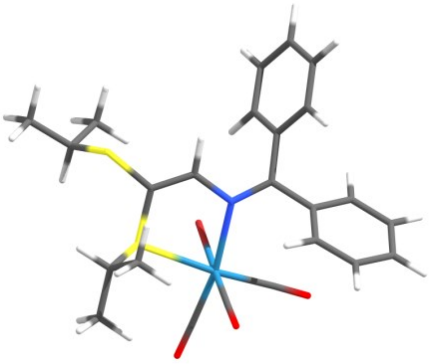

Figure S45. Optimized geometry for **1a** applying a THF solvent field.

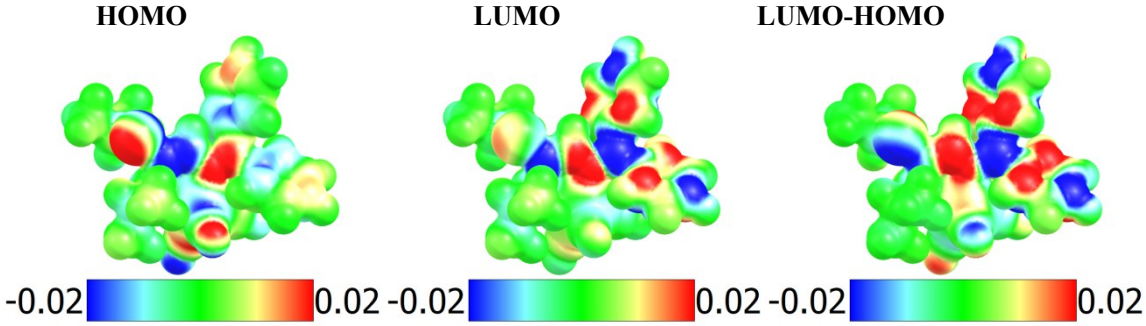

Figure S46. Electron-density map of the HOMO and LUMO; Electron-density difference (LUMO-HOMO)

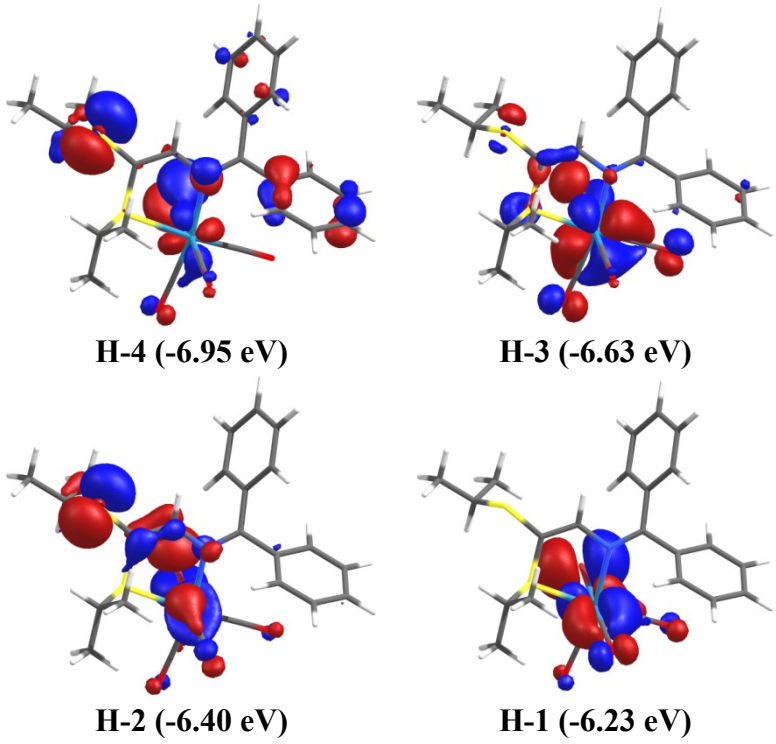

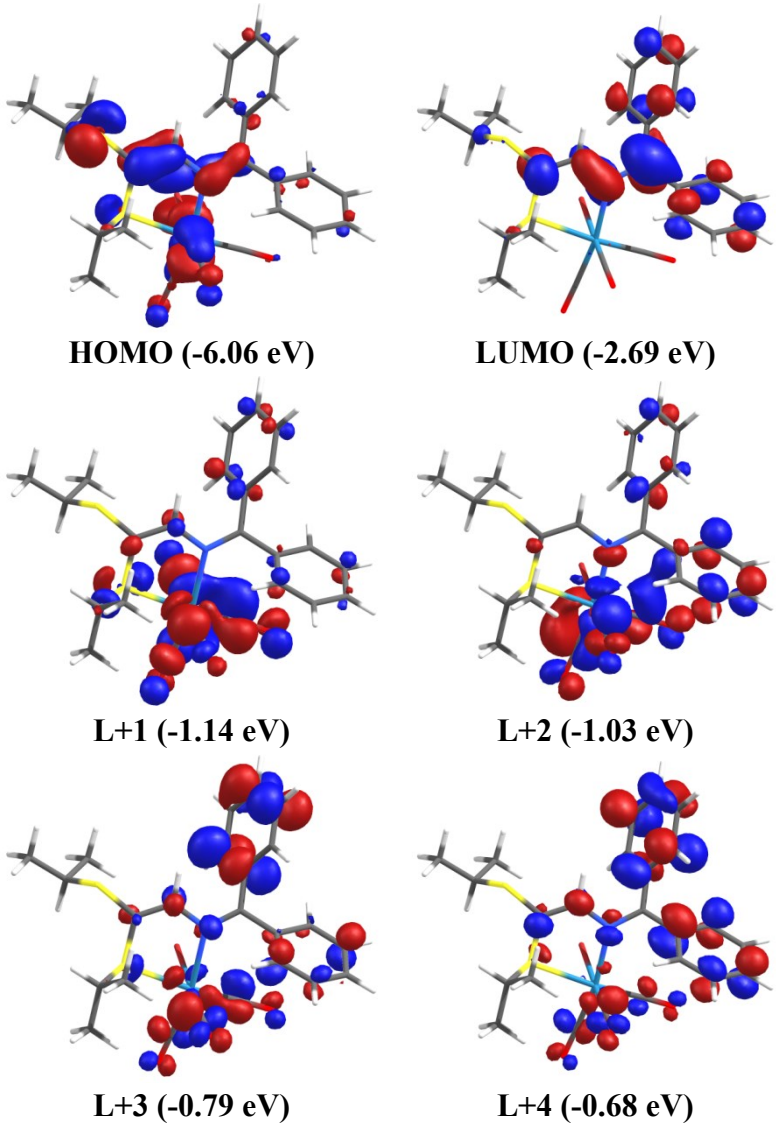

Figure S47. Representations of the frontier MOs for **1a** applying a THF solvent field. The isoval = 0.04.

Table S10. Relative atomic contributions (%) of the various fragments to the frontier MOs of **1a**. [a]

Fragments	H-4	H-3	H-2	H-1	HOMO	LUMO	L+1	L+2	L+3	L+4
Re	11%	**44%**	18%	38%	20%	2%	22%	20%	13%	7%
3CO	6%	19%	7%	17%	10%	2%	28%	30%	15%	11%
Br	18%	10%	20%	**39%**	16%	0%	12%	3%	1%	1%
N-S_Ligands	**65%**	27%	**55%**	6%	**54%**	**95%**	**37%**	**46%**	**70%**	**82%**

[a]H = HOMO, L = LUMO; the values in bold represent the largest contributions.

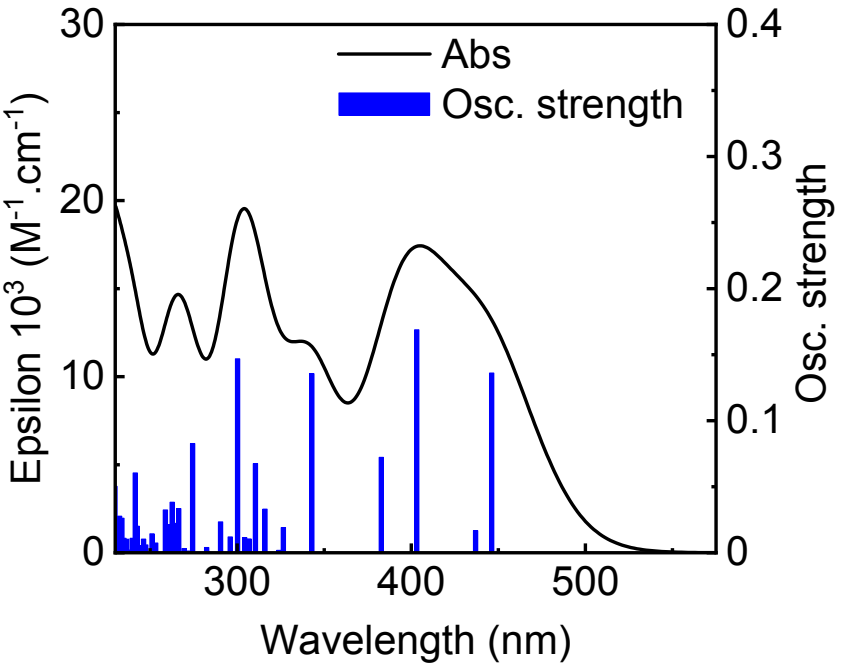

Figure S48. Simulated absorption spectrum for **1a** by TDDFT computations. Bar graph reporting the calculated oscillator strength and calculated position of the 100st electronic transitions calculated by TDDFT for **1a** (bar graph; f = computed oscillator strength).

Table S11. Calculated position, oscillator strength (f) and major contributions (%) of the first 100 singlet-singlet electronic transitions for **1a**.

No.	λ (nm)	f	Major contributions (%)
1	446.2	0.1361	HOMO→LUMO (86%)
2	436.9	0.0167	H-1→LUMO (92%)
3	403.1	0.1688	H-2→LUMO (86%)
4	382.8	0.0723	H-3→LUMO (91%)
5	342.9	0.1356	H-4→LUMO (96%)
6	326.6	0.0191	H-6→LUMO (20%), H-5→LUMO (79%)
7	323.9	0.0018	H-6→LUMO (78%), H-5→LUMO (20%)
8	316.0	0.0331	H-7→LUMO (94%)
9	310.5	0.0675	H-8→LUMO (93%)
10	306.8	0.0105	H-1→L+1 (55%), HOMO→L+1 (15%)
11	304.3	0.0115	HOMO→L+1 (50%), HOMO→L+2 (12%)
12	300.3	0.1469	H-9→LUMO (85%)
13	296.0	0.012	H-1→L+2 (21%), HOMO→L+2 (44%)
14	290.4	0.0234	H-1→L+1 (11%), H-1→L+2 (57%)
15	282.9	0.001	H-10→LUMO (14%), H-3→L+1 (54%)
16	282.5	0.004	H-10→LUMO (84%)
17	274.4	0.0827	H-11→LUMO (19%), H-2→L+1 (24%), HOMO→L+1 (11%), HOMO→L+3 (26%)
18	271.5	0.0013	H-12→LUMO (11%), H-11→LUMO (50%), H-2→L+1 (25%)
19	269.5	0.0032	H-2→L+1 (26%), HOMO→L+3 (33%)
20	266.5	0.0335	H-2→L+2 (52%), HOMO→L+2 (12%)
21	264.5	0.0223	H-12→LUMO (66%)

22	262.7	0.0383	H-3→L+2 (52%)
23	261.1	0.0212	H-2→L+2 (11%), H-1→L+3 (40%), HOMO→L+3 (10%), HOMO→L+4 (18%)
24	258.8	0.0324	H-1→L+3 (15%), HOMO→L+4 (55%)
25	253.3	0.0074	H-2→L+3 (10%), H-1→L+4 (56%)
26	251.2	0.0144	H-2→L+3 (38%), H-1→L+4 (18%)
27	247.5	0.006	H-4→L+1 (19%), H-2→L+3 (11%), HOMO→L+5 (35%)
28	246.3	0.0104	H-4→L+1 (35%), HOMO→L+5 (23%)
29	244.2	0.0053	H-2→L+4 (11%), HOMO→L+6 (15%), HOMO→L+7 (17%)
30	242.6	0.0201	H-1→L+5 (13%), H-1→L+8 (12%), HOMO→L+6 (13%)
31	242.4	0.0069	H-5→L+1 (12%), H-2→L+4 (54%)
32	241.5	0.0605	H-5→L+1 (11%), H-2→L+4 (13%)
33	239.8	0.011	H-3→L+3 (28%), H-1→L+5 (23%)
34	238.8	0.0013	H-4→L+2 (49%)
35	237.5	0.0021	H-1→L+5 (25%), H-1→L+6 (16%), H-1→L+7 (11%)
36	236.6	0.0103	H-14→LUMO (20%), H-13→LUMO (44%)
37	235.4	0.0019	H-3→L+4 (36%)
38	235.0	0.011	H-6→L+2 (15%), H-5→L+2 (16%)
39	233.8	0.0262	H-7→L+1 (13%), H-5→L+2 (13%), H-2→L+5 (12%)
40	232.5	0.0277	H-3→L+4 (27%), HOMO→L+6 (14%), HOMO→L+7 (22%)
41	231.8	0.0077	HOMO→L+8 (29%)
42	231.1	0.0044	H-2→L+6 (18%), H-2→L+7 (21%), H-1→L+8 (12%)
43	229.8	0.0503	H-7→L+1 (29%), H-2→L+5 (23%)
44	227.7	0.0114	H-7→L+2 (20%), H-6→L+1 (17%), H-2→L+5 (12%)
45	226.9	0.0167	H-6→L+1 (10%)
46	226.2	0.0011	H-1→L+6 (33%), H-1→L+7 (35%)
47	225.4	0.0226	H-3→L+5 (14%)
48	224.4	0.026	H-7→L+2 (12%), H-4→L+3 (15%), H-1→L+8 (15%)
49	223.3	0.0182	H-6→L+1 (19%), H-6→L+2 (14%), H-5→L+2 (11%)
50	222.2	0.0098	H-6→L+2 (18%), H-4→L+3 (12%), H-3→L+5 (28%)
51	221.7	0.0297	H-4→L+3 (13%), H-3→L+5 (14%), H-3→L+8 (21%)
52	221.2	0.0056	H-3→L+8 (20%)
53	219.4	0.0102	H-3→L+6 (10%), H-1→L+10 (17%), HOMO→L+10 (12%)
54	219.3	0.02	H-8→L+1 (32%), H-4→L+4 (16%)
55	218.6	0.007	H-8→L+1 (20%), H-2→L+6 (12%)
56	217.9	0.0199	H-8→L+1 (11%), H-4→L+4 (13%), H-2→L+6 (21%), H-2→L+7 (12%)
57	217.7	0.0242	H-4→L+4 (37%)
58	215.9	0.0073	H-6→L+3 (29%), H-5→L+3 (22%)
59	215.4	0.007	H-5→L+3 (22%)
60	214.5	0.0044	H-1→L+10 (27%), HOMO→L+9 (28%)
61	214.3	0.0117	H-14→LUMO (12%), H-2→L+8 (29%), H-1→L+9 (18%)
62	214.0	0.0242	H-14→LUMO (41%), H-13→LUMO (19%), H-2→L+8 (23%)
63	213.4	0.0345	H-2→L+8 (15%), H-1→L+9 (21%)
64	212.3	0.0235	H-9→L+1 (29%), H-8→L+2 (14%), H-7→L+3 (14%)
65	211.9	0.0252	H-7→L+3 (39%)
66	211.2	0.0218	H-10→L+2 (13%), H-3→L+6 (11%)
67	210.9	0.0034	H-9→L+1 (10%), H-6→L+4 (27%), H-5→L+4 (23%)

68	210.6	0.0206	H-3→L+6 (13%), H-3→L+7 (16%), H-2→L+9 (10%)
69	209.9	0.0304	H-9→L+2 (40%), H-6→L+3 (11%)
70	209.7	0.0188	H-9→L+1 (11%), H-6→L+3 (11%)
71	209.3	0.0353	H-10→L+2 (17%), H-5→L+4 (30%), H-3→L+7 (10%)
72	208.6	0.0081	H-10→L+2 (13%), HOMO→L+11 (18%)
73	207.8	0.0108	H-9→L+3 (14%), H-8→L+3 (13%), H-4→L+5 (19%)
74	206.6	0.0152	H-7→L+4 (18%), HOMO→L+11 (13%)
75	206.2	0.0317	H-9→L+2 (13%), H-6→L+4 (14%), H-4→L+5 (16%)
76	205.8	0.0285	H-7→L+4 (42%)
77	205.2	0.0061	H-11→L+1 (19%), H-8→L+3 (14%)
78	205.1	0.0206	HOMO→L+12 (15%)
79	204.5	0.0147	H-15→LUMO (41%)
80	204.3	0.009	H-15→LUMO (24%), H-1→L+11 (20%)
81	203.8	0.0293	H-11→L+1 (17%), H-8→L+3 (21%)
82	203.1	0.0437	H-18→LUMO (13%)
83	202.8	0.0062	H-18→LUMO (27%), H-16→LUMO (16%), H-15→LUMO (11%)
84	202.4	0.0224	H-6→L+5 (11%), H-5→L+5 (10%), H-4→L+6 (18%)
85	202.1	0.0633	H-11→L+2 (12%)
86	201.3	0.0084	H-11→L+2 (21%), H-5→L+5 (24%), H-4→L+6 (10%)
87	200.8	0.0304	H-12→L+1 (11%), H-5→L+5 (19%)
88	200.2	0.009	HOMO→L+14 (33%)
89	199.9	0.0144	H-19→LUMO (28%), H-9→L+3 (13%), H-8→L+4 (14%)
90	199.5	0.0092	H-12→L+1 (10%), H-11→L+2 (18%), H-7→L+5 (15%), H-4→L+7 (12%)
91	199.3	0.1636	H-12→L+1 (30%), H-6→L+5 (16%), H-4→L+7 (11%)
92	199.1	0.0053	H-12→L+1 (11%), H-9→L+4 (12%), H-6→L+5 (15%), H-5→L+5 (13%)
93	198.5	0.0191	H-19→LUMO (22%), H-7→L+5 (24%)
94	198.0	0.0086	H-5→L+6 (10%), H-4→L+8 (28%)
95	197.4	0.0231	H-9→L+4 (10%), H-4→L+8 (11%), H-2→L+9 (13%)
96	196.8	0.0198	H-12→L+2 (20%), H-5→L+8 (13%)
97	196.3	0.0302	H-10→L+3 (13%), H-5→L+6 (11%)
98	196.1	0.0069	H-10→L+3 (17%), H-8→L+5 (11%)
99	196.0	0.0213	H-10→L+3 (23%), H-2→L+10 (11%)
100	195.6	0.0017	H-2→L+10 (32%), HOMO→L+10 (11%)

Complex 1a (triplet state)

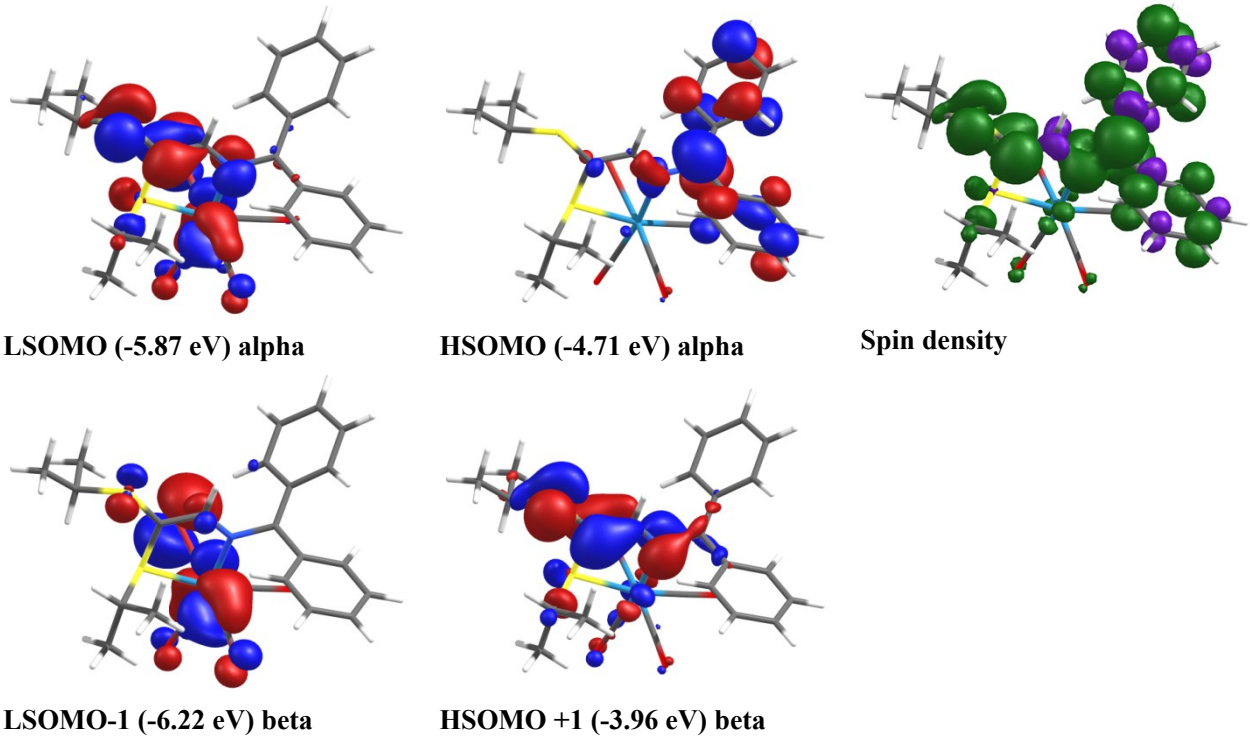

Figure S49. Left, representations of the semi-occupied MOs for **1a** in its lowest energy triplet state. The isoval = 0.04. Right, Alpha – beta SCF spin density. The isoval = 0.003 (green lobe positive, purple lobe negative).

Table S12. Relative atomic contributions (%) of the various fragments to the semi-occupied MOs of **1a**.[b]

Fragments	LS-1	LSOMO	HSOMO	HS+1
Re	**37%**	19%	2%	5%
3(CO)	16%	9%	2%	4%
Br	32%	10%	0%	2%
N-S_Ligands	15%	**62%**	**95%**	**89%**

[b]HS = HSOMO, LS = LSOMO; the values in bold represent the largest contributions.

Complex 1b (singlet state)

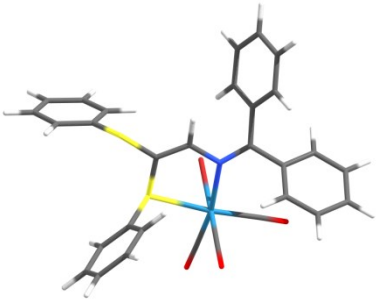

Figure S50. Optimized geometry for **1b** applying a THF solvent field.

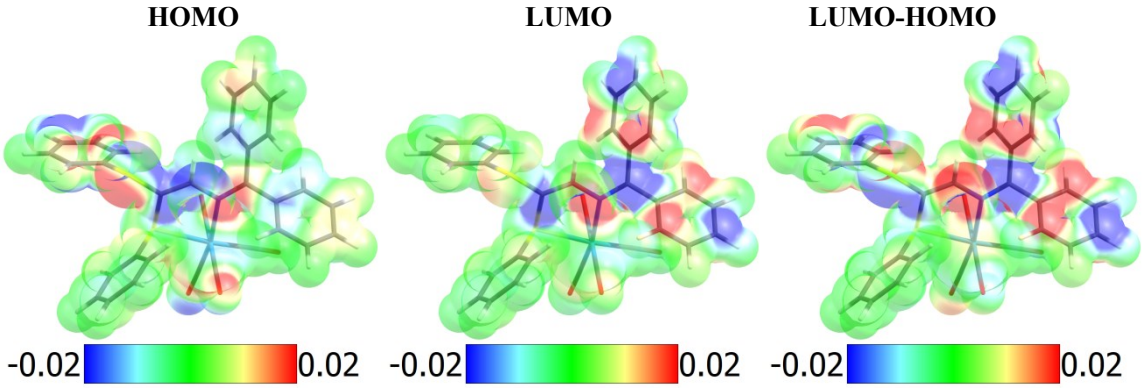

Figure S51. Electron-density map of the HOMO and LUMO ; Electron-density difference (LUMO-HOMO)

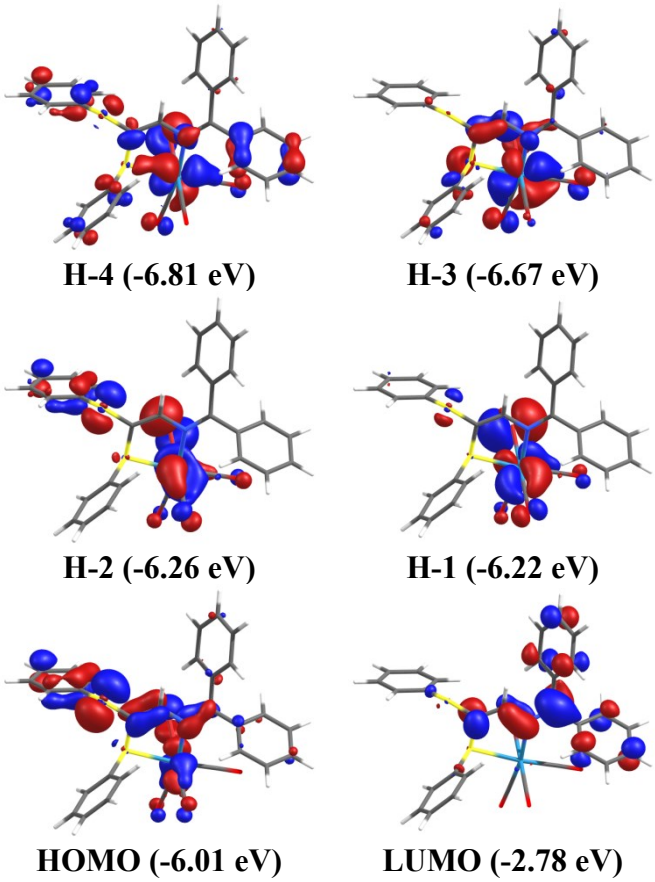

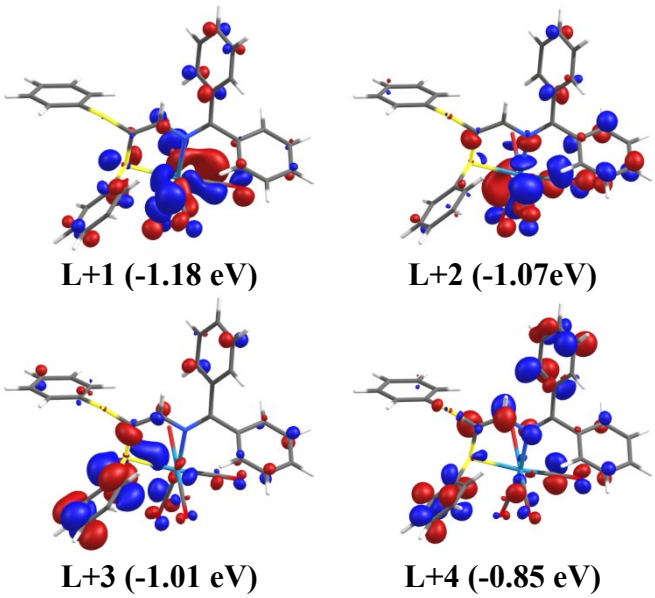

Figure S52. Representations of the frontier MOs for **1b** applying a THF solvent field. The isoval = 0.04.

Table S13. Relative atomic contributions (%) of the various fragments to the frontier MOs of **1b**.[a]

Fragments	H-4	H-3	H-2	H-1	HOMO	LUMO	L+1	L+2	L+3	L+4
Re	22%	37%	30%	**35%**	13%	2%	24%	18%	12%	8%
3(CO)	10%	16%	13%	16%	6%	2%	25%	28%	9%	10%
Br	10%	10%	27%	37%	8%	0%	8%	4%	2%	1%
N-S_Ligands	**58%**	**38%**	**31%**	12%	**73%**	**96%**	**42%**	**51%**	**77%**	**81%**

[a]H = HOMO, L = LUMO; the values in bold represent the largest contributions.

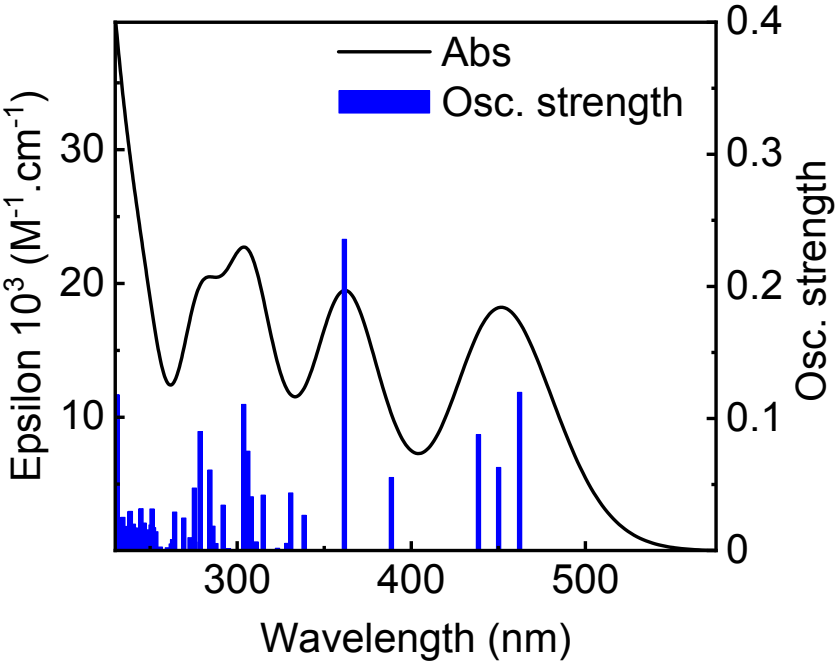

Figure S53. Simulated absorption spectrum for **1b** by TDDFT computations. Bar graph reporting the calculated oscillator strength and calculated position of the 100st electronic transitions calculated by TDDFT for **1b** (bar graph; f = computed oscillator strength).

Table S14. Calculated position, oscillator strength (f) and major contributions (%) of the first 100 singlet-singlet electronic transitions for **1b**.

No.	λ (nm)	f	Major contributions (%)
1	462.2	0.1198	H-1→LUMO (29%), HOMO→LUMO (68%)
2	450.1	0.0629	H-2→LUMO (27%), H-1→LUMO (56%), HOMO→LUMO (16%)
3	438.5	0.0879	H-2→LUMO (70%), H-1→LUMO (14%), HOMO→LUMO (14%)
4	388.6	0.0553	H-4→LUMO (15%), H-3→LUMO (83%)
5	361.6	0.2357	H-4→LUMO (83%), H-3→LUMO (14%)
6	338.4	0.0267	H-6→LUMO (27%), H-5→LUMO (67%)
7	330.7	0.0436	H-9→LUMO (11%), H-7→LUMO (85%)
8	328.5	0.0054	H-8→LUMO (94%)
9	323.2	0.0017	H-6→LUMO (65%), H-5→LUMO (30%)
10	315.0	0.042	H-11→LUMO (20%), H-10→LUMO (72%)
11	310.9	0.0066	H-11→LUMO (15%), H-1→L+1 (36%), HOMO→L+1 (26%)
12	309.6	0.002	H-9→LUMO (84%), H-7→LUMO (11%)
13	308.1	0.0408	H-11→LUMO (53%), H-10→LUMO (15%), H-1→L+1 (10%)
14	306.1	0.0752	H-12→LUMO (52%), H-2→L+1 (13%)
15	303.7	0.1107	H-12→LUMO (40%), H-2→L+1 (23%), HOMO→L+1 (10%)
16	295.0	0.0015	H-2→L+2 (33%), H-1→L+2 (44%)
17	292.0	0.0344	H-2→L+1 (10%), H-1→L+1 (17%), H-1→L+2 (12%), HOMO→L+2 (32%)
18	287.8	0.0053	H-13→LUMO (92%)
19	286.1	0.0185	H-3→L+1 (15%), H-2→L+1 (20%), H-1→L+1 (10%), HOMO→L+1 (21%)
20	284.4	0.061	HOMO→L+2 (14%), HOMO→L+3 (73%)
21	278.7	0.0901	H-3→L+1 (23%), HOMO→L+1 (15%)
22	275.8	0.0065	H-14→LUMO (65%), H-1→L+3 (13%)
23	275.4	0.0473	H-1→L+3 (48%), HOMO→L+4 (11%)
24	273.0	0.0098	H-3→L+1 (14%), H-2→L+2 (22%), H-1→L+3 (18%), HOMO→L+2 (10%), HOMO→L+3 (11%)
25	271.4	7E-4	H-2→L+3 (68%)
26	269.3	0.0246	H-14→LUMO (10%), H-2→L+3 (13%), HOMO→L+4 (55%)
27	264.1	0.0291	H-3→L+2 (21%), HOMO→L+5 (40%)
28	263.0	0.0083	H-3→L+2 (15%), H-2→L+4 (17%), HOMO→L+5 (33%)
29	262.2	0.005	H-2→L+4 (14%), H-1→L+4 (68%)
30	260.0	0.0022	H-2→L+4 (49%), H-1→L+4 (11%)
31	255.9	0.0027	H-2→L+5 (11%), H-1→L+5 (76%)
32	253.3	0.0143	H-15→LUMO (65%), H-2→L+5 (10%)
33	252.0	0.0173	H-4→L+1 (31%), H-3→L+3 (13%), H-2→L+5 (17%)
34	251.4	0.0147	H-4→L+1 (12%), H-2→L+5 (35%)
35	251.2	0.0315	HOMO→L+6 (14%), HOMO→L+7 (22%), HOMO→L+8 (11%)
36	250.5	0.0194	H-3→L+2 (12%), H-3→L+3 (48%)
37	249.6	0.0157	HOMO→L+6 (55%)
38	246.6	0.0208	HOMO→L+7 (37%), HOMO→L+8 (29%)
39	244.8	0.0317	H-4→L+2 (51%)
40	244.0	0.0023	H-5→L+1 (11%), H-1→L+6 (34%)
41	243.2	0.015	H-5→L+1 (11%), HOMO→L+8 (13%), HOMO→L+9 (12%)
42	242.2	0.0169	H-3→L+4 (12%), H-1→L+6 (32%)

43	241.4	0.017	H-17→LUMO (12%), H-16→LUMO (41%), H-2→L+6 (16%)
44	240.9	0.0092	H-16→LUMO (28%), H-3→L+4 (12%), H-2→L+6 (15%)
45	240.4	0.02	H-4→L+3 (40%)
46	240.0	0.0025	H-4→L+3 (13%), H-3→L+4 (12%)
47	238.7	0.0297	H-3→L+4 (22%), H-2→L+6 (16%)
48	238.3	0.0294	H-1→L+8 (16%)
49	238.1	0.0038	H-4→L+3 (11%)
50	237.0	0.0183	H-7→L+1 (11%), H-3→L+5 (10%), HOMO→L+9 (10%), HOMO→L+10 (10%)
51	236.3	0.0018	H-1→L+7 (41%)
52	235.9	0.0123	H-2→L+7 (32%), H-1→L+8 (35%)
53	235.4	0.0055	H-3→L+5 (32%), H-1→L+7 (13%)
54	235.1	0.0026	H-2→L+8 (39%)
55	234.4	0.0251	H-5→L+2 (12%), H-3→L+5 (11%), H-2→L+7 (12%)
56	233.7	0.0124	H-2→L+7 (10%), HOMO→L+11 (16%)
57	233.1	8E-4	H-2→L+8 (14%), H-1→L+12 (10%)
58	232.7	0.0077	H-17→LUMO (12%), H-7→L+2 (18%), H-4→L+4 (14%)
59	232.1	0.0062	H-17→LUMO (17%), H-7→L+2 (14%), H-4→L+4 (15%)
60	231.0	0.118	H-17→LUMO (28%)
61	229.6	0.0075	H-5→L+1 (11%), H-5→L+3 (11%)
62	229.4	0.0242	H-2→L+9 (11%), H-1→L+9 (23%)
63	228.0	0.0084	H-5→L+1 (12%), H-2→L+9 (12%), H-1→L+9 (24%)
64	227.7	0.023	H-5→L+1 (15%), H-5→L+3 (16%), H-1→L+9 (23%)
65	227.5	0.0178	H-5→L+3 (11%), H-2→L+9 (21%)
66	227.3	0.0078	H-8→L+1 (12%), H-6→L+1 (22%), H-4→L+5 (13%)
67	226.1	0.0226	H-6→L+1 (20%), H-4→L+5 (42%)
68	225.6	0.0116	H-3→L+6 (40%)
69	224.9	8E-4	H-1→L+10 (28%), HOMO→L+12 (12%)
70	224.5	0.0299	H-10→L+1 (14%), H-8→L+2 (13%)
71	223.5	0.0022	H-1→L+10 (20%), H-1→L+11 (12%)
72	223.4	0.0325	H-7→L+3 (10%), H-2→L+10 (20%)
73	223.3	0.0068	H-11→L+1 (10%), H-7→L+3 (19%)
74	223.0	0.0121	H-9→L+1 (26%)
75	222.6	0.0365	H-9→L+1 (21%), H-5→L+2 (11%)
76	222.2	0.0257	H-5→L+2 (12%), H-2→L+11 (13%)
77	221.7	0.0115	H-11→L+2 (10%), H-8→L+1 (10%), H-8→L+2 (12%), H-6→L+2 (11%)
78	221.6	0.0273	H-7→L+3 (10%), H-3→L+6 (14%)
79	221.4	0.0501	H-6→L+3 (35%), H-5→L+3 (15%), H-2→L+10 (10%)
80	220.1	0.0294	H-11→L+2 (11%), H-6→L+2 (14%), H-6→L+3 (16%)
81	219.7	0.0604	H-6→L+2 (16%), H-3→L+7 (11%)
82	219.2	0.0018	H-11→L+1 (14%), H-3→L+7 (28%)
83	218.8	0.0266	H-9→L+2 (18%), H-5→L+4 (19%), H-3→L+8 (13%)
84	218.7	0.003	H-11→L+1 (15%), H-10→L+1 (14%), H-9→L+2 (19%)
85	218.1	0.0496	H-9→L+2 (34%), H-5→L+4 (12%), H-3→L+7 (11%)
86	217.8	0.0035	H-3→L+7 (13%), H-3→L+8 (20%)
87	217.4	0.0318	H-8→L+2 (20%), H-4→L+6 (11%)
88	216.4	0.0411	--

89	216.2	0.0258	H-11→L+3 (12%), H-10→L+3 (28%)
90	215.7	0.0013	H-7→L+4 (33%)
91	214.9	0.016	H-7→L+4 (11%), H-6→L+4 (12%), H-5→L+5 (27%)
92	214.7	0.0164	H-6→L+4 (34%), H-5→L+5 (10%)
93	214.4	0.0482	H-8→L+3 (12%), H-6→L+4 (21%)
94	213.8	0.0143	H-8→L+3 (24%), H-7→L+4 (10%)
95	213.6	0.027	H-3→L+12 (12%)
96	213.1	0.0462	H-8→L+3 (12%), H-4→L+6 (11%), H-4→L+7 (10%)
97	212.9	0.0048	H-3→L+11 (13%)
98	212.5	0.01	H-3→L+9 (15%)
99	212.0	0.0604	H-4→L+7 (30%)
100	211.7	0.0112	H-13→L+1 (22%), H-13→L+2 (12%), H-7→L+5 (11%)

Complex 1b (triplet state)

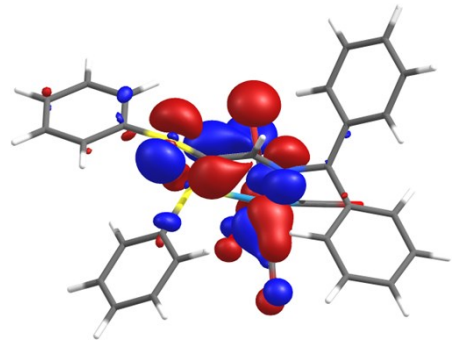

LSOMO (-5.91 eV) alpha

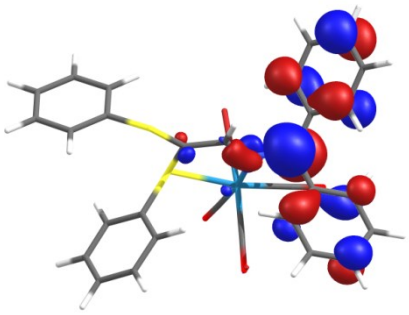

HSOMO (-4.05 eV) alpha

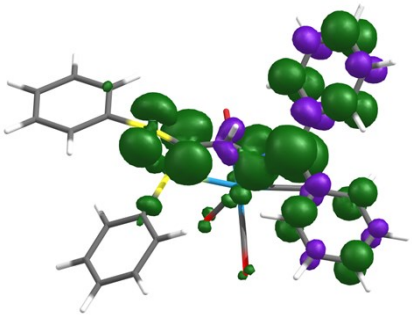

Spin density

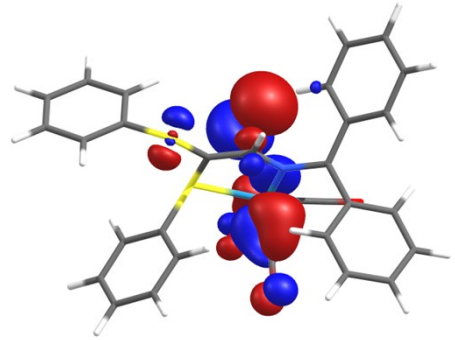

LSOMO -1 (-6.19 eV) beta

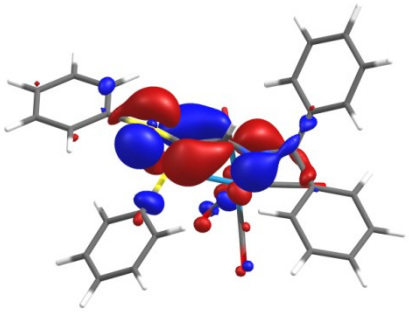

HSOMO +1 (-4.05 eV) beta

Figure S54. Left, representations of the semi-occupied MOs for **1b** in its lowest energy triplet state. The isoval = 0.04. Right, Alpha – beta SCF spin density. The isoval = 0.003 (green lobe positive, purple lobe negative).

Table S15. Relative atomic contributions (%) of the various fragments to the semi-occupied MOs of **1b**.[b]

Fragments	LS-1	LSOMO	HSOMO	HS+1
Re	**36%**	20%	2%	5%
3(CO)	15%	9%	2%	4%
Br	33%	10%	0%	2%
N-S_Ligands	16%	**60%**	**95%**	**89%**

[b]HS = HSOMO, LS = LSOMO; the values in bold represent the largest contributions.

Complex 1c (singlet state)

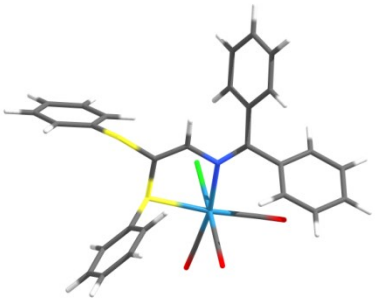

Figure S55. Optimized geometry for **1c** applying a THF solvent field.

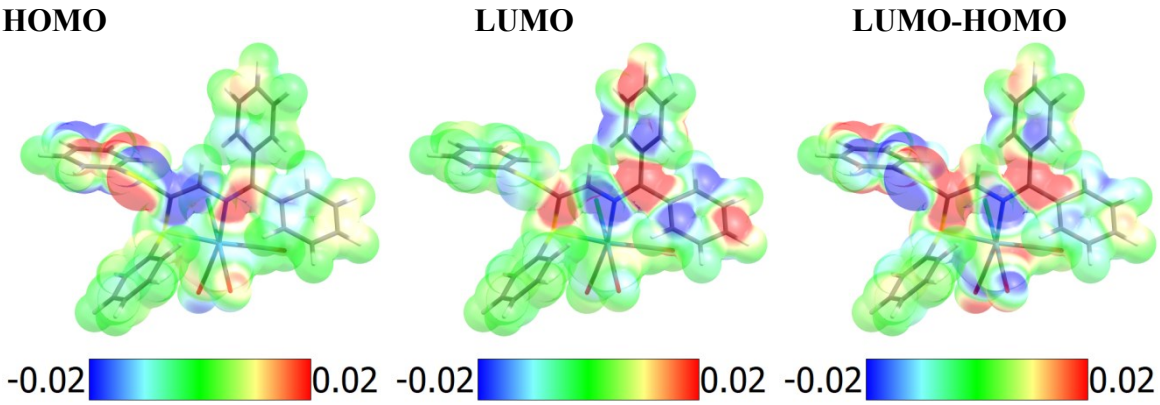

Figure S56. Electron-density map of the HOMO and LUMO ; Electron-density difference (LUMO-HOMO)

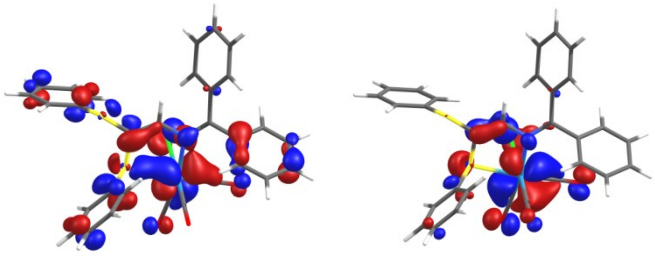

H-4 (-6.84 eV) **H-3 (-6.68 eV)**

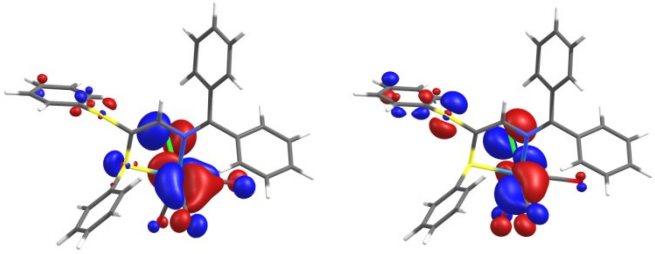

H-2 (-6.33 eV) **H-1 (-6.29 eV)**

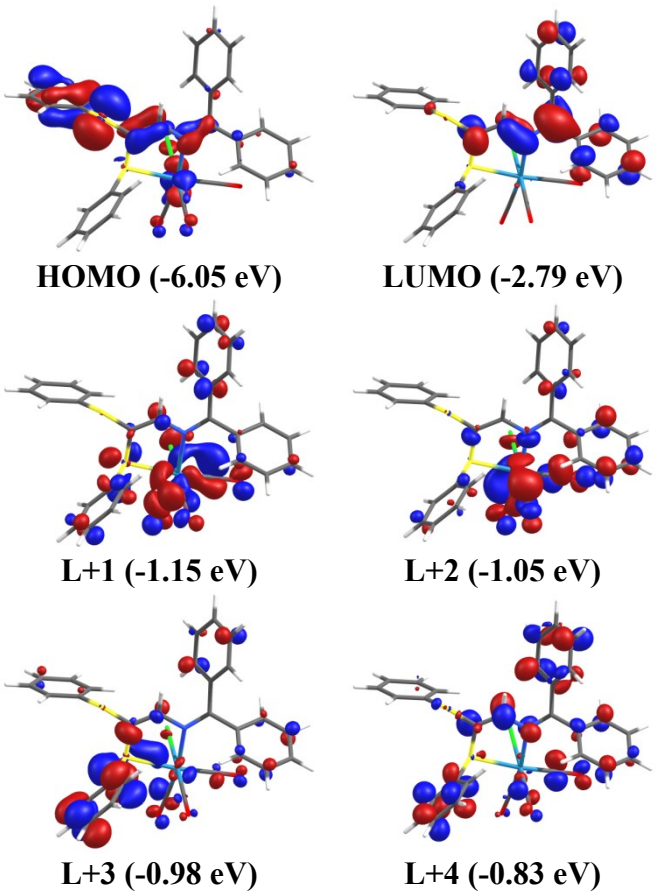

Figure S57. Representations of the frontier MOs for **1c** applying a THF solvent field. The isoval = 0.04.

Table S16. Relative atomic contributions (%) of the various fragments to the frontier MOs of **1c**.[a]

Fragments	H-4	H-3	H-2	H-1	HOMO	LUMO	L+1	L+2	L+3	L+4
Re	21%	**45%**	**42%**	**41%**	9%	2%	23%	17%	11%	7%
3(CO)	10%	19%	18%	18%	4%	2%	23%	29%	9%	10%
Cl	6%	7%	20%	19%	3%	0%	5%	4%	2%	1%
N-S_Ligands	**63%**	29%	19%	22%	**84%**	**96%**	**49%**	**50%**	**78%**	**81%**

[a]H = HOMO, L = LUMO; the values in bold represent the largest contributions.

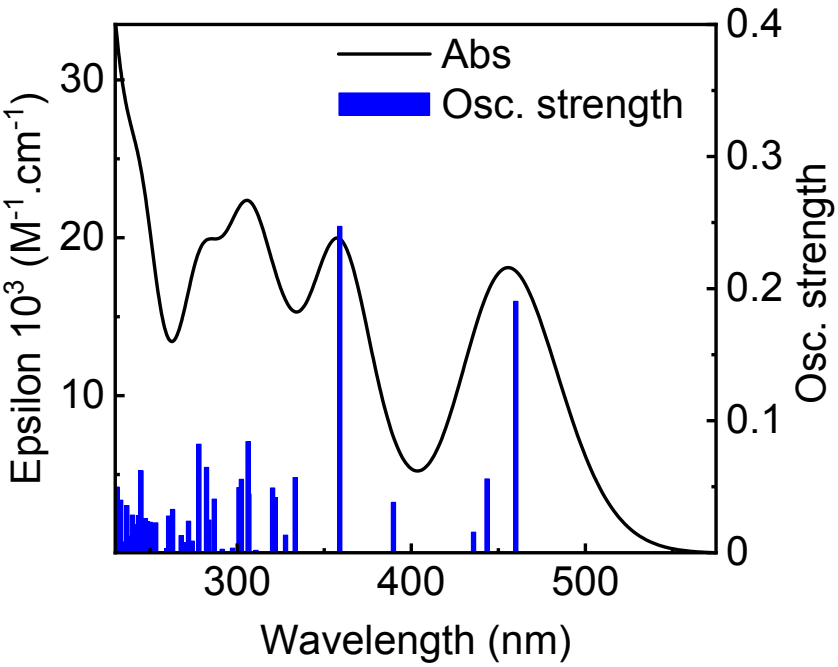

Figure S58. Simulated absorption spectrum for **1c** by TDDFT computations. Bar graph reporting the calculated oscillator strength and calculated position of the 100st electronic transitions calculated by TDDFT for **1c** (bar graph; f = computed oscillator strength).

Table S17. Calculated positions, oscillator strengths (f) and major contributions (%) of the first 100 singlet-singlet electronic transitions for **1c**.

No.	λ (nm)	f	Major contributions (%)
1	460.0	0.1904	H-1→LUMO (12%), HOMO→LUMO (85%)
2	443.5	0.0559	H-2→LUMO (27%), H-1→LUMO (60%), HOMO→LUMO (13%)
3	435.8	0.0156	H-2→LUMO (70%), H-1→LUMO (27%)
4	389.7	0.0382	H-3→LUMO (89%)
5	359.0	0.2472	H-4→LUMO (88%)
6	333.3	0.057	H-7→LUMO (14%), H-6→LUMO (41%), H-5→LUMO (39%)
7	327.8	0.0133	H-7→LUMO (30%), H-5→LUMO (51%)
8	321.9	0.0418	H-9→LUMO (12%), H-7→LUMO (29%), H-6→LUMO (42%)
9	320.4	0.0491	H-9→LUMO (80%)
10	310.8	0.0018	H-8→LUMO (69%), H-7→LUMO (25%)
11	306.8	0.0444	H-10→LUMO (39%), H-1→L+1 (25%), HOMO→L+1 (22%)
12	306.3	0.0842	H-11→LUMO (11%), H-10→LUMO (47%), H-1→L+1 (13%)
13	302.5	0.0556	H-11→LUMO (79%)
14	301.1	0.0494	H-2→L+1 (36%), H-1→L+2 (14%), HOMO→L+1 (13%)
15	297.4	0.0035	H-12→LUMO (87%)
16	291.4	0.0027	H-2→L+2 (53%), H-1→L+2 (18%)
17	286.9	0.0406	H-2→L+1 (23%), H-2→L+2 (10%), HOMO→L+2 (38%)
18	283.9	0.0247	H-1→L+1 (21%), HOMO→L+1 (33%)
19	282.4	0.0647	HOMO→L+3 (76%)
20	278.0	0.0822	H-3→L+1 (21%), H-3→L+2 (11%), HOMO→L+1 (16%)
21	274.2	0.0088	H-13→LUMO (75%)
22	272.1	0.0239	H-1→L+2 (15%), H-1→L+3 (33%), HOMO→L+2 (10%), HOMO→L+4 (14%)

23	270.6	0.0076	H-3→L+1 (16%), H-1→L+3 (33%), HOMO→L+2 (10%), HOMO→L+3 (11%)
24	268.8	0.0069	H-2→L+3 (20%), HOMO→L+4 (38%)
25	267.9	0.013	H-2→L+3 (54%), HOMO→L+4 (12%)
26	264.2	6E-4	H-14→LUMO (80%)
27	262.9	0.0328	HOMO→L+5 (60%)
28	260.7	0.0278	H-3→L+1 (11%), H-3→L+2 (25%)
29	259.5	0.0031	H-1→L+4 (67%)
30	257.1	5E-4	H-2→L+4 (68%)
31	253.2	0.0227	H-15→LUMO (68%)
32	252.5	0.0014	H-2→L+5 (34%), H-1→L+5 (44%)
33	250.7	0.0218	HOMO→L+6 (33%), HOMO→L+8 (25%), HOMO→L+9 (11%)
34	250.1	0.0231	H-2→L+5 (34%), H-1→L+5 (31%)
35	248.8	0.0082	HOMO→L+6 (46%), HOMO→L+8 (17%)
36	248.3	0.0235	H-3→L+2 (15%), H-3→L+3 (62%)
37	247.3	0.0259	H-4→L+1 (59%), HOMO→L+7 (13%)
38	244.8	0.0621	HOMO→L+7 (65%)
39	243.4	0.0281	H-17→LUMO (10%), H-16→LUMO (18%), H-4→L+2 (19%), HOMO→L+8 (10%)
40	242.4	0.0212	H-16→LUMO (47%), H-4→L+2 (19%)
41	242.1	0.0088	H-4→L+2 (13%), HOMO→L+8 (12%), HOMO→L+9 (13%)
42	239.9	0.0285	H-3→L+4 (39%), H-1→L+6 (28%)
43	239.3	0.0068	H-3→L+4 (22%), H-2→L+6 (34%), H-1→L+6 (10%)
44	238.2	0.0126	H-4→L+3 (47%)
45	237.0	0.0104	H-2→L+6 (10%)
46	236.6	0.0357	H-4→L+3 (16%), H-2→L+6 (21%), H-1→L+6 (27%)
47	236.4	0.0046	H-3→L+5 (22%), HOMO→L+10 (23%)
48	235.2	0.0045	H-3→L+5 (24%)
49	234.9	0.0082	H-3→L+5 (10%), H-1→L+7 (18%)
50	234.1	0.0044	H-2→L+7 (16%), H-2→L+8 (24%)
51	233.1	0.0398	H-17→LUMO (31%)
52	232.9	0.0011	H-6→L+1 (27%), H-5→L+1 (23%)
53	232.3	0.0077	H-17→LUMO (15%), H-4→L+4 (12%), H-2→L+7 (14%)
54	231.6	0.0219	H-1→L+7 (45%)
55	231.0	0.0498	H-2→L+8 (12%), H-1→L+12 (12%), HOMO→L+9 (11%)
56	230.3	0.014	H-4→L+4 (10%), H-2→L+7 (18%), H-1→L+8 (25%)
57	229.4	0.0318	H-4→L+4 (18%), H-2→L+7 (22%), H-2→L+8 (12%)
58	227.7	0.0022	H-6→L+2 (20%), H-5→L+2 (16%), H-2→L+8 (12%)
59	227.1	0.0047	H-8→L+1 (12%)
60	226.6	0.0027	H-6→L+1 (23%), H-5→L+1 (38%)
61	226.5	0.0031	H-2→L+12 (10%)
62	225.7	0.0149	H-1→L+9 (41%), HOMO→L+10 (15%)
63	225.4	0.0234	H-2→L+9 (16%)
64	224.7	0.0507	H-4→L+5 (24%)
65	224.4	0.0066	H-9→L+2 (12%), H-4→L+5 (12%), H-3→L+6 (17%)
66	224.1	0.0121	H-8→L+1 (10%), H-5→L+3 (11%), H-2→L+9 (11%)
67	223.8	0.0249	H-5→L+3 (15%), H-3→L+6 (14%)
68	223.0	0.0179	H-2→L+9 (10%), HOMO→L+12 (10%)

69	222.8	0.0168	H-9→L+1 (12%), H-3→L+6 (12%)
70	222.3	0.0254	H-1→L+10 (16%)
71	221.7	0.0098	H-7→L+1 (12%)
72	221.4	0.0083	H-8→L+1 (35%), H-8→L+3 (12%)
73	220.8	0.01	H-6→L+2 (14%), H-5→L+2 (12%), H-1→L+10 (22%)
74	220.4	0.028	H-8→L+2 (12%), H-6→L+2 (10%), H-5→L+2 (19%)
75	219.9	0.0021	H-6→L+3 (13%), H-2→L+10 (22%)
76	219.8	0.0403	H-6→L+3 (26%), H-5→L+3 (21%), H-2→L+10 (21%)
77	219.4	0.0184	H-12→L+1 (10%), H-2→L+10 (15%)
78	218.8	0.0279	H-7→L+2 (14%)
79	217.8	0.0122	H-3→L+7 (12%), H-3→L+8 (18%)
80	217.4	0.0505	H-8→L+2 (26%), H-7→L+2 (24%)
81	217.2	0.0198	H-10→L+1 (13%), H-9→L+1 (14%), H-3→L+8 (18%)
82	216.6	0.0439	H-5→L+4 (16%)
83	216.4	0.0101	H-12→L+1 (14%), H-3→L+7 (10%)
84	216.3	0.0614	H-5→L+4 (40%), H-3→L+7 (16%)
85	216.0	0.0156	H-5→L+4 (17%), H-4→L+6 (11%), H-3→L+7 (24%)
86	215.2	0.0116	--
87	214.7	0.0111	H-12→L+2 (24%)
88	213.5	0.082	H-8→L+3 (12%), H-7→L+3 (26%), H-6→L+4 (15%), H-5→L+5 (11%)
89	213.4	0.0039	H-3→L+11 (16%)
90	213.2	0.0215	H-6→L+4 (17%), H-6→L+5 (10%), H-5→L+5 (15%), H-4→L+6 (18%)
91	212.9	0.0047	H-7→L+3 (11%), H-6→L+4 (18%)
92	212.4	0.0428	H-9→L+3 (16%)
93	212.3	0.0081	H-6→L+4 (16%), H-3→L+12 (10%)
94	211.3	0.0671	H-11→L+2 (11%), H-10→L+1 (11%), H-9→L+3 (28%)
95	211.1	0.0655	H-4→L+6 (14%)
96	210.7	0.0054	H-3→L+9 (31%)
97	210.5	0.0115	H-7→L+4 (31%), H-4→L+7 (10%)
98	210.0	0.0171	H-10→L+1 (16%), H-8→L+4 (11%)
99	209.5	0.0014	H-10→L+1 (10%), H-10→L+2 (11%)
100	209.2	0.0351	H-8→L+4 (24%), H-7→L+4 (10%)

Complex 1c (triplet state)

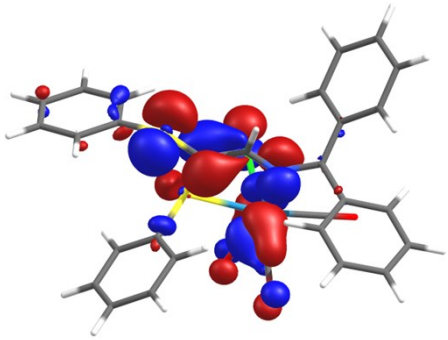

LSOMO (-5.94 eV) alpha

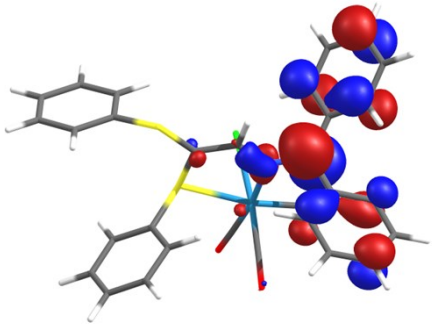

HSOMO (-4.72 eV) alpha

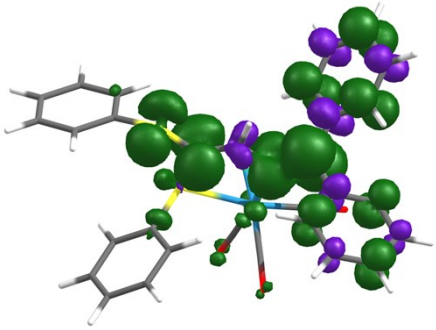

Spin density

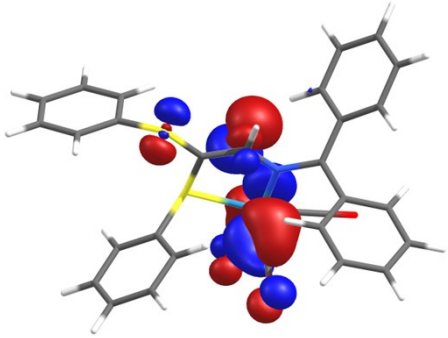

LSOMO-1 (-6.26 eV) beta

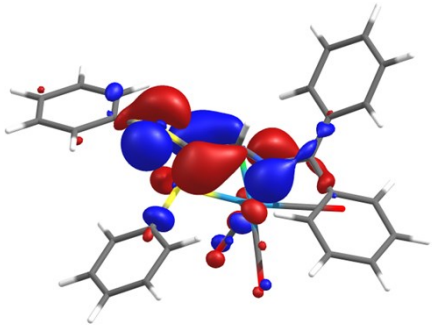

HSOMO+1 (-4.04 eV) beta

Figure S59. Left, representations of the semi-occupied MOs for **1c** in its lowest energy triplet state. The isoval = 0.04. Right, Alpha – beta SCF spin density. The isoval = 0.003 (green lobe positive, purple lobe negative).

Table S18. Relative atomic contributions (%) of the various fragments to the semi-occupied MOs of **1c**.[b]

Fragments	LS-1	LSOMO	HSOMO	HS+1
Re	**43%**	19%	2%	5%
3(CO)	18%	9%	2%	4%
Cl	20%	6%	0%	1%
N-S_Ligands	19%	**65%**	**95%**	**90%**

[b]HS = HSOMO, LS = LSOMO; the values in bold represent the largest contributions.

Complex 1e (singlet state)

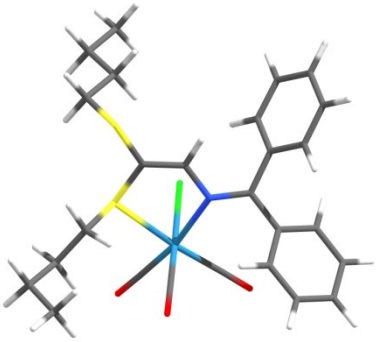

Figure S60. Optimized geometry for **1e** applying a THF solvent field.

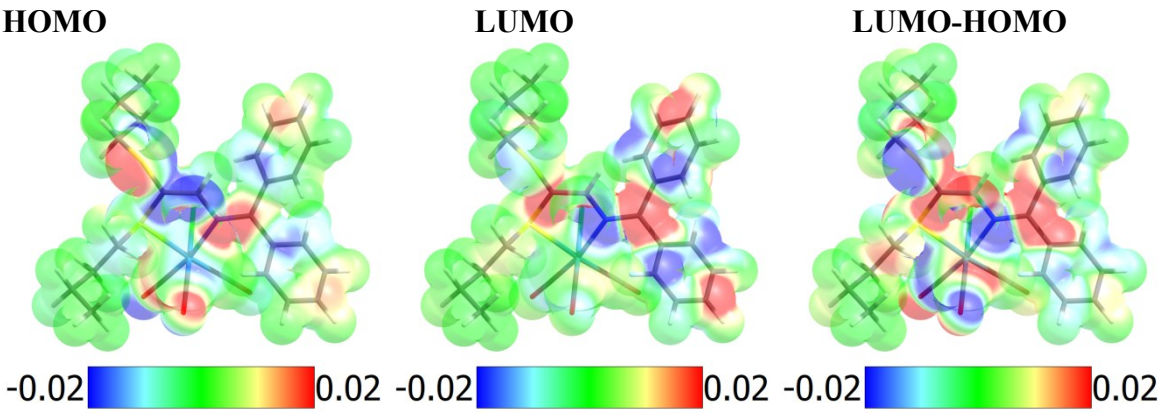

Figure S61. Electron-density map of the HOMO and LUMO ; Electron-density difference (LUMO-HOMO)

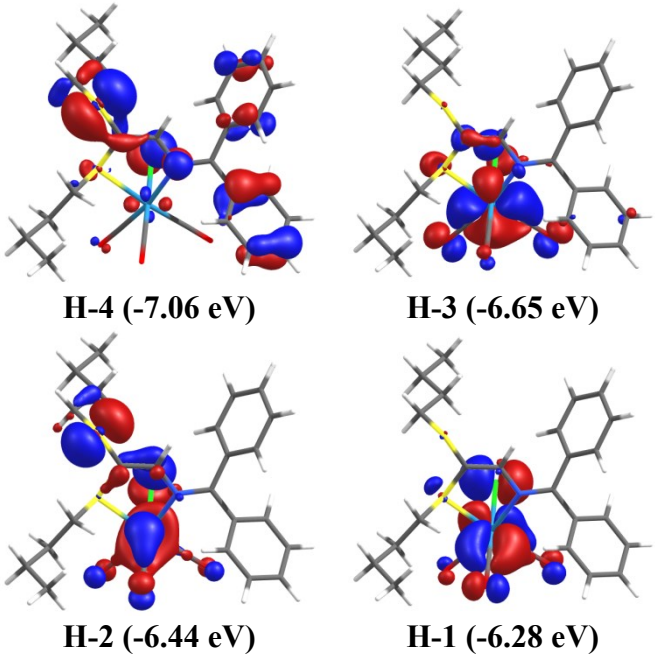

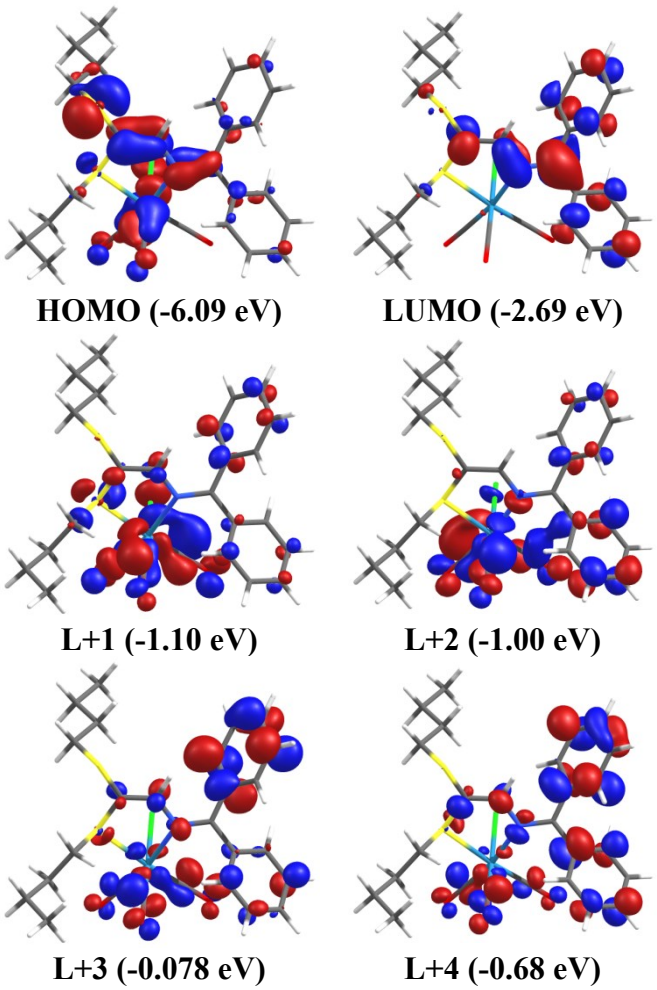

Figure S62. Representations of the frontier MOs for **1e** applying a THF solvent field. The isoval = 0.04.

Table S19. Relative atomic contributions (%) of the various fragments to the frontier MOs of **1e**. [a]

Fragments	H-4	H-3	H-2	H-1	HOMO	LUMO	L+1	L+2	L+3	L+4
Re	3%	**52%**	31%	**46%**	19%	2%	21%	19%	13%	7%
3(CO)	2%	22%	13%	21%	9%	2%	28%	31%	15%	13%
Cl	9%	7%	14%	24%	8%	0%	8%	4%	1%	1%
N-S_Ligands	**85%**	20%	**42%**	9%	**64%**	**95%**	**43%**	**46%**	**72%**	**79%**

[a]H = HOMO, L = LUMO; the values in bold represent the largest contributions.

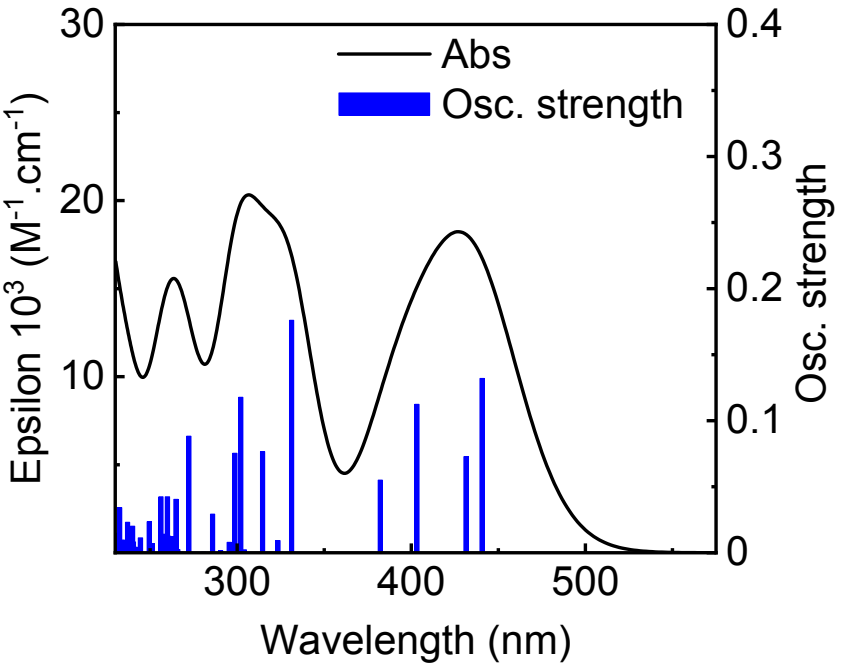

Figure S63. Simulated absorption spectrum for **1e** by TDDFT computations. Bar graph reporting the calculated oscillator strength and calculated position of the 100st electronic transitions calculated by TDDFT for **1e** (bar graph; f = computed oscillator strength).

Table S20. Calculated positions, oscillator strengths (f) and major contributions (%) of the first 100 singlet-singlet electronic transitions for **1e**.

No.	λ (nm)	f	Major contributions (%)
1	440.6	0.132	H-1→LUMO (24%), HOMO→LUMO (72%)
2	431.5	0.0728	H-1→LUMO (75%), HOMO→LUMO (20%)
3	403.2	0.1124	H-2→LUMO (87%)
4	382.2	0.055	H-3→LUMO (93%)
5	331.3	0.176	H-4→LUMO (96%)
6	323.4	0.0092	H-5→LUMO (97%)
7	314.6	0.0766	H-6→LUMO (96%)
8	304.1	0.0023	H-1→L+1 (46%), HOMO→L+1 (27%)
9	302.1	0.1177	H-7→LUMO (82%)
10	298.7	0.0753	H-7→LUMO (13%), H-2→L+1 (13%), HOMO→L+1 (30%), HOMO→L+2 (11%)
11	298.3	0.0041	H-8→LUMO (91%)
12	295.4	0.0079	H-9→LUMO (87%)
13	290.5	0.0016	H-2→L+2 (10%), H-1→L+2 (54%), HOMO→L+2 (13%)
14	285.9	0.0293	H-1→L+1 (22%), H-1→L+2 (14%), HOMO→L+2 (34%)
15	280.7	4E-4	H-3→L+1 (50%), H-3→L+2 (21%)
16	272.3	0.0883	H-2→L+1 (21%), HOMO→L+1 (20%), HOMO→L+3 (25%)
17	267.8	3E-4	H-11→LUMO (25%), H-10→LUMO (50%)
18	266.0	0.0024	H-11→LUMO (25%), H-2→L+1 (29%), HOMO→L+3 (29%)
19	264.9	0.0404	H-2→L+2 (41%), HOMO→L+2 (21%)
20	263.7	0.0122	H-11→LUMO (36%), H-10→LUMO (19%), HOMO→L+3 (12%)
21	260.7	0.0125	H-12→LUMO (65%), H-3→L+2 (14%)
22	260.0	0.0424	H-12→LUMO (32%), H-3→L+2 (29%)
23	258.1	0.0141	H-2→L+2 (14%), H-1→L+3 (20%), HOMO→L+4 (37%)
24	256.3	0.0424	H-1→L+3 (34%), HOMO→L+4 (33%)
25	251.3	0.007	H-2→L+3 (12%), H-1→L+4 (59%)
26	249.5	0.0235	H-2→L+3 (41%), H-1→L+4 (18%)

27	244.5	0.0113	HOMO→L+5 (63%)
28	241.5	0.0042	H-2→L+4 (57%)
29	240.4	0.0082	HOMO→L+5 (10%), HOMO→L+6 (26%)
30	239.9	0.0201	H-3→L+3 (48%)
31	238.4	0.014	H-1→L+5 (27%), HOMO→L+6 (15%)
32	237.1	0.0231	H-15→LUMO (49%), H-13→LUMO (15%)
33	235.8	0.0015	H-1→L+5 (54%)
34	234.6	0.0032	H-3→L+4 (54%)
35	234.1	0.0096	H-4→L+1 (71%)
36	232.5	0.0342	H-3→L+4 (12%), HOMO→L+6 (16%), HOMO→L+8 (14%)
37	231.2	0.0142	H-1→L+8 (15%), HOMO→L+8 (18%)
38	230.5	0.0148	H-2→L+5 (19%), H-2→L+7 (10%), H-1→L+8 (12%)
39	229.5	0.0023	H-2→L+5 (22%), HOMO→L+7 (18%)
40	227.9	0.011	H-4→L+2 (63%)
41	227.0	0.013	H-9→L+1 (10%), H-2→L+6 (10%), H-2→L+7 (21%)
42	225.8	0.0113	H-5→L+1 (32%), H-2→L+5 (20%)
43	224.6	0.0129	H-8→L+1 (17%), H-6→L+1 (14%), H-3→L+8 (14%)
44	223.9	0.0074	H-1→L+6 (50%), H-1→L+7 (27%)
45	223.4	0.034	H-13→LUMO (29%)
46	223.2	0.018	H-13→LUMO (29%), H-6→L+2 (10%), H-3→L+5 (15%)
47	222.3	0.0119	H-13→LUMO (10%), H-9→L+1 (27%)
48	222.0	0.0242	H-6→L+1 (12%), H-5→L+2 (12%), H-3→L+5 (23%)
49	220.9	0.0101	H-5→L+1 (16%), H-5→L+2 (23%)
50	219.6	0.0081	H-3→L+5 (11%), H-1→L+10 (22%), HOMO→L+10 (13%)
51	218.6	0.0249	H-9→L+1 (13%), H-1→L+10 (10%)
52	218.0	0.0171	H-8→L+2 (14%), H-4→L+3 (22%), H-2→L+6 (14%)
53	217.2	0.0018	H-8→L+2 (11%), H-7→L+1 (10%), H-6→L+1 (10%), H-2→L+6 (30%), H-2→L+7 (12%)
54	216.9	0.0319	H-4→L+3 (24%)
55	216.8	0.0058	H-8→L+1 (16%), H-6→L+1 (26%), H-5→L+2 (11%)
56	216.5	0.0011	H-14→LUMO (92%)
57	216.0	0.0227	H-9→L+2 (19%), H-3→L+5 (10%), H-1→L+10 (10%)
58	215.7	0.0368	H-9→L+2 (22%)
59	213.8	0.0028	H-5→L+3 (26%), H-5→L+4 (10%), H-4→L+4 (17%)
60	213.7	0.0077	H-2→L+8 (24%), HOMO→L+8 (11%), HOMO→L+9 (11%)
61	213.3	0.0225	H-4→L+4 (43%)
62	212.5	0.0234	H-2→L+8 (15%), HOMO→L+9 (20%)
63	211.1	0.0292	H-7→L+1 (15%), H-3→L+6 (18%), H-1→L+9 (12%)
64	210.1	0.0143	H-5→L+4 (16%)
65	209.3	0.0023	H-17→LUMO (17%), H-16→LUMO (66%)
66	209.0	0.0146	H-7→L+1 (24%), H-7→L+2 (10%), H-6→L+4 (11%)
67	208.8	0.0279	H-7→L+2 (15%), H-5→L+3 (20%), H-3→L+6 (15%)
68	208.4	0.0233	--
69	208.2	0.0116	H-1→L+9 (10%), HOMO→L+11 (23%)
70	207.8	0.0564	H-6→L+3 (19%), H-3→L+7 (10%)
71	207.4	0.0086	H-17→LUMO (52%), H-16→LUMO (24%)
72	207.0	0.0082	H-7→L+3 (12%), H-6→L+3 (31%)
73	205.5	0.1149	H-8→L+3 (15%), H-7→L+2 (21%), H-6→L+3 (10%), H-5→L+4 (11%)
74	205.0	0.0031	H-19→LUMO (10%), H-18→LUMO (69%), H-17→LUMO (12%)
75	204.5	0.0081	H-3→L+10 (11%), H-1→L+11 (12%), H-1→L+12 (18%)
76	204.0	0.0059	HOMO→L+11 (15%)
77	203.6	0.0057	H-22→LUMO (13%), H-19→LUMO (37%), H-18→LUMO (12%)
78	203.4	0.0033	H-21→LUMO (18%)
79	203.2	0.035	H-21→LUMO (10%), H-4→L+5 (24%)

80	202.9	0.0403	H-21→LUMO (30%), H-4→L+5 (13%)
81	202.6	0.0049	H-1→L+11 (10%), HOMO→L+12 (14%)
82	202.2	0.0095	H-9→L+3 (11%), H-8→L+3 (28%), H-1→L+11 (10%)
83	201.3	0.0041	H-9→L+3 (39%), H-8→L+3 (16%)
84	200.3	0.0349	H-9→L+3 (18%), H-8→L+4 (11%), H-6→L+4 (12%)
85	200.1	0.0288	H-11→L+1 (15%), H-10→L+1 (25%)
86	199.3	0.0058	H-4→L+6 (19%)
87	199.2	0.0095	H-10→L+2 (16%)
88	198.4	0.0219	H-22→LUMO (10%), H-11→L+1 (16%), H-10→L+1 (19%), H-7→L+4 (10%)
89	198.0	3E-4	H-11→L+1 (14%), H-8→L+4 (17%), H-7→L+4 (11%), H-5→L+5 (27%)
90	197.8	0.0083	H-22→LUMO (13%), H-8→L+4 (17%)
91	197.3	0.0417	H-9→L+4 (26%), H-8→L+4 (14%)
92	197.2	0.0041	H-11→L+2 (18%), H-10→L+2 (17%), H-2→L+10 (12%)
93	197.0	0.0059	H-12→L+1 (23%), H-12→L+2 (12%), H-9→L+4 (21%)
94	196.5	0.0049	H-9→L+4 (13%), H-2→L+10 (14%), HOMO→L+14 (12%)
95	196.0	0.0619	H-22→LUMO (13%), H-5→L+6 (10%)
96	195.8	0.0422	H-7→L+4 (14%), H-6→L+5 (29%)
97	194.9	0.0198	H-6→L+5 (21%), H-4→L+7 (14%)
98	194.5	0.0199	H-11→L+2 (27%)
99	194.1	0.001	H-2→L+11 (18%)
100	193.7	0.0015	H-23→LUMO (11%), H-21→LUMO (12%), H-20→LUMO (37%)

Complex 1e (triplet state)

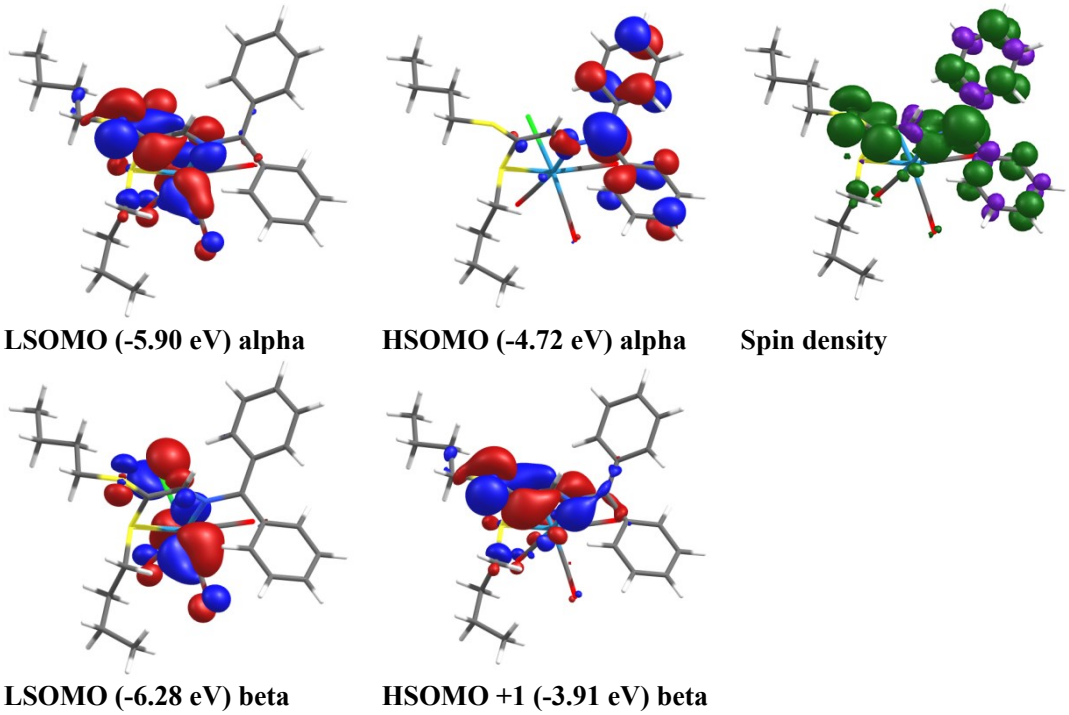

Figure S64. Left, representations of the semi-occupied MOs for **1e** in its lowest energy triplet state. The isoval = 0.04. Right, Alpha – beta SCF spin density. The isoval = 0.003 (green lobe positive, purple lobe negative).

Table S21. Relative atomic contributions (%) of the various fragments to the semi-occupied MOs of **1e**.[b]

Fragments	LS-1	LSOMO	HSOMO	HS+1
Re	**44%**	19%	2%	5%
3(CO)	19%	9%	2%	4%
Cl	20%	6%	0%	1%
N-S_Ligands	17%	**65%**	**95%**	**90%**

[b]HS = HSOMO, LS = LSOMO; the values in bold represent the largest contributions.

Complex 1f (singlet state)

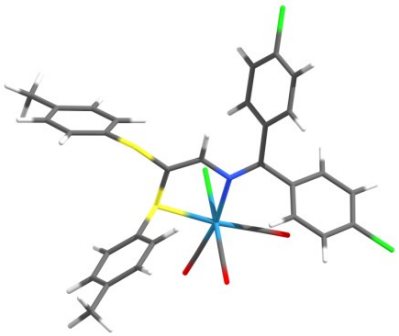

Figure S65. Optimized geometry for **1f** applying a THF solvent field.

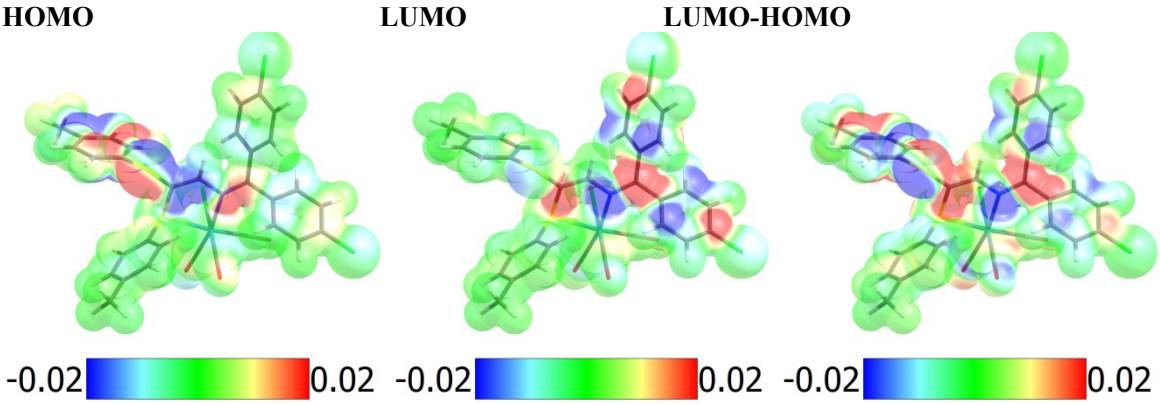

Figure S66. Electron-density map of the HOMO and LUMO ; Electron-density difference (LUMO-HOMO)

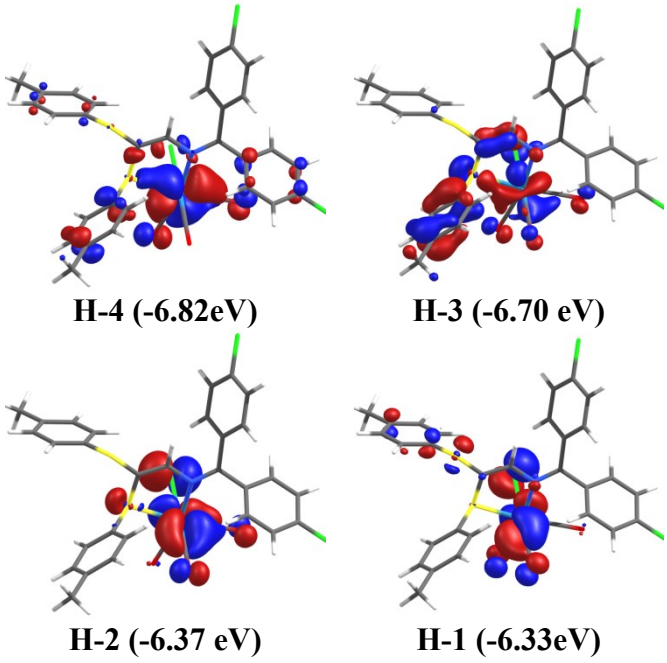

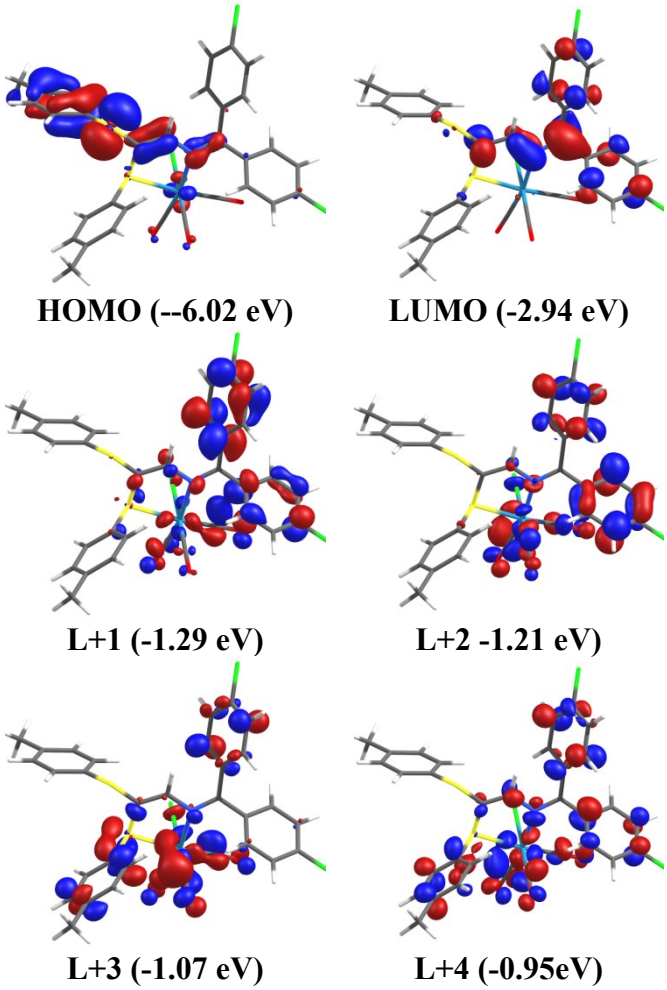

Figure S67. Representations of the frontier MOs for **1f** applying a THF solvent field. The isoval = 0.04.

Table S22. Relative atomic contributions (%) of the various fragments to the frontier MOs of **1f**. [a]

Fragments	H-4	H-3	H-2	H-1	HOMO	LUMO	L+1	L+2	L+3	L+4
Re	**43%**	28%	**43%**	**41%**	4%	2%	10%	13%	19%	14%
3(CO)	19%	12%	19%	19%	2%	2%	12%	15%	20%	16%
Cl	3%	7%	23%	18%	1%	0%	2%	4%	3%	1%
N-S_Ligands	35%	**53%**	14%	22%	**92%**	**96%**	**76%**	**68%**	**58%**	**70%**

[a]H = HOMO, L = LUMO; the values in bold represent the largest contributions.

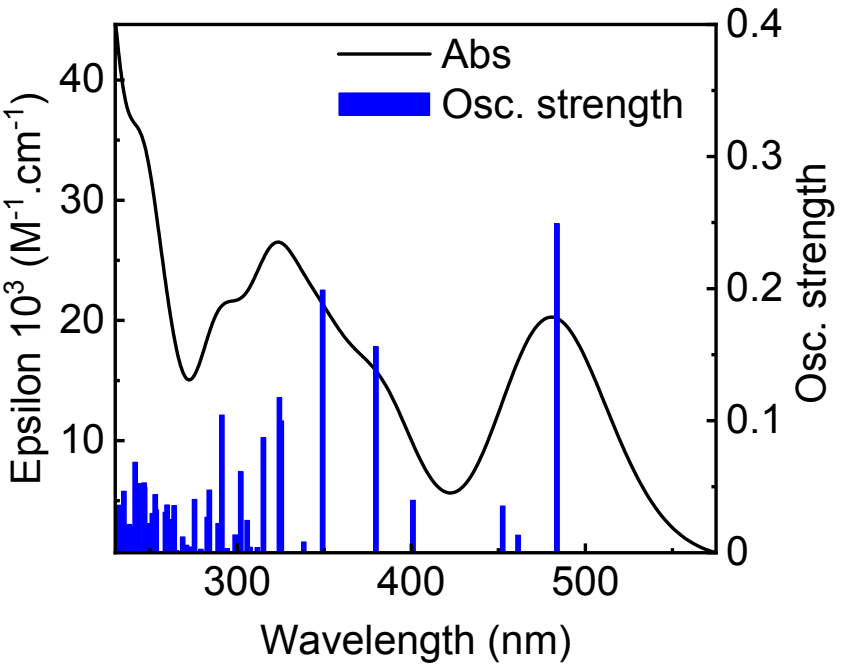

Figure S68. Simulated absorption spectrum for **1f** by TDDFT computations. Bar graph reporting the calculated oscillator strength and calculated position of the 100st electronic transitions calculated by TDDFT for **1f** (bar graph; f = computed oscillator strength).

Table S23. Calculated positions, oscillator strengths (f) and major contributions (%) of the first 100 singlet-singlet electronic transitions for **1f**.

No.	λ (nm)	f	Major contributions (%)
1	483.7	0.2492	HOMO→LUMO (94%)
2	461.3	0.0133	H-2→LUMO (33%), H-1→LUMO (62%)
3	452.5	0.0354	H-2→LUMO (64%), H-1→LUMO (33%)
4	401.0	0.0397	H-4→LUMO (39%), H-3→LUMO (59%)
5	379.7	0.156	H-4→LUMO (59%), H-3→LUMO (38%)
6	349.1	0.1989	H-5→LUMO (92%)
7	338.3	0.0082	H-6→LUMO (93%)
8	325.3	0.0999	H-8→LUMO (40%), H-7→LUMO (55%)
9	324.3	0.1175	H-8→LUMO (53%), H-7→LUMO (44%)
10	315.1	0.0871	H-9→LUMO (81%)
11	311.6	0.004	H-10→LUMO (91%)
12	307.4	0.0042	H-11→LUMO (87%)
13	305.7	0.0245	H-1→L+1 (15%), H-1→L+3 (19%), HOMO→L+1 (14%)
14	302.1	0.0614	H-2→L+1 (13%), H-1→L+1 (15%), H-1→L+2 (11%), HOMO→L+1 (16%)
15	298.9	0.0136	H-13→LUMO (80%)
16	294.2	0.0031	H-2→L+1 (14%), H-2→L+2 (34%), H-2→L+4 (13%)
17	291.3	0.1043	H-12→LUMO (21%), HOMO→L+1 (32%)
18	290.4	0.0112	H-2→L+1 (11%), HOMO→L+2 (40%)
19	289.1	0.0222	H-12→LUMO (53%), HOMO→L+1 (13%)
20	284.0	0.0475	H-1→L+2 (12%), HOMO→L+3 (48%)
21	282.9	0.0269	HOMO→L+2 (27%), HOMO→L+3 (15%)
22	279.2	0.0027	HOMO→L+4 (10%), HOMO→L+5 (46%)

23	275.5	0.0404	H-1→L+1 (24%), H-1→L+3 (13%), HOMO→L+4 (33%), HOMO→L+5 (17%)
24	274.0	0.0034	H-14→LUMO (16%), HOMO→L+4 (17%)
25	272.6	0.0044	H-1→L+2 (11%), H-1→L+3 (33%), HOMO→L+4 (13%)
26	270.9	0.0057	H-15→LUMO (25%), H-14→LUMO (51%)
27	268.7	0.012	H-2→L+2 (12%), H-2→L+3 (51%)
28	265.1	0.0015	H-15→LUMO (25%), H-1→L+2 (10%), HOMO→L+6 (11%)
29	263.8	0.0356	H-15→LUMO (29%), H-3→L+1 (11%), H-2→L+4 (13%)
30	262.6	0.0069	H-2→L+1 (15%), H-2→L+4 (29%), H-2→L+5 (25%)
31	262.1	3E-4	H-2→L+4 (10%), H-1→L+4 (21%), H-1→L+5 (25%)
32	261.6	0.0251	H-1→L+1 (11%), H-1→L+4 (22%), H-1→L+5 (36%)
33	259.7	0.0362	H-3→L+1 (13%), H-2→L+4 (13%), H-2→L+5 (24%), H-1→L+5 (17%)
34	258.8	0.0307	H-2→L+5 (13%), HOMO→L+6 (47%)
35	253.5	0.0325	HOMO→L+7 (64%)
36	253.0	0.044	H-4→L+1 (22%), H-3→L+1 (28%), HOMO→L+7 (15%)
37	252.7	0.0069	H-1→L+6 (11%), HOMO→L+9 (37%), HOMO→L+10 (12%)
38	251.3	0.0297	H-16→LUMO (86%)
39	250.8	0.0023	H-4→L+2 (15%), H-3→L+3 (35%)
40	249.4	0.0214	H-4→L+1 (13%), H-3→L+2 (17%), H-3→L+3 (15%), H-2→L+6 (25%)
41	248.6	0.0221	H-3→L+2 (12%), H-2→L+6 (28%), H-1→L+6 (26%)
42	246.8	0.0497	H-2→L+6 (23%), H-1→L+6 (31%)
43	246.6	0.053	HOMO→L+8 (74%)
44	245.1	0.0036	H-4→L+3 (25%), H-3→L+4 (19%)
45	243.6	0.0523	H-4→L+2 (21%), H-4→L+3 (17%), H-3→L+4 (30%)
46	242.5	0.0355	H-3→L+5 (16%), HOMO→L+9 (17%), HOMO→L+10 (27%)
47	241.4	0.0686	H-3→L+5 (41%), H-1→L+7 (12%)
48	240.4	0.0203	H-5→L+1 (13%), H-1→L+7 (26%)
49	240.2	0.0046	H-5→L+1 (27%), H-2→L+7 (15%), H-1→L+7 (23%)
50	239.2	8E-4	H-5→L+1 (10%), H-2→L+7 (29%)
51	238.0	0.0215	H-2→L+7 (35%)
52	236.5	0.0139	H-5→L+2 (36%)
53	235.4	0.0184	H-4→L+4 (12%), H-4→L+5 (15%)
54	235.0	0.0466	H-4→L+4 (11%), H-4→L+5 (26%)
55	234.3	0.0081	H-1→L+9 (18%), H-1→L+11 (13%), H-1→L+12 (15%)
56	233.4	0.0185	H-19→LUMO (26%)
57	232.6	0.0187	H-4→L+5 (12%), H-2→L+9 (18%)
58	232.0	0.036	H-19→LUMO (10%), H-4→L+4 (12%), H-3→L+6 (12%)
59	231.5	8E-4	H-6→L+1 (52%)
60	231.2	0.0326	H-4→L+6 (16%), H-3→L+6 (18%)
61	231.1	0.0035	H-6→L+1 (22%), H-1→L+8 (13%)
62	229.8	0.0309	H-2→L+8 (12%), H-1→L+8 (25%), H-1→L+9 (30%)
63	229.6	0.0043	H-5→L+3 (11%), H-1→L+8 (26%)
64	229.5	0.0039	H-17→LUMO (89%)
65	228.9	0.0016	H-8→L+2 (28%)
66	228.4	0.0013	H-18→LUMO (94%)
67	228.2	0.008	H-2→L+8 (54%)
68	227.0	0.0373	H-6→L+2 (45%), H-5→L+2 (14%)

69	226.7	0.0411	H-7→L+1 (19%), H-6→L+2 (24%)
70	226.4	0.0176	H-7→L+1 (25%), HOMO→L+11 (12%)
71	225.8	0.0135	H-5→L+5 (12%), H-2→L+9 (14%), H-2→L+12 (12%)
72	225.5	0.0751	H-7→L+1 (16%)
73	224.8	0.0183	H-5→L+4 (10%), H-5→L+5 (24%)
74	224.7	0.0067	H-2→L+12 (11%)
75	224.5	0.0072	H-6→L+3 (14%), H-1→L+10 (10%), HOMO→L+11 (11%)
76	223.6	0.0205	H-2→L+11 (11%)
77	223.5	0.0169	H-7→L+2 (14%), H-5→L+4 (20%)
78	222.8	0.0155	H-7→L+2 (42%)
79	222.5	0.0365	H-7→L+2 (15%), H-6→L+3 (22%), H-1→L+10 (10%)
80	222.1	0.0072	H-4→L+6 (19%), H-3→L+7 (22%)
81	221.6	0.0584	H-9→L+1 (12%), H-1→L+10 (13%)
82	221.3	0.0081	H-8→L+1 (12%), H-3→L+7 (10%)
83	220.2	0.0676	H-8→L+1 (21%)
84	220.0	0.0203	H-8→L+1 (20%)
85	219.6	0.0147	H-2→L+10 (58%), H-1→L+10 (15%)
86	219.1	0.0521	H-6→L+4 (26%), H-6→L+5 (30%)
87	218.7	0.0044	HOMO→L+12 (22%)
88	218.2	0.0076	H-11→L+2 (15%), H-4→L+7 (13%)
89	218.1	0.0512	H-11→L+1 (18%), H-4→L+7 (20%)
90	217.6	0.0121	H-4→L+7 (14%), H-3→L+9 (21%)
91	216.9	0.0026	H-6→L+4 (25%), H-6→L+5 (29%)
92	216.7	0.0711	H-7→L+3 (47%), H-3→L+8 (13%)
93	215.8	0.0063	H-2→L+16 (19%), H-1→L+15 (10%), H-1→L+16 (12%)
94	215.2	0.0228	H-3→L+8 (29%), H-3→L+9 (12%)
95	214.5	0.031	H-8→L+3 (17%), H-5→L+6 (27%)
96	214.0	0.008	H-8→L+3 (29%), H-5→L+6 (25%)
97	213.1	0.0096	H-3→L+9 (10%), HOMO→L+15 (10%)
98	212.9	0.02	H-7→L+4 (39%), H-7→L+5 (23%)
99	212.8	0.0066	H-7→L+4 (14%), HOMO→L+15 (27%)
100	212.4	0.0309	H-9→L+3 (16%)

Complex 1f (triplet state)

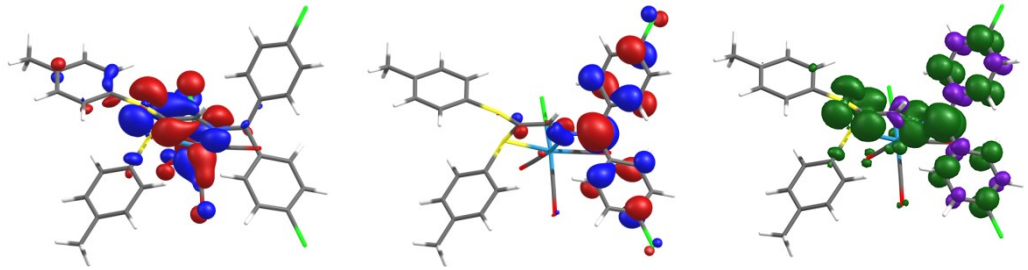

LSOMO (-5.93 eV) alpha **HSOMO (-4.91 eV) alpha** **Spin density**

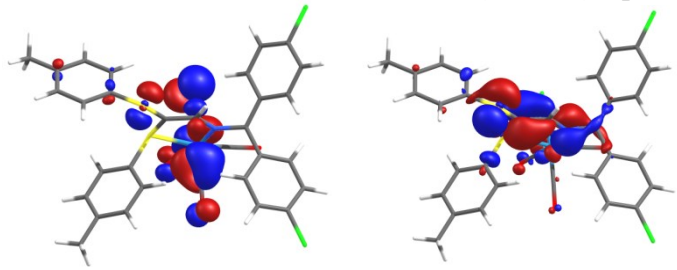

LSOMO-1 (-6.30 eV) beta **HSOMO+1 (-4.10 eV) beta**

Figure S69. Left, representations of the semi-occupied MOs for **1f** in its lowest energy triplet state. The isoval = 0.04. Right, Alpha – beta SCF spin density. The isoval = 0.003 (green lobe positive, purple lobe negative).

Table S24. Relative atomic contributions (%) of the various fragments to the semi-occupied MOs of **1f**.[b]

Fragments	LS-1	LSOMO	HSOMO	HS+1
Re	**42%**	17%	2%	5%
3(CO)	18%	8%	2%	4%
Cl	18%	5%	0%	1%
N-S_Ligands	22%	**69%**	**96%**	**90%**

[b]HS = HSOMO, LS = LSOMO; the values in bold represent the largest contributions.

Complex 1g (singlet state)

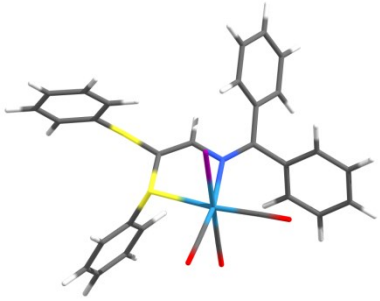

Figure S70. Optimized geometry for **1g** applying a THF solvent field.

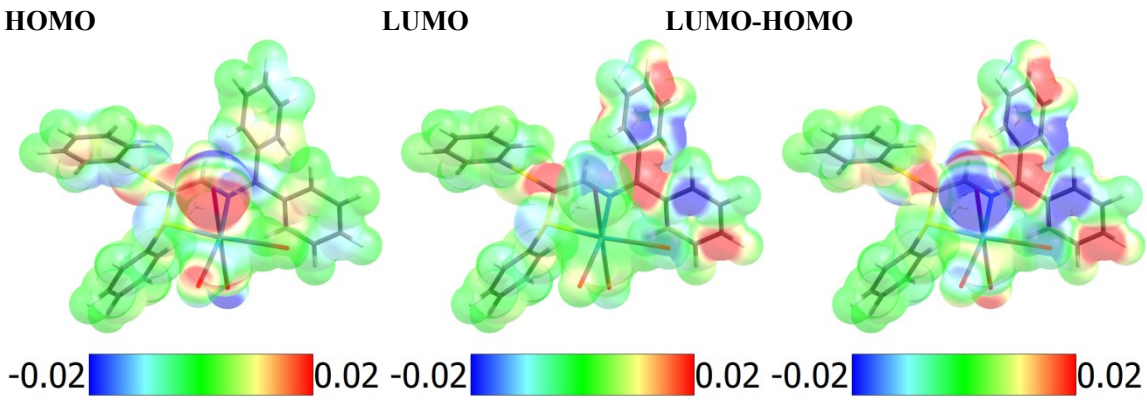

Figure S71. Electron-density map of the HOMO and LUMO ; Electron-density difference (LUMO-HOMO)

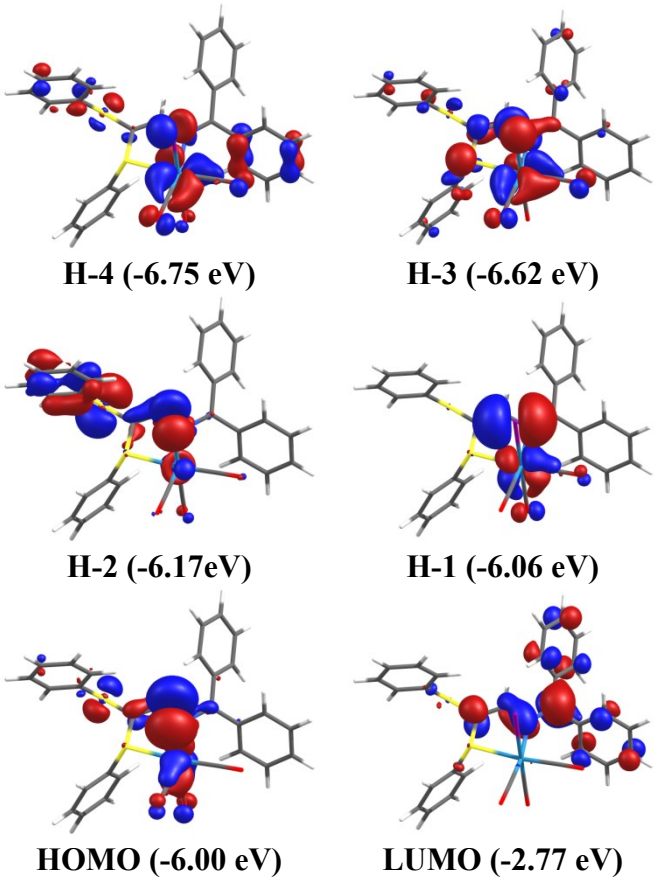

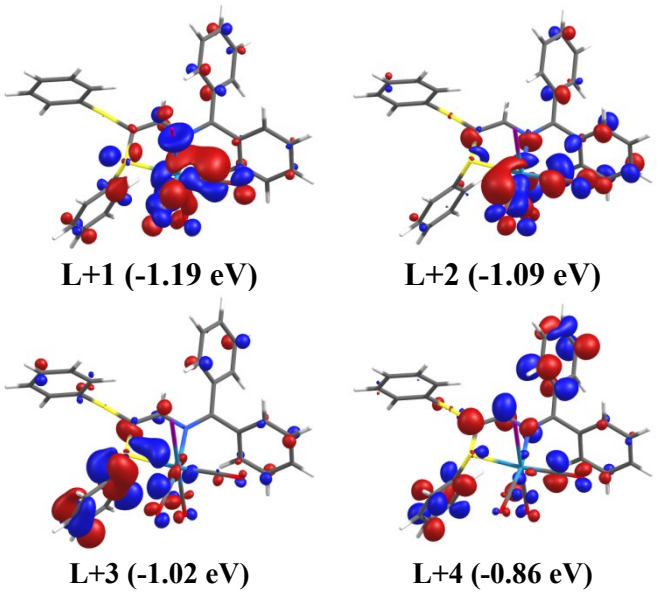

Figure S72. Representations of the frontier MOs for **1g** applying a THF solvent field. The isoval = 0.04.

Table S25. Relative atomic contributions (%) of the various fragments to the frontier MOs of **1g.**[a]

Fragments	H-4	H-3	H-2	H-1	HOMO	LUMO	L+1	L+2	L+3	L+4
Re	**37%**	27%	8%	24%	22%	2%	27%	19%	15%	8%
3(CO)	15%	12%	3%	11%	10%	2%	24%	27%	9%	10%
I	9%	12%	16%	**59%**	**35%**	0%	12%	4%	3%	2%
N-S_Ligands	36%	**44%**	**71%**	6%	30%	**85%**	**36%**	**42%**	**74%**	**76%**

[a]H = HOMO, L = LUMO; the values in bold represent the largest contributions.

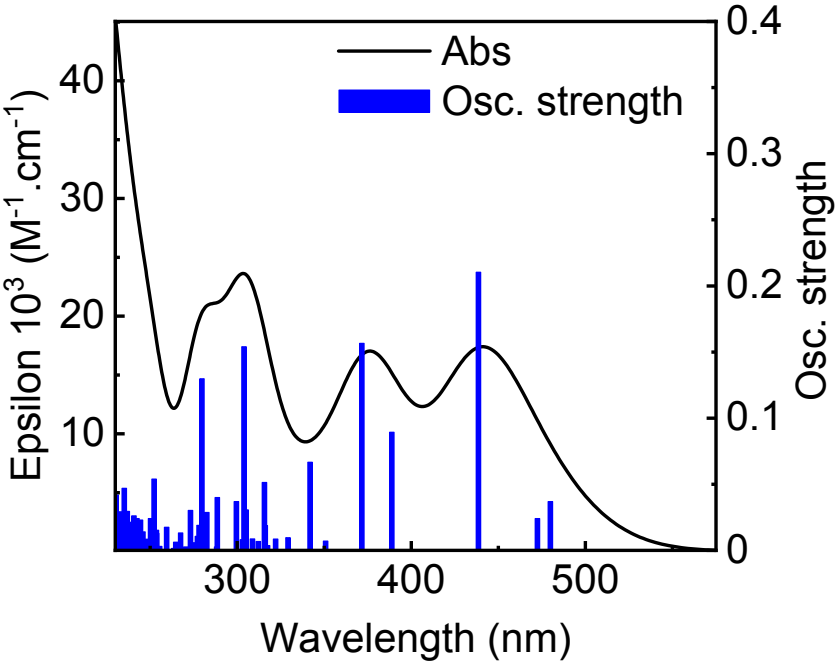

Figure S73. Simulated absorption spectrum for **1g** by TDDFT computations. Bar graph reporting the calculated oscillator strength and calculated position of the 100st electronic transitions calculated by TDDFT for **1g** (bar graph; f = computed oscillator strength).

Table S26. Calculated position, oscillator strength (f) and major contributions (%) of the first 100 singlet-singlet electronic transitions for **1g**.

No.	λ (nm)	f	Major contributions (%)
1	479.9	0.037	H-1→LUMO (24%), HOMO→LUMO (72%)
2	472.4	0.0241	H-1→LUMO (74%), HOMO→LUMO (19%)
3	438.6	0.2104	H-2→LUMO (88%)
4	388.8	0.0894	H-4→LUMO (28%), H-3→LUMO (69%)
5	371.6	0.1566	H-4→LUMO (69%), H-3→LUMO (26%)
6	350.8	0.0071	H-6→LUMO (12%), H-5→LUMO (84%)
7	341.9	0.0667	H-7→LUMO (25%), H-6→LUMO (61%)
8	329.2	0.0096	H-8→LUMO (93%)
9	322.1	0.0086	H-7→LUMO (66%), H-6→LUMO (22%)
10	317.4	0.0037	H-10→LUMO (28%), H-1→L+1 (29%), HOMO→L+1 (22%)
11	316.1	0.0188	H-12→LUMO (15%), H-11→LUMO (11%), H-10→LUMO (42%), HOMO→L+1 (17%)
12	315.7	0.0514	H-11→LUMO (70%)
13	312.1	0.0068	H-1→L+1 (24%), HOMO→L+1 (35%), HOMO→L+2 (10%)
14	308.8	0.0087	H-9→LUMO (84%)
15	305.1	0.0307	H-12→LUMO (61%)
16	303.9	0.1541	H-13→LUMO (78%), H-12→LUMO (11%)
17	302.9	0.0081	H-1→L+2 (56%), HOMO→L+2 (14%)
18	299.5	0.037	H-1→L+1 (18%), H-1→L+2 (19%), HOMO→L+2 (32%)
19	288.6	0.04	HOMO→L+2 (13%), HOMO→L+3 (66%)
20	288.2	0.0027	H-4→L+1 (15%), H-2→L+1 (47%)
21	282.6	0.0287	H-1→L+3 (81%)
22	279.8	0.1298	H-14→LUMO (10%), H-3→L+1 (16%), H-2→L+1 (18%), H-2→L+2 (22%)
23	278.1	0.019	H-2→L+2 (31%), H-2→L+3 (21%), HOMO→L+4 (21%)
24	277.2	0.0107	H-14→LUMO (55%), H-2→L+1 (12%)
25	274.3	0.0058	H-3→L+1 (10%), H-2→L+2 (16%), H-2→L+3 (34%), HOMO→L+4 (10%)
26	273.2	0.0303	H-14→LUMO (14%), H-2→L+3 (27%), HOMO→L+4 (44%)
27	270.5	0.0027	H-1→L+4 (71%)
28	267.5	0.0132	H-3→L+2 (19%), H-1→L+4 (10%), HOMO→L+5 (36%)
29	267.1	0.0019	H-3→L+2 (10%), H-2→L+4 (10%), HOMO→L+5 (49%)
30	264.7	0.0063	H-2→L+4 (62%)
31	263.6	0.0015	H-1→L+5 (87%)
32	259.5	0.0176	H-4→L+1 (38%), H-3→L+1 (24%)
33	255.5	0.0031	H-15→LUMO (11%), H-2→L+5 (45%)
34	254.6	0.0012	H-5→L+1 (10%), H-3→L+3 (35%), H-2→L+5 (20%)
35	253.8	0.0129	H-3→L+2 (20%), H-2→L+5 (10%), H-1→L+6 (10%)
36	253.6	0.0153	HOMO→L+6 (64%)
37	252.6	0.0047	H-15→LUMO (15%), H-4→L+2 (27%)
38	252.3	0.054	H-15→LUMO (48%)
39	251.4	0.0155	H-4→L+2 (10%), HOMO→L+7 (16%), HOMO→L+8 (13%)
40	250.3	0.0241	H-1→L+6 (38%)
41	248.5	0.0085	H-5→L+2 (18%), H-1→L+6 (11%), HOMO→L+7 (15%)
42	248.2	0.0053	H-5→L+2 (11%), HOMO→L+7 (16%), HOMO→L+8 (27%)

43	246.9	0.0028	H-4→L+3 (11%), H-1→L+7 (18%), HOMO→L+8 (20%)
44	245.9	0.0141	H-3→L+4 (10%)
45	245.3	0.0058	H-2→L+6 (35%), H-1→L+7 (17%), HOMO→L+8 (11%)
46	244.5	0.023	H-2→L+6 (15%), H-2→L+7 (17%), H-1→L+8 (26%)
47	243.5	0.0136	H-4→L+3 (31%), H-1→L+7 (30%)
48	243.2	0.0206	H-5→L+1 (10%), H-1→L+8 (37%)
49	242.4	0.0241	H-3→L+4 (25%), H-2→L+7 (25%)
50	241.2	0.0228	H-3→L+4 (25%), H-2→L+6 (11%), H-2→L+7 (11%)
51	240.7	0.0262	H-4→L+3 (11%), HOMO→L+9 (23%), HOMO→L+10 (13%)
52	240.1	0.003	H-16→LUMO (20%)
53	239.5	0.007	H-17→LUMO (18%), H-16→LUMO (47%)
54	238.6	0.0136	H-2→L+8 (16%), HOMO→L+11 (22%)
55	238.2	0.0035	H-3→L+5 (11%), H-2→L+8 (10%), H-1→L+9 (12%), HOMO→L+9 (14%)
56	237.4	0.0215	H-4→L+4 (16%), HOMO→L+11 (14%)
57	236.9	0.0296	H-3→L+5 (40%), HOMO→L+9 (14%)
58	236.5	0.0028	H-3→L+5 (13%), H-2→L+8 (17%), H-1→L+9 (15%)
59	235.8	0.006	H-1→L+9 (29%), HOMO→L+12 (10%)
60	235.2	0.047	H-5→L+3 (14%), H-4→L+4 (36%)
61	234.9	0.0034	H-1→L+9 (18%), H-1→L+10 (24%), H-1→L+12 (18%)
62	233.4	0.0214	H-5→L+3 (18%), HOMO→L+10 (22%)
63	233.2	0.0293	H-5→L+3 (13%), H-2→L+9 (13%), HOMO→L+10 (10%)
64	231.5	0.0147	H-17→LUMO (25%), H-6→L+3 (14%), H-1→L+10 (14%)
65	230.7	0.0175	H-8→L+1 (18%), H-2→L+10 (10%)
66	230.5	0.042	H-17→LUMO (15%), H-6→L+3 (16%)
67	230.2	0.0359	H-10→L+1 (12%), H-1→L+10 (21%), H-1→L+12 (12%)
68	229.4	0.0394	H-10→L+2 (12%)
69	229.0	0.0315	H-6→L+3 (15%), H-1→L+12 (10%)
70	228.4	0.006	H-4→L+5 (38%), H-2→L+10 (11%)
71	228.0	0.0094	H-1→L+11 (22%), HOMO→L+12 (24%)
72	227.6	0.0058	H-7→L+1 (38%), H-6→L+1 (18%)
73	226.5	0.0461	H-3→L+6 (24%), H-2→L+11 (12%)
74	225.6	0.0053	H-10→L+1 (20%), H-10→L+2 (10%), H-8→L+2 (17%), H-7→L+1 (11%)
75	225.0	0.0198	H-8→L+1 (22%), H-2→L+11 (10%)
76	224.8	0.0223	H-6→L+4 (10%), H-5→L+4 (50%)
77	224.0	0.013	H-9→L+1 (34%), H-7→L+2 (10%)
78	223.8	0.0651	H-9→L+1 (10%), H-2→L+11 (20%)
79	223.1	0.003	H-9→L+1 (15%), H-8→L+2 (14%)
80	223.0	0.0326	H-9→L+1 (10%), H-7→L+2 (13%)
81	222.2	0.0191	H-7→L+3 (13%)
82	221.8	0.0089	H-3→L+7 (46%)
83	221.4	0.0487	H-7→L+3 (12%), H-6→L+4 (33%)
84	220.9	0.0235	H-5→L+5 (25%), H-1→L+14 (14%)
85	220.6	0.0066	H-5→L+5 (19%), H-3→L+8 (13%), H-2→L+11 (10%)
86	220.3	0.0038	H-8→L+2 (11%), H-7→L+2 (13%), H-7→L+3 (11%), H-4→L+6 (11%)
87	219.7	0.0076	H-10→L+3 (27%), H-9→L+2 (27%)
88	219.5	0.0283	H-5→L+5 (10%), HOMO→L+14 (10%)

89	219.3	0.0124	H-12→L+1 (12%), H-11→L+1 (34%)
90	218.8	4E-4	H-9→L+2 (20%), H-3→L+8 (15%)
91	218.7	0.1369	H-9→L+2 (29%)
92	218.1	0.0588	--
93	216.6	0.027	H-11→L+2 (14%), H-11→L+3 (12%), H-8→L+3 (23%)
94	216.3	0.0291	H-12→L+2 (12%), H-4→L+6 (11%), H-2→L+12 (13%)
95	216.3	0.011	H-6→L+5 (14%), H-3→L+9 (19%)
96	216.0	5E-4	H-4→L+7 (15%), H-1→L+14 (20%), HOMO→L+13 (11%)
97	215.6	0.0062	H-7→L+4 (17%), H-6→L+5 (15%)
98	215.4	0.0507	H-4→L+7 (12%)
99	215.2	0.0393	H-7→L+4 (35%), H-6→L+4 (11%)
100	214.7	0.0023	H-4→L+7 (16%)

Complex 1g (triplet state)

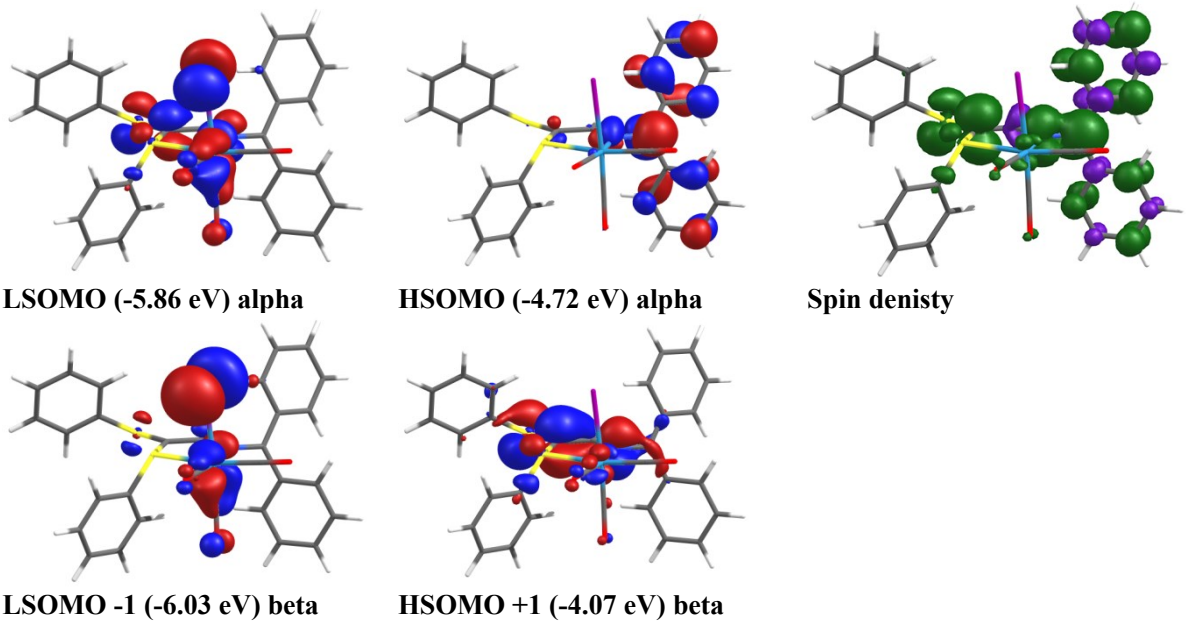

Figure S74. Left, representations of the semi-occupied MOs for **1g** in its lowest energy triplet state. The isoval = 0.04. Right, Alpha – beta SCF spin density. The isoval = 0.003 (green lobe positive, purple lobe negative).

Table S27. Relative atomic contributions (%) of the various fragments to the semi-occupied MOs of **1g**.[b]

Fragments	LS-1	LSOMO	HSOMO	HS+1
Re	25%	21%	2%	5%
3(CO)	11%	10%	2%	4%
I	**51%**	21%	0%	2%
N-S_Ligands	13%	**38%**	**91%**	**70%**

[b]HS = HSOMO, LS = LSOMO; the values in bold represent the largest contributions.

Complex 1h (singlet state)

Figure S75. Optimized geometry for **1h** applying a THF solvent field.

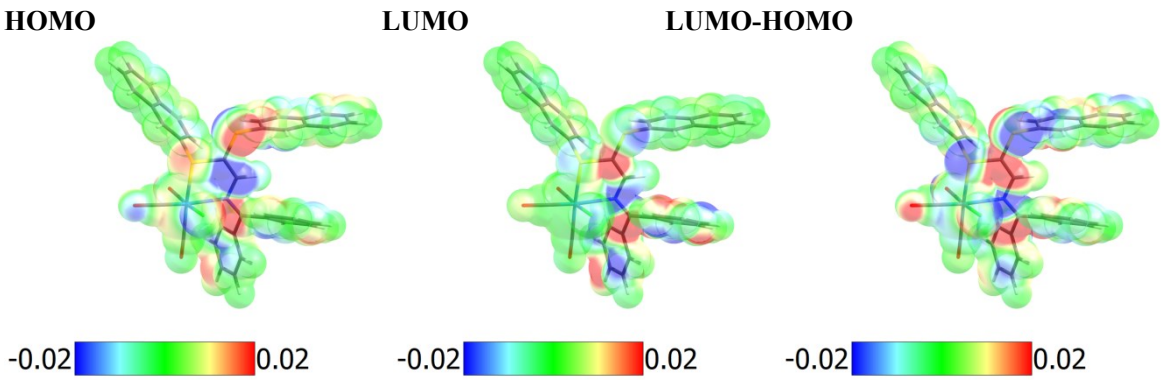

Figure S76. Electron-density map of the HOMO and LUMO ; Electron-density difference (LUMO-HOMO)

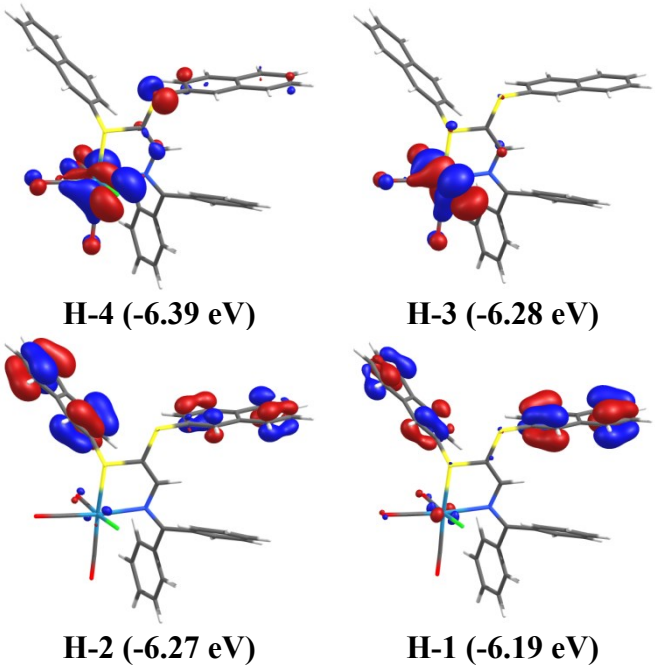

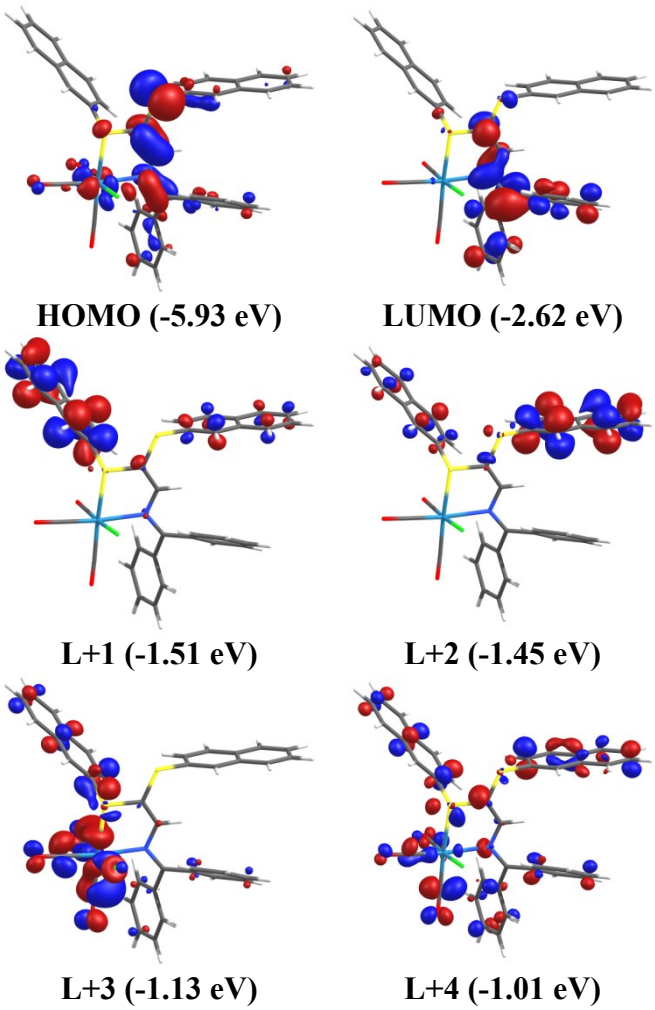

Figure S77. Representations of the frontier MOs for **1h** (optimized) applying a THF solvent field. The isoval = 0.04.

Table S28. Relative atomic contributions (%) of the various fragments to the frontier MOs of **1h.**[a]

Fragments	H-4	H-3	H-2	H-1	HOMO	LUMO	L+1	L+2	L+3	L+4
Re	**39%**	**44%**	3%	5%	8%	2%	3%	1%	25%	7%
3(CO)	17%	20%	2%	2%	4%	2%	3%	1%	26%	14%
Cl	21%	24%	1%	2%	3%	0%	0%	0%	6%	0%
N-S_Ligands	23%	12%	**94%**	**91%**	**85%**	**95%**	**94%**	**98%**	**44%**	**78%**

[a]H = HOMO, L = LUMO; the values in bold represent the largest contributions.

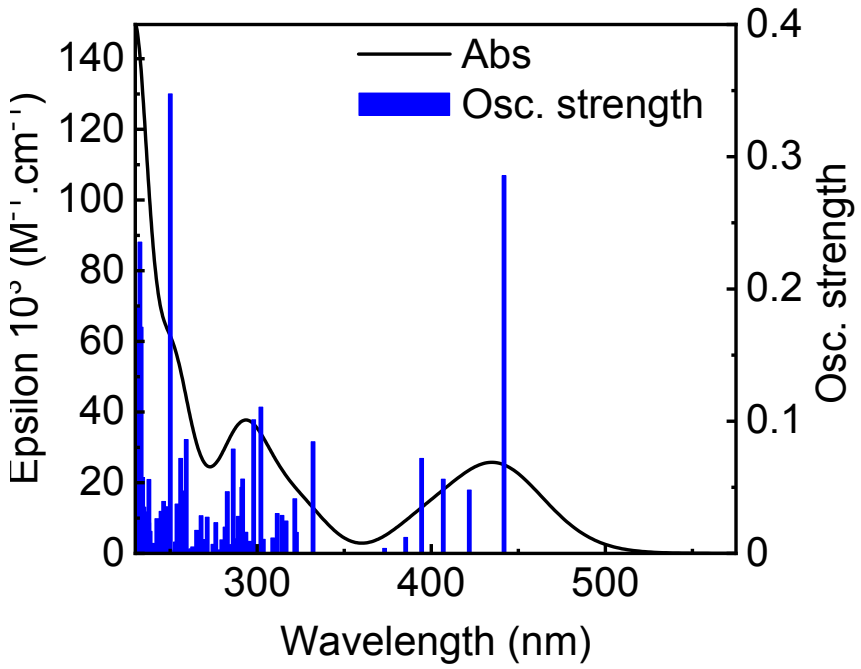

Figure S78. Simulated absorption spectrum for **1h** by TDDFT computations. Bar graph reporting the calculated oscillator strength and calculated position of the 100st electronic transitions calculated by TDDFT for **1h** (bar graph; f = computed oscillator strength).

Table S29. Calculated positions, oscillator strengths (f) and major contributions (%) of the first 100 singlet-singlet electronic transitions for **1h**.

No.	λ (nm)	f	Major contributions (%)
1	441.7	0.2858	HOMO→LUMO (87%)
2	421.8	0.0479	H-3→LUMO (84%)
3	406.9	0.0561	H-4→LUMO (47%), H-1→LUMO (40%)
4	394.5	0.0719	H-4→LUMO (38%), H-1→LUMO (52%)
5	385.3	0.0121	H-2→LUMO (89%)
6	373.2	0.0038	H-5→LUMO (96%)
7	332.1	0.0845	H-6→LUMO (95%)
8	322.5	0.0159	H-8→LUMO (44%), H-7→LUMO (18%), HOMO→L+1 (22%), HOMO→L+2 (11%)
9	321.6	0.0414	H-8→LUMO (29%), HOMO→L+1 (38%), HOMO→L+2 (21%)
10	316.6	0.0245	HOMO→L+1 (34%), HOMO→L+2 (58%)
11	314.3	0.0287	H-9→LUMO (14%), H-8→LUMO (20%), H-7→LUMO (57%)
12	311.5	0.0302	H-9→LUMO (79%), H-7→LUMO (11%)
13	308.9	0.0117	H-3→L+3 (27%), HOMO→L+3 (49%)
14	303.6	0.0107	H-4→L+3 (11%), H-3→L+3 (16%), HOMO→L+4 (11%), HOMO→L+5 (10%)
15	302.1	0.1107	H-10→LUMO (82%)
16	298.0	0.1011	H-11→LUMO (85%)
17	295.9	0.0091	H-3→L+1 (42%), H-3→L+2 (11%)
18	293.5	0.016	H-1→L+1 (13%), HOMO→L+4 (31%)
19	291.6	0.0562	H-12→LUMO (57%), H-1→L+1 (11%)
20	291.2	0.05	H-12→LUMO (30%), H-2→L+1 (12%), H-1→L+1 (29%)
21	290.2	0.0206	H-4→L+1 (17%), H-1→L+2 (14%)
22	289.1	0.028	H-2→L+1 (13%), H-1→L+1 (10%), HOMO→L+5 (12%)

23	287.6	0.0111	H-3→L+1 (28%), H-1→L+1 (15%), H-1→L+2 (21%)
24	286.3	0.0789	H-4→L+1 (11%), H-2→L+1 (29%), H-1→L+2 (20%), HOMO→L+4 (12%), HOMO→L+5 (10%)
25	284.1	0.0067	H-4→L+1 (29%), HOMO→L+5 (35%)
26	282.8	0.0467	H-4→L+3 (38%), HOMO→L+3 (18%)
27	281.9	0.0034	H-4→L+1 (18%), H-2→L+1 (14%), H-1→L+2 (16%)
28	281.5	0.0199	H-2→L+2 (37%)
29	279.7	0.0103	H-5→L+3 (10%), H-3→L+2 (32%)
30	278.8	0.0012	H-13→LUMO (15%), H-5→L+3 (34%), H-5→L+5 (14%)
31	277.8	0.0027	H-13→LUMO (62%)
32	276.2	0.0233	H-2→L+2 (22%), HOMO→L+6 (17%)
33	274.6	0.0069	H-4→L+2 (37%), H-3→L+2 (20%), HOMO→L+6 (16%)
34	271.3	0.0274	H-4→L+5 (11%), HOMO→L+6 (35%)
35	270.2	0.0105	H-4→L+2 (20%), H-4→L+5 (19%)
36	268.5	0.0101	H-5→L+1 (30%), H-3→L+4 (19%)
37	267.8	0.0285	HOMO→L+7 (76%)
38	266.1	0.0122	H-5→L+1 (13%), H-3→L+5 (10%), H-1→L+3 (28%)
39	265.2	0.0175	H-5→L+1 (17%), H-3→L+5 (18%), H-1→L+3 (23%)
40	263.0	0.0049	HOMO→L+8 (79%)
41	261.8	0.0035	H-2→L+3 (56%), H-1→L+3 (21%)
42	260.4	0.0028	H-4→L+4 (30%), H-4→L+5 (18%)
43	259.3	0.0861	H-5→L+1 (12%), H-5→L+4 (11%), H-2→L+5 (10%)
44	258.6	0.0472	H-1→L+4 (22%), H-1→L+5 (29%)
45	257.7	0.0134	H-16→LUMO (72%), H-14→LUMO (10%)
46	256.0	0.0718	H-4→L+4 (12%), H-1→L+4 (12%), H-1→L+5 (16%), H-1→L+6 (12%)
47	254.9	0.0011	H-5→L+2 (51%), H-5→L+5 (11%)
48	254.0	0.0374	H-16→LUMO (12%), H-14→LUMO (52%)
49	253.0	0.0086	H-3→L+6 (34%), H-3→L+7 (22%)
50	252.7	0.0026	H-2→L+4 (20%), H-2→L+5 (22%), H-1→L+5 (16%)
51	250.1	0.3475	H-6→L+1 (29%), H-2→L+5 (20%)
52	248.8	0.0353	H-15→LUMO (21%), H-14→LUMO (12%), HOMO→L+9 (46%)
53	248.6	0.0224	H-15→LUMO (44%), H-3→L+8 (20%), HOMO→L+9 (15%)
54	248.3	0.0098	H-15→LUMO (23%), H-3→L+8 (35%)
55	248.1	0.0157	H-4→L+6 (21%), H-4→L+7 (12%), H-1→L+7 (10%)
56	246.3	0.0393	H-6→L+2 (45%)
57	245.2	0.0106	H-2→L+6 (44%), H-1→L+6 (20%)
58	244.8	0.0318	H-7→L+1 (24%), H-6→L+1 (13%), H-2→L+6 (12%), H-1→L+7 (20%)
59	244.1	0.015	H-5→L+4 (20%), H-4→L+8 (10%)
60	243.8	0.0064	H-5→L+4 (18%), H-4→L+8 (14%), H-1→L+8 (12%)
61	243.1	0.0124	H-2→L+7 (16%), H-1→L+7 (10%)
62	242.6	0.0055	H-3→L+6 (17%), H-3→L+7 (36%)
63	242.4	0.0263	H-17→LUMO (51%)
64	240.7	4E-4	H-1→L+8 (24%), HOMO→L+10 (53%)
65	240.0	0.0076	H-4→L+6 (11%), H-4→L+8 (14%), H-3→L+8 (10%), H-1→L+8 (18%), HOMO→L+10 (13%)
66	238.5	0.0167	H-6→L+3 (12%), H-4→L+6 (14%), H-4→L+7 (26%), H-4→L+8 (12%)
67	237.8	0.0559	H-4→L+8 (14%), H-2→L+7 (23%), H-2→L+8 (36%)

68	237.7	0.0232	H-6→L+3 (61%)
69	237.3	0.002	H-8→L+1 (35%), H-8→L+2 (32%), H-7→L+2 (14%)
70	236.9	0.0314	H-20→LUMO (13%), H-18→LUMO (39%), H-17→LUMO (12%)
71	236.7	0.0037	H-3→L+9 (55%)
72	235.0	0.035	HOMO→L+11 (28%)
73	234.2	0.0574	H-8→L+1 (28%), H-8→L+2 (18%)
74	233.3	0.1711	H-4→L+9 (11%)
75	233.1	0.0342	H-5→L+6 (18%), H-5→L+7 (17%)
76	232.7	0.2355	H-3→L+12 (11%), HOMO→L+12 (10%)
77	232.3	0.1871	H-6→L+4 (25%)
78	231.7	0.0784	H-4→L+9 (15%), H-1→L+9 (22%)
79	231.5	0.0105	H-7→L+3 (16%), H-1→L+9 (10%)
80	230.9	0.0201	H-10→L+1 (22%), H-9→L+1 (23%), H-6→L+4 (20%)
81	230.5	0.0037	H-10→L+2 (18%), H-9→L+1 (22%), H-5→L+8 (13%)
82	230.0	0.0242	H-9→L+1 (20%), H-6→L+4 (16%), H-5→L+8 (14%)
83	229.1	0.0196	H-5→L+8 (22%), H-4→L+9 (22%), H-1→L+9 (14%)
84	228.6	0.0289	H-3→L+12 (12%)
85	228.0	0.2881	H-6→L+5 (39%)
86	227.6	0.0358	H-10→L+1 (14%), H-9→L+2 (10%), H-2→L+9 (18%)
87	227.2	0.0171	H-9→L+2 (54%), H-2→L+9 (11%)
88	226.9	0.1979	H-10→L+1 (10%), H-10→L+2 (13%), H-2→L+9 (18%)
89	226.7	0.2293	H-4→L+9 (11%)
90	226.0	0.1026	H-12→L+3 (11%), H-9→L+3 (10%), H-3→L+10 (11%), HOMO→L+12 (10%)
91	225.3	0.2149	H-2→L+9 (16%)
92	225.1	0.0698	H-8→L+3 (21%), H-7→L+3 (17%)
93	224.3	0.068	H-5→L+6 (27%), H-5→L+7 (29%)
94	224.0	0.0017	H-8→L+4 (10%), H-7→L+4 (14%)
95	223.5	0.0306	H-12→L+1 (19%)
96	223.1	0.0058	H-4→L+11 (15%), HOMO→L+11 (13%)
97	222.8	0.0218	H-12→L+1 (16%), H-11→L+1 (17%), H-11→L+2 (22%)
98	222.7	0.0245	H-11→L+1 (14%), H-3→L+10 (12%), H-1→L+10 (11%)
99	222.5	0.0145	H-11→L+1 (15%), H-7→L+4 (14%)
100	222.1	0.0254	H-12→L+1 (12%)

Complex 1h (triplet state)

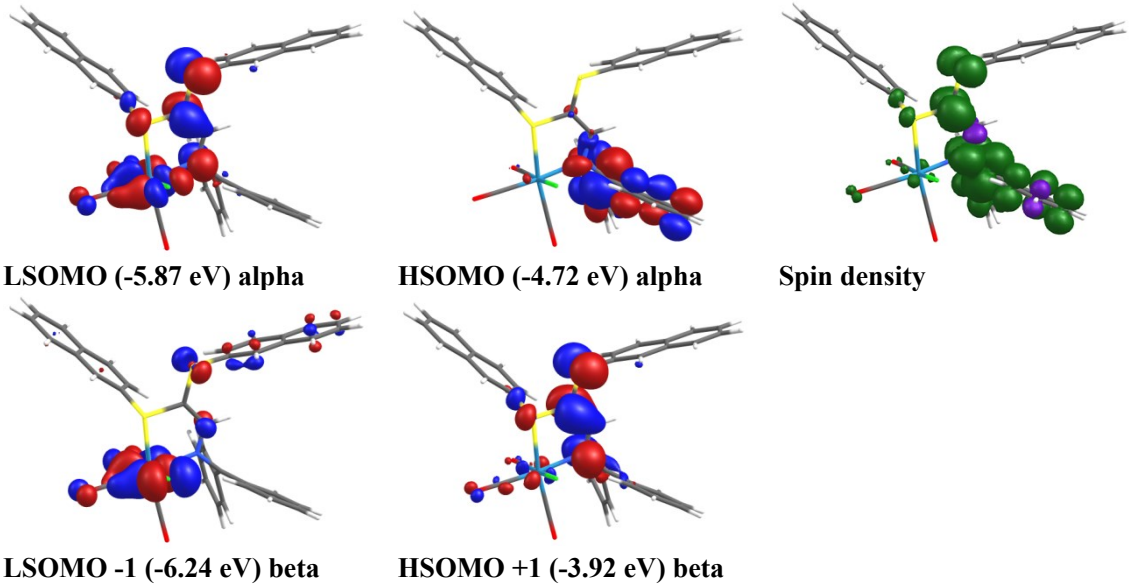

Figure S79. Left, representations of the semi-occupied MOs for **1h** in its lowest energy triplet state. The isoval = 0.04. Right, Alpha – beta SCF spin density. The isoval = 0.003 (green lobe positive, purple lobe negative).

Table S30. Relative atomic contributions (%) of the various fragments to the semi-occupied MOs of **1h**.[b]

Fragments	LS-1	LSOMO	HSOMO	HS+1
Re	**38%**	18%	2%	5%
3(CO)	16%	9%	2%	4%
Cl	18%	6%	0%	1%
N-S_Ligands	28%	**67%**	**95%**	**90%**

[b]HS = HSOMO, LS = LSOMO; the values in bold represent the largest contributions.

Complex 1i (singlet state)

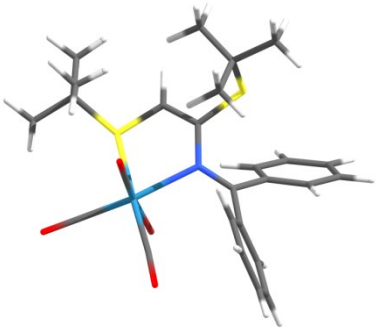

Figure S80. Optimized geometry for **1i** applying a THF solvent field.

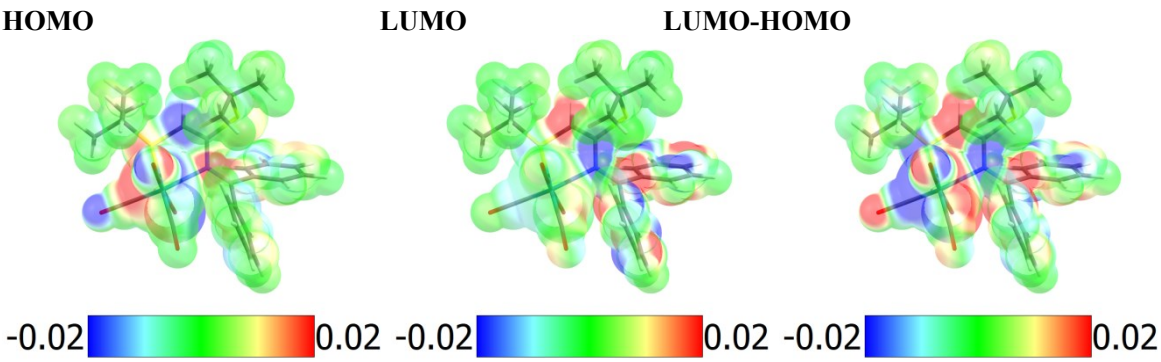

Figure S81. Electron-density map of the HOMO and LUMO ; Electron-density difference (LUMO-HOMO)

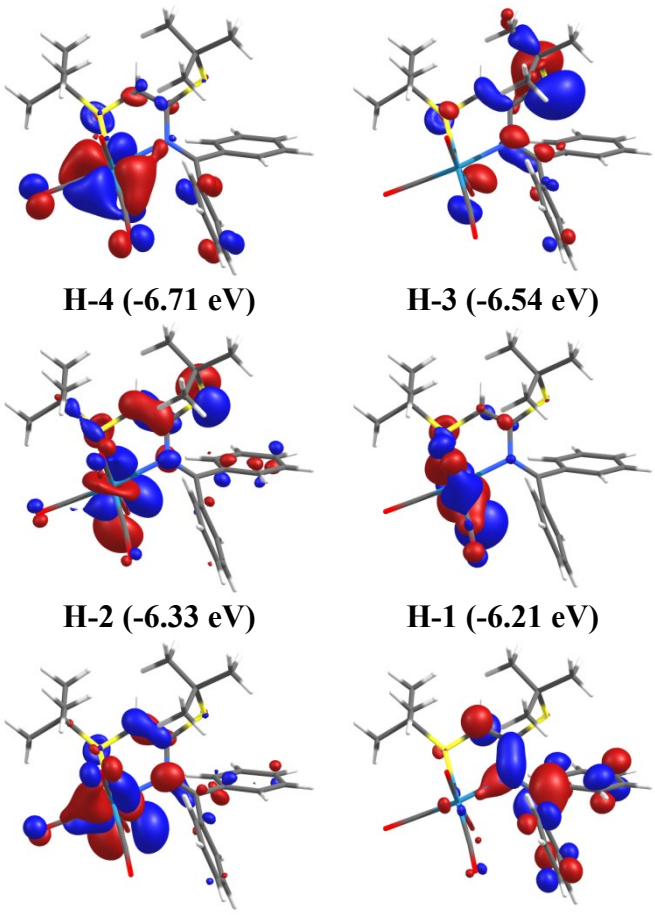

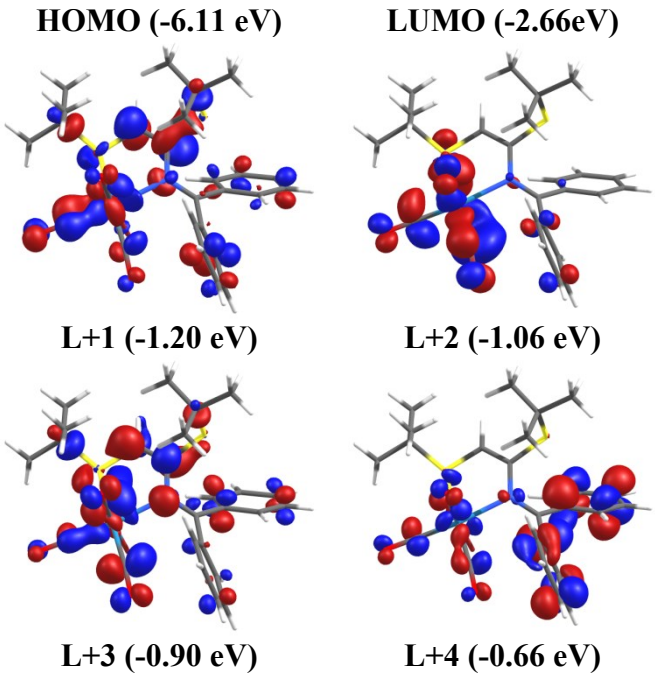

Figure S82. Representations of the frontier MOs for **1i** applying a THF solvent field. The isoval = 0.04.

Table S31. Relative atomic contributions (%) of the various fragments to the frontier MOs of **1i**.[a]

Fragments	H-4	H-3	H-2	H-1	HOMO	LUMO	L+1	L+2	L+3	L+4
Re	**48%**	1%	16%	**34%**	28%	4%	15%	29%	9%	9%
3(CO)	21%	1%	6%	15%	14%	3%	14%	**35%**	20%	12%
Br	4%	7%	24%	**34%**	24%	0%	3%	11%	1%	1%
N-S_Ligands	27%	**91%**	**54%**	17%	**35%**	**93%**	**68%**	25%	**70%**	**79%**

[a]H = HOMO, L = LUMO; the values in bold represent the largest contributions.

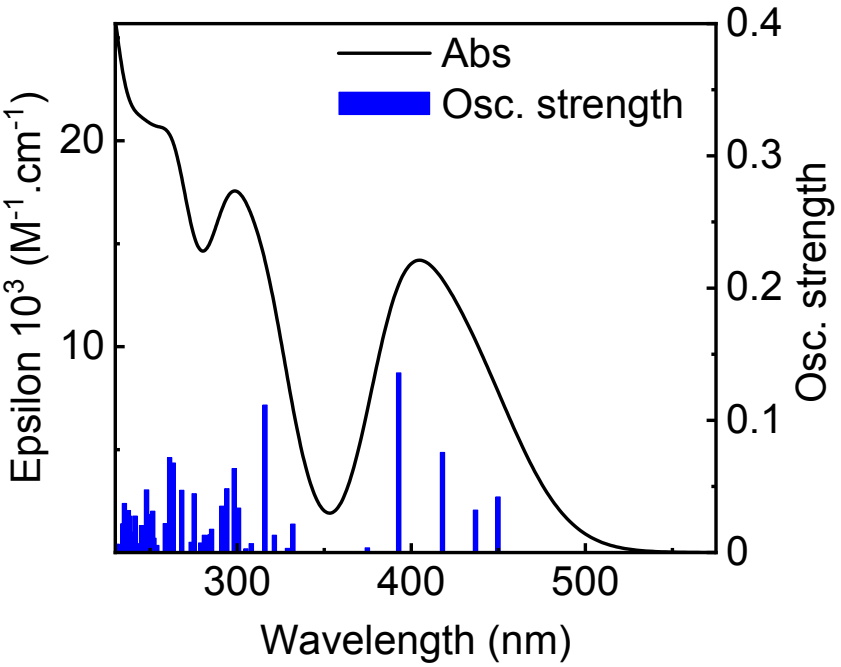

Figure S83. Simulated absorption spectrum for **1i** by TDDFT computations. Bar graph reporting the calculated oscillator strength and calculated position of the 100st electronic transitions calculated by TDDFT for **1i** (bar graph; f = computed oscillator strength).

Table S32. Calculated position, oscillator strength (f) and major contributions (%) of the first 100 singlet-singlet electronic transitions for **1i**.

No.	λ (nm)	f	Major contributions (%)
1	449.8	0.0421	H-1→LUMO (10%), HOMO→LUMO (87%)
2	436.9	0.0321	H-1→LUMO (86%)
3	417.9	0.0757	H-3→LUMO (18%), H-2→LUMO (77%)
4	392.8	0.1359	H-3→LUMO (79%), H-2→LUMO (14%)
5	374.8	0.0036	H-4→LUMO (96%)
6	332.0	0.0216	H-6→LUMO (15%), H-5→LUMO (82%)
7	328.9	0.0032	H-6→LUMO (83%), H-5→LUMO (14%)
8	321.4	0.0131	H-7→LUMO (94%)
9	316.0	0.1116	H-8→LUMO (95%)
10	308.1	0.0068	H-1→L+2 (24%), HOMO→L+1 (32%), HOMO→L+2 (17%)
11	305.0	0.0029	HOMO→L+1 (25%), HOMO→L+2 (56%)
12	300.8	0.0337	H-9→LUMO (26%), H-1→L+1 (49%), H-1→L+3 (11%)
13	298.3	0.0635	H-9→LUMO (60%), H-1→L+1 (15%)
14	294.0	0.0483	H-10→LUMO (77%)
15	291.1	0.0351	H-1→L+2 (37%), HOMO→L+1 (24%)
16	285.3	0.0177	H-11→LUMO (81%)
17	284.4	0.0136	H-11→LUMO (14%), H-2→L+1 (45%)
18	281.2	0.0131	H-4→L+2 (23%), H-2→L+2 (30%)
19	279.0	0.0073	H-1→L+3 (41%), HOMO→L+3 (34%)
20	275.3	0.0445	H-2→L+1 (10%), H-1→L+3 (28%), HOMO→L+3 (38%)
21	273.6	0.0078	H-3→L+1 (58%), H-2→L+3 (17%)
22	268.2	0.0471	H-4→L+1 (14%), H-4→L+2 (29%), H-2→L+2 (32%)
23	263.3	0.0677	H-4→L+1 (43%), H-4→L+2 (23%)
24	261.2	0.0718	H-3→L+1 (13%), H-2→L+3 (63%)
25	258.7	0.022	HOMO→L+4 (81%)
26	253.9	0.0054	H-3→L+2 (69%)
27	252.2	0.0109	H-1→L+4 (79%)
28	251.5	0.0313	H-12→LUMO (26%), H-3→L+3 (36%)
29	250.1	0.0288	H-12→LUMO (45%), H-3→L+3 (31%)
30	248.9	0.0114	HOMO→L+5 (63%)
31	248.0	0.0474	H-4→L+3 (49%)
32	246.5	0.0188	H-2→L+4 (64%), HOMO→L+5 (13%)
33	245.1	0.0204	H-6→L+1 (14%), H-1→L+5 (38%)
34	243.6	0.0068	H-6→L+2 (17%), H-1→L+5 (19%), HOMO→L+6 (10%)
35	241.4	0.0276	H-6→L+1 (17%), H-5→L+1 (14%), H-1→L+5 (25%), HOMO→L+6 (13%)
36	239.9	0.0155	H-2→L+5 (30%), HOMO→L+6 (16%)
37	238.7	0.0025	H-7→L+2 (17%), H-3→L+4 (10%)
38	238.4	0.0275	H-7→L+1 (10%), H-6→L+2 (11%), H-5→L+2 (13%), H-2→L+5 (30%)
39	237.5	0.0318	H-3→L+4 (75%)
40	236.1	0.0038	H-13→LUMO (49%)
41	235.6	0.0061	H-13→LUMO (12%), H-1→L+6 (11%), HOMO→L+7 (14%)
42	235.2	0.0372	H-13→LUMO (18%), H-7→L+1 (22%), H-1→L+6 (16%)
43	234.4	0.0219	H-2→L+5 (10%), HOMO→L+7 (13%), HOMO→L+8 (13%)
44	232.5	0.0061	H-7→L+2 (24%), H-3→L+5 (18%), H-1→L+6 (12%)
45	231.1	0.0064	H-4→L+4 (14%), H-3→L+5 (12%), H-1→L+7 (17%)
46	229.4	0.0138	H-6→L+1 (18%), H-5→L+1 (21%), H-4→L+4 (11%), H-2→L+6 (11%)
47	228.8	0.0171	H-5→L+3 (20%), H-4→L+4 (15%)
48	228.4	0.0282	H-6→L+1 (10%), H-4→L+4 (15%), H-3→L+5 (31%)
49	227.5	0.0019	H-6→L+2 (10%), H-5→L+2 (14%), HOMO→L+8 (13%)
50	227.1	0.0364	H-8→L+1 (30%)

51	226.1	0.0082	H-6→L+3 (15%), H-5→L+3 (10%), H-1→L+7 (15%), HOMO→L+8 (14%)
52	226.0	0.0276	H-8→L+1 (23%), H-2→L+6 (22%)
53	224.6	0.0191	H-14→LUMO (10%), H-6→L+2 (10%)
54	223.7	0.024	H-1→L+6 (13%), H-1→L+8 (29%)
55	223.1	0.0859	H-14→LUMO (49%), H-4→L+5 (10%)
56	222.4	0.0171	H-2→L+7 (21%)
57	221.7	0.0117	H-7→L+3 (23%), H-2→L+6 (17%)
58	221.0	0.0107	H-4→L+5 (10%), HOMO→L+9 (18%)
59	219.5	0.0115	H-8→L+2 (17%), H-4→L+5 (13%), H-2→L+7 (18%)
60	218.9	2E-4	H-8→L+2 (26%), H-3→L+6 (22%)
61	218.7	0.0215	H-4→L+6 (15%), H-1→L+9 (16%)
62	218.3	0.0057	H-6→L+3 (13%), H-5→L+3 (14%), H-3→L+6 (24%)
63	217.3	0.0182	H-10→L+1 (15%), H-9→L+1 (29%), H-8→L+2 (13%)
64	217.0	0.0027	H-10→L+1 (24%), H-9→L+1 (10%), H-8→L+3 (17%), H-3→L+6 (13%)
65	216.4	0.0217	H-11→L+1 (25%), H-9→L+2 (11%)
66	215.2	0.0204	H-5→L+4 (11%), H-4→L+7 (10%), H-2→L+8 (11%)
67	214.8	0.011	H-10→L+2 (34%), H-9→L+2 (12%)
68	214.4	0.0033	H-10→L+2 (11%), H-2→L+8 (10%)
69	213.6	0.0082	H-8→L+3 (30%)
70	213.4	0.0231	H-11→L+1 (16%), H-8→L+3 (26%), H-6→L+4 (10%), H-5→L+4 (18%)
71	212.7	0.019	H-6→L+4 (30%), H-3→L+7 (16%), H-2→L+8 (12%)
72	211.9	0.0071	H-6→L+4 (16%), HOMO→L+10 (16%)
73	210.8	0.0153	H-10→L+2 (16%), H-9→L+2 (27%), H-3→L+7 (10%)
74	210.2	0.0043	H-9→L+2 (13%), H-3→L+7 (34%)
75	209.9	0.0052	H-1→L+10 (11%)
76	209.4	0.008	H-10→L+3 (20%), H-9→L+3 (11%), H-1→L+10 (17%)
77	208.7	0.0152	H-15→LUMO (12%), H-8→L+4 (15%)
78	208.4	9E-4	H-15→LUMO (61%)
79	207.8	0.0135	H-7→L+4 (33%)
80	207.3	0.0114	H-10→L+3 (25%), H-7→L+4 (22%), H-6→L+5 (12%)
81	206.9	0.0284	H-9→L+3 (13%), H-5→L+5 (10%)
82	206.2	6E-4	H-19→LUMO (25%), H-17→LUMO (17%)
83	206.0	0.0021	HOMO→L+11 (14%)
84	205.4	0.0119	H-11→L+3 (22%), H-6→L+5 (21%), H-5→L+5 (10%)
85	205.2	0.0077	H-5→L+5 (11%), H-3→L+8 (15%)
86	204.9	0.0062	H-3→L+8 (21%), H-2→L+9 (12%)
87	204.3	0.0105	H-19→LUMO (17%), H-18→LUMO (14%), H-16→LUMO (29%)
88	203.9	0.0126	H-11→L+3 (21%), H-4→L+6 (11%), H-4→L+8 (12%)
89	203.8	0.0188	H-16→LUMO (11%), H-11→L+3 (24%)
90	202.8	0.0265	H-6→L+5 (15%), H-5→L+5 (16%)
91	202.6	0.016	H-3→L+8 (13%), H-2→L+9 (13%)
92	202.1	0.0421	H-7→L+5 (18%)
93	201.3	0.0836	H-7→L+5 (23%), H-3→L+8 (10%)
94	201.1	0.0329	H-7→L+5 (16%)
95	200.9	0.0186	H-19→LUMO (17%), H-17→LUMO (34%)
96	200.6	0.076	H-9→L+4 (19%), H-8→L+5 (14%), H-6→L+6 (10%)
97	200.3	0.0204	H-18→LUMO (14%), H-16→LUMO (12%), HOMO→L+12 (12%)
98	199.5	0.0526	H-11→L+2 (13%), H-2→L+10 (10%)
99	199.0	0.0205	H-19→LUMO (10%), H-18→LUMO (17%), H-17→LUMO (13%), H-8→L+5 (10%)
100	198.0	0.0034	HOMO→L+13 (11%)

Complex 1i (triplet state)

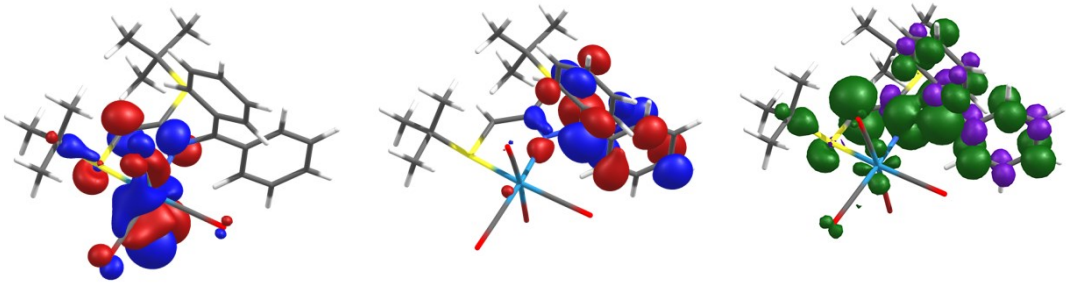

LSOMO (-6.05 eV) alpha **HSOMO (-4.76 eV) alpha** **Spin density**

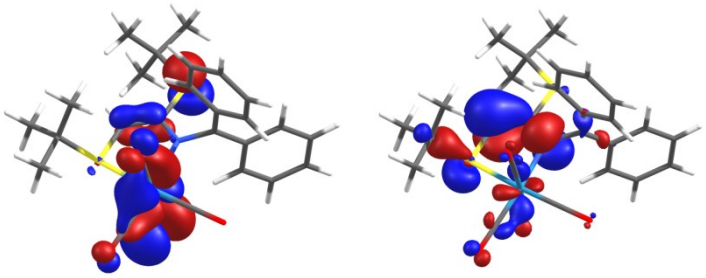

LSOMO (-6.17 eV) beta **HSOMO (-4.09 eV) beta**

Figure S84. Left, representations of the semi-occupied MOs for **1i** in its lowest energy triplet state. The isoval = 0.04. Right, Alpha – beta SCF spin density. The isoval = 0.003 (green lobe positive, purple lobe negative).

Table S33. Relative atomic contributions (%) of the various fragments to the semi-occupied MOs of **1i**.[b]

Fragments	LS-1	LSOMO	HSOMO	HS+1
Re	**33%**	32%	3%	7%
3(CO)	14%	14%	2%	5%
Br	22%	19%	0%	3%
N-S_Ligands	31%	**36%**	**95%**	**85%**

[b]HS = HSOMO, LS = LSOMO; the values in bold represent the largest contributions.

Complex 1j (singlet state)

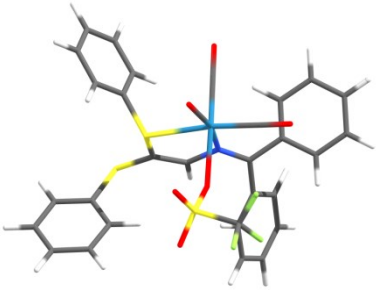

Figure S85. Optimized geometry for **1j** applying a THF solvent field.

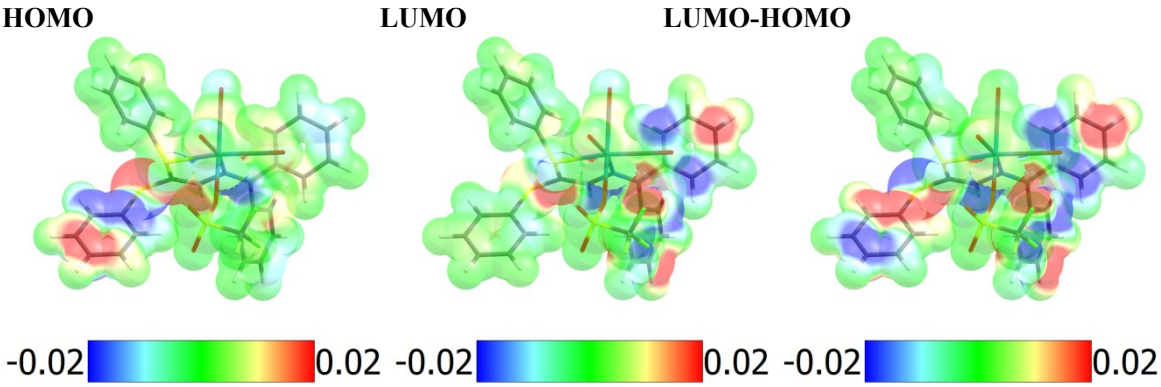

Figure S86. Electron-density map of the HOMO and LUMO ; Electron-density difference (LUMO-HOMO)

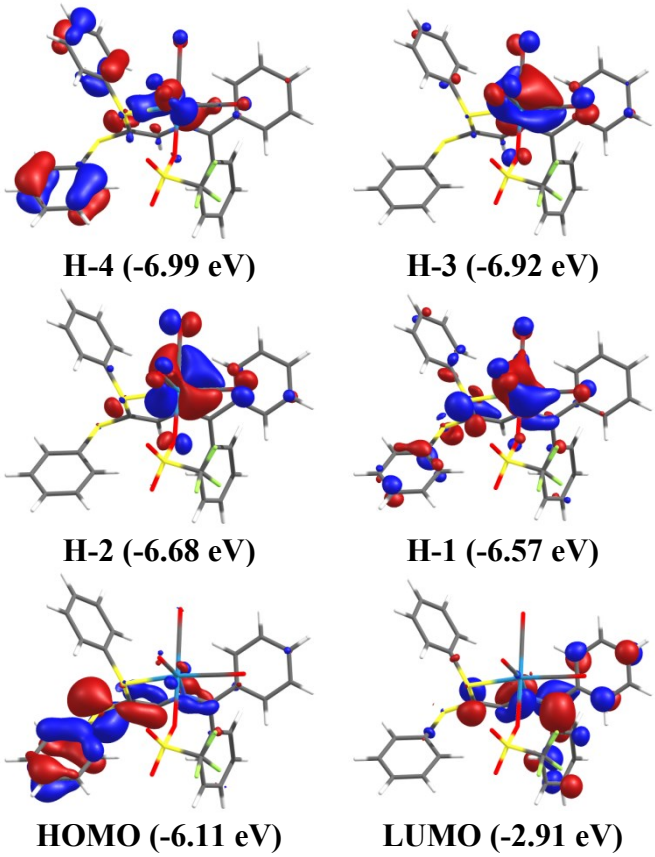

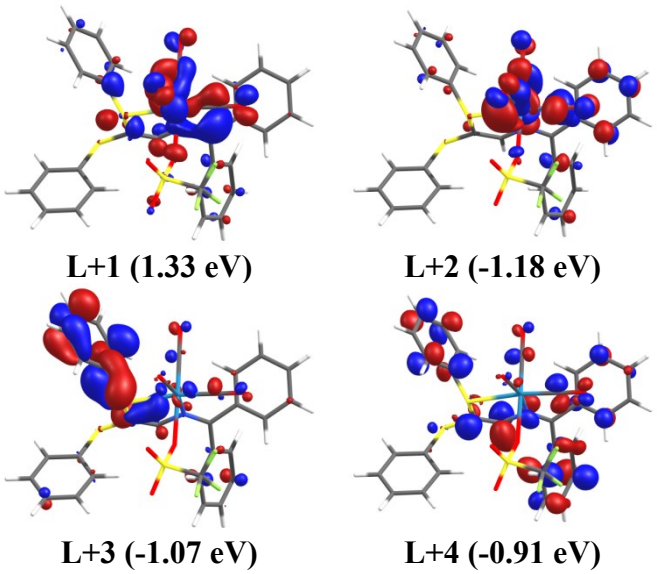

Figure S87. Representations of the frontier MOs for **1j** applying a THF solvent field. The isoval = 0.04.

Table S34. Relative atomic contributions (%) of the various fragments to the frontier MOs of **1j**.[a]

Fragments	H-4	H-3	H-2	H-1	HOMO	LUMO	L+1	L+2	L+3	L+4
Re	23%	**59%**	**58%**	33%	3%	2%	25%	22%	11%	6%
3(CO)	11%	24%	23%	15%	2%	2%	29%	30%	8%	9%
$CF_3SO_3^-$ (TfO^-)	1%	4%	5%	2%	0%	0%	9%	3%	1%	0%
N-S_Ligands	**65%**	13%	14%	**50%**	**95%**	**95%**	**36%**	**45%**	**80%**	**85%**

[a]H = HOMO, L = LUMO; the values in bold represent the largest contributions.

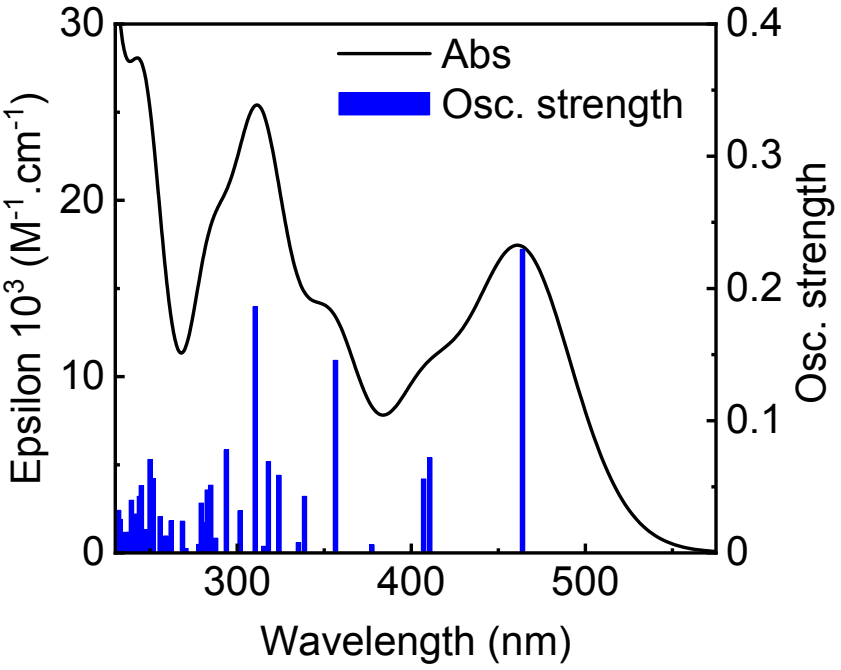

Figure S88. Simulated absorption spectrum for **1j** by TDDFT computations. Bar graph reporting the calculated oscillator strength and calculated position of the 100st electronic transitions calculated by TDDFT for **1j** (bar graph; f = computed oscillator strength).

Table S35. Calculated position, oscillator strength (f) and major contributions (%) of the first 100 singlet-singlet electronic transitions for **1j**.

No.	λ (nm)	f	Major contributions (%)
1	463.9	0.2296	HOMO→LUMO (98%)
2	410.6	0.0721	H-2→LUMO (57%), H-1→LUMO (40%)
3	407.1	0.0559	H-2→LUMO (42%), H-1→LUMO (54%)
4	377.4	0.0062	H-3→LUMO (96%)
5	356.5	0.1457	H-5→LUMO (18%), H-4→LUMO (74%)
6	338.7	0.0428	H-5→LUMO (70%), H-4→LUMO (18%)
7	335.2	0.0078	H-8→LUMO (15%), H-7→LUMO (15%), H-6→LUMO (57%)
8	324.0	0.0587	H-9→LUMO (24%), H-8→LUMO (32%), H-7→LUMO (19%), H-6→LUMO (21%)
9	317.9	0.0691	H-9→LUMO (68%)
10	315.3	0.005	H-8→LUMO (43%), H-7→LUMO (56%)
11	310.4	0.1862	H-10→LUMO (92%)
12	301.7	0.0318	H-2→L+1 (31%), HOMO→L+1 (55%)
13	293.8	0.0779	H-2→L+1 (21%), H-1→L+1 (26%), H-1→L+2 (12%), HOMO→L+1 (13%)
14	287.6	0.0112	H-1→L+1 (32%), H-1→L+2 (10%), HOMO→L+1 (13%)
15	284.8	0.0512	H-2→L+1 (17%), HOMO→L+2 (58%)
16	282.8	0.0476	HOMO→L+3 (75%)
17	281.1	0.023	H-11→LUMO (51%), HOMO→L+3 (10%)
18	279.4	0.0377	H-11→LUMO (20%), H-2→L+2 (32%)
19	278.0	0.0065	H-11→LUMO (10%), H-3→L+1 (17%), H-3→L+2 (16%), H-2→L+2 (26%), HOMO→L+2 (10%)
20	273.6	2E-4	H-12→LUMO (99%)
21	270.6	0.0034	HOMO→L+4 (73%)
22	268.6	0.024	H-3→L+1 (33%), H-1→L+2 (20%)
23	262.1	0.0242	HOMO→L+5 (79%)
24	259.7	0.012	H-3→L+2 (11%), H-1→L+3 (62%)
25	259.1	0.0128	H-3→L+2 (23%), H-2→L+3 (30%), H-1→L+3 (17%)
26	256.2	0.0023	H-13→LUMO (49%), H-2→L+3 (20%)
27	255.8	0.0274	H-13→LUMO (29%), H-2→L+3 (25%)
28	251.8	0.0561	H-1→L+4 (20%), HOMO→L+6 (16%), HOMO→L+8 (10%)
29	250.0	0.0706	H-5→L+1 (12%), H-4→L+1 (29%), HOMO→L+6 (11%)
30	248.0	0.0177	HOMO→L+6 (59%), HOMO→L+7 (12%), HOMO→L+8 (13%)
31	247.2	0.0056	H-4→L+1 (13%), H-1→L+4 (49%)
32	245.0	0.0509	HOMO→L+7 (31%), HOMO→L+8 (38%)
33	243.9	0.0428	H-2→L+4 (49%)
34	243.6	0.0074	H-14→LUMO (15%), H-4→L+2 (20%)
35	243.0	0.0085	H-14→LUMO (19%), H-1→L+5 (25%)
36	242.2	0.0295	H-14→LUMO (22%), H-1→L+5 (18%), HOMO→L+7 (10%)
37	241.5	0.0279	H-3→L+3 (11%), H-1→L+5 (14%), HOMO→L+7 (11%), HOMO→L+10 (15%)
38	239.3	0.0398	H-3→L+3 (54%), H-1→L+5 (11%)
39	238.4	0.0029	H-2→L+5 (60%)
40	237.6	0.0157	H-6→L+1 (11%), H-5→L+1 (16%)
41	236.4	0.0099	H-5→L+1 (33%), H-4→L+1 (13%), H-4→L+3 (14%)
42	235.6	0.0116	H-17→LUMO (11%), H-4→L+3 (19%)

43	234.5	0.0156	HOMO→L+9 (24%), HOMO→L+10 (16%)
44	234.2	0.003	H-15→LUMO (61%), H-14→LUMO (20%)
45	233.3	0.0124	H-17→LUMO (11%), H-6→L+1 (30%), H-3→L+4 (13%)
46	232.8	0.0254	H-17→LUMO (32%), H-6→L+1 (16%)
47	231.9	0.0322	H-6→L+1 (11%), H-3→L+4 (49%)
48	230.3	0.023	H-8→L+1 (14%), H-1→L+6 (34%)
49	229.4	0.0056	H-3→L+5 (12%), H-2→L+6 (10%), H-1→L+6 (12%), HOMO→L+11 (11%)
50	228.9	0.0072	H-7→L+1 (38%), HOMO→L+11 (13%)
51	228.4	0.0047	H-6→L+2 (11%), H-5→L+2 (37%), H-4→L+2 (18%)
52	228.2	0.0074	H-8→L+1 (42%), H-7→L+1 (24%)
53	227.7	0.0054	H-3→L+5 (40%), H-2→L+6 (13%)
54	227.2	0.0189	H-4→L+4 (15%), H-2→L+6 (11%)
55	226.6	0.0396	HOMO→L+11 (25%)
56	226.2	0.008	H-5→L+3 (27%), H-4→L+3 (11%), H-2→L+6 (10%)
57	225.3	0.0401	H-2→L+6 (18%), H-2→L+12 (11%), HOMO→L+12 (13%)
58	225.1	0.003	H-16→LUMO (72%)
59	225.0	0.0339	H-16→LUMO (21%), H-6→L+2 (13%), H-5→L+3 (13%)
60	224.4	0.0108	H-2→L+7 (18%), H-1→L+7 (18%)
61	223.9	0.0045	H-9→L+1 (15%), H-6→L+2 (19%)
62	223.3	0.0033	H-10→L+1 (14%), H-9→L+1 (23%), H-9→L+2 (16%)
63	222.8	0.0186	H-1→L+7 (10%), H-1→L+8 (16%)
64	222.5	0.0284	H-7→L+2 (11%), H-4→L+4 (10%)
65	221.5	0.0211	H-1→L+8 (49%)
66	221.4	0.0334	H-2→L+7 (17%), H-1→L+7 (11%), HOMO→L+12 (10%)
67	220.7	0.0105	H-4→L+5 (15%), H-2→L+7 (13%)
68	220.3	0.0012	H-8→L+2 (20%), H-8→L+3 (16%), H-7→L+2 (20%)
69	219.6	0.0536	H-7→L+2 (18%), H-6→L+3 (12%), H-2→L+7 (17%)
70	219.3	0.0428	H-6→L+3 (14%), H-5→L+4 (11%)
71	219.1	0.0466	H-5→L+4 (47%), H-4→L+4 (11%)
72	218.2	0.048	H-8→L+2 (23%), H-3→L+6 (19%)
73	218.0	0.0136	H-18→LUMO (91%)
74	217.6	0.0357	H-10→L+1 (10%), H-2→L+8 (10%), H-1→L+9 (27%)
75	217.1	0.0354	H-3→L+6 (13%), HOMO→L+12 (12%)
76	216.3	0.0079	H-1→L+11 (12%)
77	215.7	0.0126	H-10→L+1 (13%), H-9→L+2 (21%), H-3→L+6 (16%)
78	215.2	0.0126	H-10→L+1 (10%), H-2→L+8 (26%)
79	215.1	0.0121	H-2→L+8 (35%)
80	214.4	0.0379	H-6→L+4 (10%), H-1→L+10 (25%)
81	214.1	0.0247	H-8→L+3 (17%), H-6→L+3 (13%), H-5→L+5 (11%)
82	213.6	0.0332	H-10→L+2 (14%), H-5→L+5 (11%)
83	213.0	0.0137	H-5→L+5 (33%)
84	212.5	0.0212	H-10→L+2 (13%), H-6→L+4 (20%)
85	212.1	0.0608	H-2→L+9 (14%)
86	211.8	0.0045	H-7→L+4 (22%), H-6→L+4 (10%)
87	211.6	0.0377	H-7→L+4 (11%), H-2→L+9 (33%)
88	210.8	0.0507	HOMO→L+13 (22%)

89	210.5	0.001	H-3→L+7 (17%), H-2→L+14 (13%)
90	210.4	0.0102	H-19→LUMO (47%)
91	210.0	0.0049	H-8→L+4 (17%), H-3→L+7 (12%)
92	209.5	0.0236	H-10→L+2 (13%)
93	209.4	0.0028	H-9→L+3 (14%), H-8→L+4 (28%)
94	208.8	0.0194	H-6→L+5 (20%), H-4→L+6 (16%)
95	208.8	0.0339	H-9→L+3 (30%), H-8→L+4 (12%)
96	208.3	0.0364	H-12→L+1 (60%), H-11→L+1 (14%)
97	207.7	0.0115	H-21→LUMO (26%)
98	207.5	0.0028	H-21→LUMO (29%), H-9→L+3 (12%)
99	207.1	0.0488	H-21→LUMO (10%), H-8→L+5 (13%), H-6→L+5 (10%)
100	207.0	0.0029	H-3→L+8 (51%), H-1→L+13 (12%)

Complex 1j (triplet state)

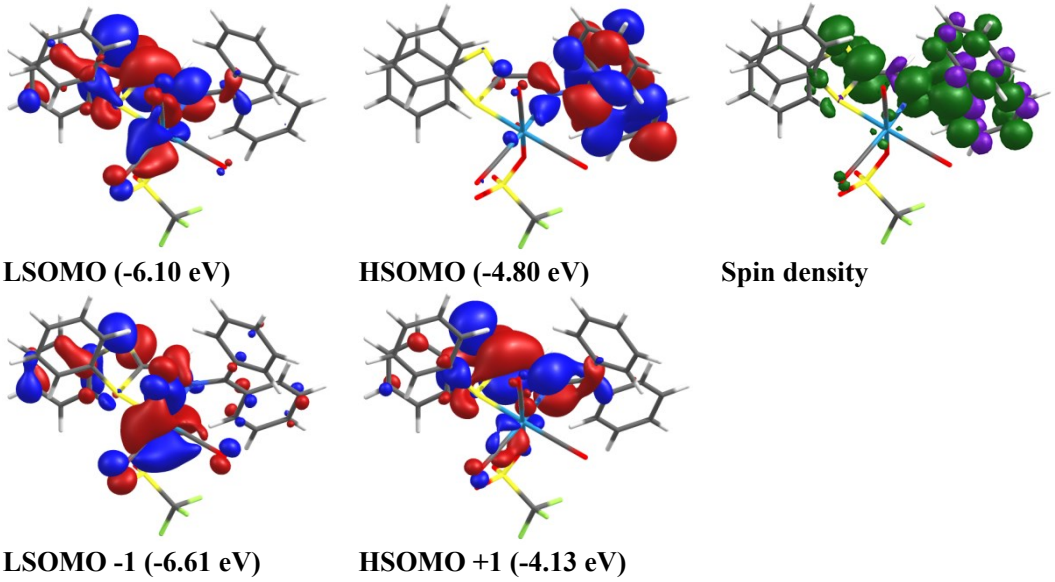

Figure S89. Right, representations of the semi-occupied MOs for **1j** in its lowest energy triplet state. The isoval = 0.04. Right, Alpha – beta SCF spin density. The isoval = 0.003 (green lobe positive, purple lobe negative).

Table S36. Relative atomic contributions (%) of the various fragments to the semi-occupied MOs of **1j.**[b]

Fragments	LS-1	LSOMO	HSOMO	HS+1
Re	**44%**	12%	3%	4%
3(CO)	19%	6%	2%	3%
$CF_3SO_3^-$ (TfO^-)	3%	1%	0%	1%
N-S_Ligands	34%	**82%**	**95%**	**92%**

[b]HS = HSOMO, LS = LSOMO; the values in bold represent the largest contributions.

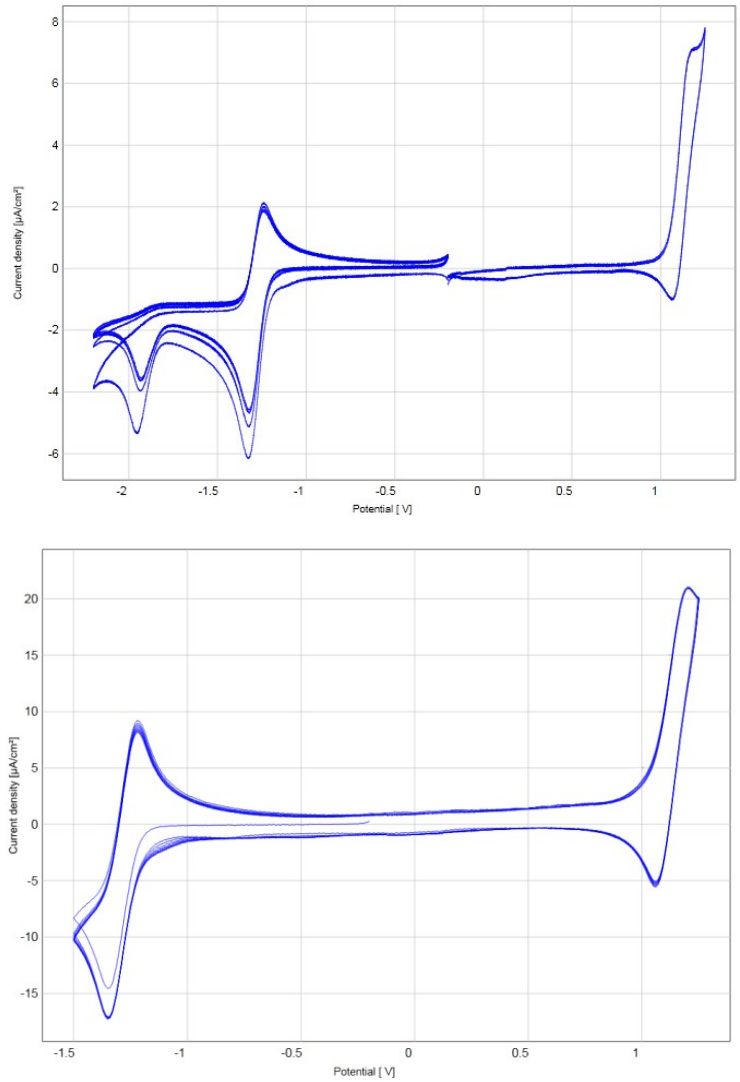

Figure S90. Cyclic voltammogram of 10 mM solution of **1h** recorded in CH_2Cl_2. Initial potential: -0.2 V. E(V) vs. Ag^+/Ag. Top: scan rate: 100 mV s^{-1}; bottom: scan rate: 1V s^{-1}.

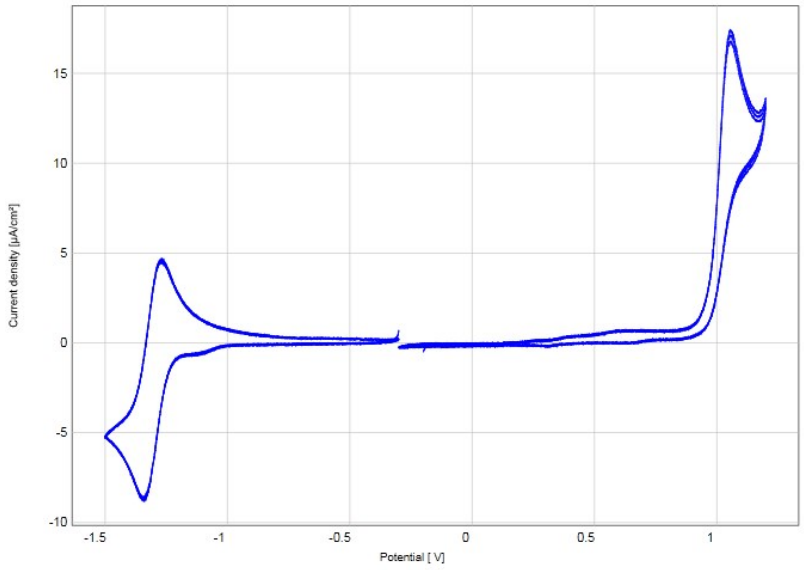

Figure S91. Cyclic voltammogram of 13 mM solution of **1b** recorded in CH_2Cl_2. Initial potential: -0.3 V. E(V) vs. Ag^+/Ag. Scan rate: 25 mV s^{-1}.

REFERENCES

1 S. Jacquot-Rousseau, A. Khatyr, G. Schmitt, M. Knorr, M. M. Kubicki and O. Blacque, *Inorg. Chem. Commun.*, 2005, **8**, 610–613.

2 S. Jacquot-Rousseau, G. Schmitt, A. Khatyr, M. Knorr, M. M. Kubicki, E. Vigier and O. Blacque, *European J. Org. Chem.*, 2006, **2006**, 1555–1562.

3 R. Kinghat, G. Schmitt, K. Ciamala, A. Khatyr, M. Knorr, S. Jacquot-Rousseau, Y. Rousselin and M. M. Kubicki, *Comptes Rendus Chim.*, 2016, **19**, 320–332.